Spectroscopic Millimeter Wave Ellipsometry

vorgelegt von
Mathias Klenner

an der Technischen Fakultät
der
Albert-Ludwigs-Universität Freiburg

Dekan

Prof. Dr. Oliver Paul

Referenten

Prof. Dr. Oliver Ambacher

Prof. Dr. Karsten Buse

Datum der Promotion: 24.07.2017

Für Sarah

She gave so much to so many...

Abstract

With the remarkable progress in high-frequency electronics, market analysts expect that the global value of millimeter wave sensors will significantly increase within the next decades. Particularly high-end radar and communication systems show great promise for complex future tasks such as fabrication automation under harsh conditions or environmental monitoring in fully autonomous driving. Clearly, sensors that are used for these applications must be highly reliable, accurate and virtually insusceptible to false detections. This can only be achieved with precise knowledge of the high-frequency material properties of modern building and plastic materials from which the sensor is made, or which interfere with its signal. However, the available catalog of material parameters is still comparably empty and partly inconsistent at millimeter wave bands, since precise measurement of the dielectric function at frequencies around 100 GHz or higher is challenging. Improvement of millimeter wave material analysis is therefore an essential prerequisite for the further development and optimization of modern sensors and sensor systems. The aim of this thesis is to establish a novel experimental method which significantly improves the measurement accuracy for characterization of the material properties of a wide variety of thin polymer materials, ceramics or composites at millimeter wave frequencies. The approach is based on adopting spectroscopic ellipsometry, a well-established technique at optical and infrared wavelengths, to the millimeter wave regime, where the signal is not only superimposed by multi-path scattering or antenna crosstalk, but also less polarized. It is demonstrated, that these limitations can be overcome by enhancing the amount of Fabry-Pérot reflections within the material under investigation so that a stronger phase rotation of the electromagnetic field is induced. This can be achieved by performing the measurements on a strongly reflecting substrate which increases the sensitivity of the measurement with respect to the critical measurands, the ellipsometer angles Ψ and Δ. By combined evaluation of the ellipsometric parameters along with spectroscopic interference effects, the novel method allows for unambiguous and more accurate material parameter measurements of thin dielectric samples than any other method. Thereby, even a slight dispersion of the dielectric function can be detected over a frequency range of 25 GHz. In addition, the novel approach allows for an approximation method which greatly reduces the necessary amount of data points that is required for analysis in the case of low-loss samples. For many practical applications, this solves the remaining drawback of millimeter wave ellipsometry compared to more established methods: insufficient measurement speed. Based on various dielectric samples, the performance and limits of the method are demonstrated throughout several experiments. It is shown that spectroscopic millimeter wave ellipsometry is a very promising approach to future material analysis that is predestined for characterization of thin dielectric layers, such as the parts of a vehicle chassis behind which millimeter radar sensors are typically placed.

Zusammenfassung

Mit der Entwicklung von kompakten, zuverlässigen und immer kosteneffizienteren Hochfrequenzschaltkreisen sehen Marktforscher in den nächsten Jahren großes Potential und eine stark wachsende Nachfrage für neuartige Millimeterwellensensoren. Insbesondere Radar- und Kommunikationssysteme werden künftig für komplexe Aufgabenstellungen in der Industrieautomation oder der Echtzeitüberwachung der Umgebung von voll autonomen Fahrzeugen eine bedeutende Rolle spielen. Die hierfür verwendeten Sensoren müssen sich durch höchste Zuverlässigkeit und Genauigkeit auszeichnen, sowie sehr robust gegen Fehldetektionen sein. Diese Eigenschaften können nur erreicht werden, wenn die Hochfrequenz-Materialparameter der Dielektrika bekannt sind, aus welchen der Sensor hergestellt ist, oder die das Sensorsignal beeinflussen. Da präzise Materialmessungen mit Millimeterwellen sehr anspruchsvoll sind, ist der derzeit vorhandene Katalog an Materialdaten für moderne, dielektrische Kunststoffe oder Laminate noch sehr lückenhaft und oft in sich nicht konsistent. Neue Messverfahren zur präzisen Bestimmung der Materialparametern von komplexen Kunststoffen bei Frequenzen um 100 GHz oder höher sind daher essentielle Voraussetzung für die Entwicklung und Optimierung von zukünftigen Sensorgenerationen in Industrie und Forschung. Zielstellung dieser Arbeit ist die Entwicklung einer neuartigen Methode zur Charakterisierung von Kunststoffen, Laminaten und Keramiken, welche die bisher erreichten Messgenauigkeiten im Millemeterwellen-Bereich deutlich übertrifft. Um dieses Ziel zu erreichen wird spektroskopische Ellipsometrie, ein Messverfahren welches bei optischen und infraroten Wellenlängen bereits etabliert ist, auch im Frequenzbereich um 100 GHz untersucht, umgesetzt und optimiert. Neben Streuung, Beugung oder dem Übersprechen der Antennen, stellt auch der geringere Polarisationsgrad des Signals eine große Herausforderung für die Millimeterwellen-Ellipsometrie dar. Im Rahmen dieser Arbeit wird gezeigt, dass diese Probleme durch deutliche Verstärkung der Fabry-Perot Reflektionen innerhalb der Materialproben gelöst werden können. Hierzu kommt ein stark reflektierendes Substrat zum Einsatz, auf welches die Proben platziert werden. Dabei wird ein stärkerer Phasenversatz des elektromagnetischen Feldes induziert, was die Sensitivität der Messung deutlich erhöht. Zusätzlich wird eine Entkopplung des Einflusses verschiedener Materialparameter auf die wesentlichen Messgrößen, die Ellipsometer Winkel Ψ und Δ, erreicht. Kombiniert mit einer klassischen reflektometrischen Messung, erlaubt dieser Ansatz eine sehr genaue und eindeutige Materialparameterbestimmung. Damit kann das Frequenzverhalten der dielektrischen Funktion über eine Bandbreite von 25 GHz sehr präzise gemessen werden. Auch schwache Dispersionseffekte sind dabei sichtbar. Viele interessante Werkstoffe absorbieren Millimeterwellen nur sehr schwach. In diesem Fall ermöglicht der neue Ansatz ein Näherungsverfahren zur Auswertung, welches wesentlich weniger Messpunkte benötigt, sodass die im Vergleich zu etablierten Verfahren langsame Messgeschwindigkeit der Ellipsometrie deutlich gesteigert werden kann. Anhand von zahlreichen Messreihen

werden die Möglichkeiten und Grenzen der neuen Methode evaluiert. Es wird gezeigt, dass das neue Verfahren besonders gut geeignet ist um die dielektrischen Eigenschaften von dünnen Materialproben, bestehend aus Polymerwerkstoffen, Keramiken oder Laminaten zu charakterisieren. Damit ist das Verfahren prädestiniert um beispielsweise den Einfluss von Karosserieteilen auf Radarsensoren für autonomes Fahren zu untersuchen.

List of Abbreviations

DC	direct current
FRP	fiber reinforced plastic
FWHM	full width at half maximum
FWTM	full width at tenth of maximum
GFRP	glass-fiber reinforced plastic
HBT	heterojunction bipolar transistor
HDPE	high-density polyethylene
IAF	Institute for Applied Solid State Physics
InGaAs	indium gallium arsenide
mHEMT	metamorphic high-electron-mobility transistor
MMIC	monolithic microwave integrated circuit
mmW	millimeter wave
MPA	medium power amplifier
PC	polycarbonate
PLL	phase-locked loop
PMMA	polymethyl methacrylate
POM	polyoxymethylene
PTFE	polytetrafluoroethylene
PVC	polyvinyl chloride
RF	radio frequency
Rx	receiving
S-parameter	scattering parameter
SiGe	silicon germanium
SNR	signal-to-noise ratio
TRL	through-reflect-line
Tx	transmitting
USB	universal serial bus

VCO	voltage-controlled oscillator
VNA	vector network analyzer

Contents

1 Introduction

Technology has not only advanced but also significantly changed in recent decades. The rapid progress in the development of microelectronics paved the way for the Information Age, also referred to as third industrial revolution or digital revolution, beginning in the 1980s [1, 2]. Today, microelectronics, or rather nanoeletronics, are still one of the driving forces of global technological change. With the development of modern networking technologies, there is an increasing desire for intelligent automation in production and assembly to create what is called a smart factory. This would be another milestone in technological advance and is sometimes already seen as the second machine age or the fourth industrial revolution [3, 4]. Apart from sophisticated algorithms for signal processing or machine learning, a variety of reliable, robust and versatile sensors is essential to gather the vast amount of information that is mandatory for realization of the so called Industry 4.0 [5, 6]. In addition, high performance data links are needed to distribute and process this information within the sensor network.

Microwave and particularly millimeter wave (mmW) technology has become more accurate, robust and cost-efficient in recent years and might fill an important gap in current sensor and communication systems [7]. The corresponding frequency range between 30 GHz and 300 GHz not only allows for large bandwidths and therefore high measurement accuracy or data rates, but also has another decisive advantage: The wavelength of a mmW signal, particularly if the frequency is higher than 100 GHz, is small enough to provide adequate resolution for most applications. On the other hand, it is still large enough to penetrate many clothing and packaging materials as well as dust particles and fog [8]. Thus, mmW sensors are suitable for measurements in harsh environmental conditions where more established sensors become unreliable or fail. Furthermore, mmW radiation is non-ionizing so that it can be safely used for security screening or biomedical applications where high-energy radiation would lead to mutation or destruction of the sample [9, 10].

Microwave and Millimeter wave material measurements

Successful development of novel, reliable sensors is closely related to precise knowledge of the materials from which they are built. In particular, the interaction of critical system components, made from dielectric polymer materials, with electromagnetic fields can significantly influence the performance of the sensor system. Therefore, a reliable catalog of material parameters at frequencies of 100 GHz and higher is indispensable to build innovative mmW senors. Apart from some summarizing data on the properties of common plastic and building materials that are suitable for microwave engineering [11–13], the catalog is still relatively empty. This is particularly problematic considering that there is

also rapid progress in the development of novel dielectric materials such as composites or polymer blends [14–17]. Accordingly, there has been increasing interest in precise measurement of the material properties of dielectric polymers at microwave and millimeter wave frequencies in recent years. This becomes especially obvious at the example of one of the driving forces in the development of industrial mmW sensors: The automotive industry.

Modern vehicles, which allow for autonomous or semi-autonomous driving must be capable of sensing their environment precisely and reliably. For this purpose, inter alia, radar systems operating at mmW frequencies are used [18–21]. Market analysts expect that the global value of millimeter wave radar sensors for autonomous driving will grow from less than 0.5 billion dollars in 2017 to about 30 billion dollars in 2030, when they will cover one third of the whole automotive sensor market [22]. However, this forecast can only be achieved if millimeter wave radars take over and improve a significant amount of functions that are now realized using optical or ultrasonic sensors. Therefore, the performance of current automotive radars must be considerably enhanced. These sensors are typically placed behind the chassis of the vehicle, which can consist of modern, complex materials or even thin varnish layers that can significantly influence the transmitted signal. In order to prevent false detection or misinterpretation of targets, the sensor itself, as well as influencing factors in its environment, must be well characterized. This becomes particularly clear by analyzing the history of automotive radar systems [23–25]. In its early stages, the new technology has been exclusively used for collision warning in high-end and later on also in consumer-class vehicles. Resolution and accuracy of these automotive radars are comparably low, particularly in vertical direction. This results in a significant false detection rate, e.g. if the vehicle drives towards a highway bridge under an angle due to an inconvenient slope of the road. With the development of adaptive cruise control systems [26, 27], the data from radar sensors is not only used for making the driver aware of potentially dangerous situations, but also to directly intervene in driving maneuvers such as breaking. Clearly, the false alert rate of these sensors must be significantly lower compared to collision warning. The next generation of automotive radars will not only be able to detect targets but also to classify them [28, 29]. The vehicle must be able to identify whether the detected target is a ball flying across the street that could be followed by a child or a harmless scenarios like a startled bird. This places enormous demands on the radar signal itself as well as on processing and analysis. It is therefore mandatory to take any interfering effects into account, such as the small dielectric layers of the vehicle chassis between the sensor and the target. Thus, precise measurement of material parameters is an obligatory requirement for the future of autonomous driving, but also in general for the development of novel and reliable mmW sensors.

A variety of different measurement techniques has been developed to achieve this ambitious goal [30]. At frequencies of 100 GHz and higher, material characterization is commonly performed using a so called free-space setup. Thereby, a mmW signal is transmitted into open space by an adequate antenna where it is reflected or transmitted at a well defined sample build from the material of interest [31–34]. The material parameters are then estimated based on evaluating the reflectivity or transmittance of the sample. This is a classical scattering parameter (S-parameter) measurement [35]. Apart

from being the most widely used method, that is also applied in commercial measurement equipment [36, 37], the method has decisive drawbacks. The material parameters are estimated based on a complex measurement of the phase and amplitude of the reflected or transmitted signal. This corresponds to a vector measurement and is typically performed using a vector network analyzer (VNA) operating at the respective mmW frequency range [38]. In consequence, complex S-parameter measurements are not only comparably cost-intensive, but also disadvantage from a fundamental point of view. The achievable measurement accuracy is greatly dependent on the calibration of the VNA setup [39]. Even though different calibration standards have been well established for complex network analysis, precise and robust calibration of a free-space configuration is particularly challenging [40–43]. Therefore, requirements on the measurement system as well as on the sample itself are high. Parasitic reflections or scattering must be reduced as far as possible, the sample needs to be well aligned and its thickness should not be considerably thinner than the wavelength of the mmW signal. This is problematic if varnish coatings or flexible materials, such as parts of a vehicle chassis, are investigated. In addition, time-stability of the method can only be assured if the setup is recalibrated frequently.

In conclusion, conventional mmW material characterization is not yet versatile enough to cope with the increasing requirements for future sensors or systems. Thus, the development of additional or alternative techniques for characterization of dielectric materials at mmW frequencies is highly desired, particularly for industrial applications.

Microwave ellipsometry

At wavelengths in the optical, infrared or ultraviolet region of the electromagnetic spectrum, the material parameters of thin, dielectric films are preferably measured using a technique known as ellipsometry [44–46]. A transparent sample is illuminated under a non-perpendicular angle using linearly polarized light. Depending on the dielectric and geometric properties of the sample, the polarization state of the reflected signal is changed and can be measured using rotatable polarizing filters. This technique has been known at least since 1887 and was documented first in the work of Paul Drude [47]. Modern ellipsometry is not only well established, but also has a reputation for being very accurate. In addition, it does not require sophisticated calibration standards, since it is based on a relative intensity measurement of the light passing through the polarizing filters [48]. If ellipsometry could be successfully applied to mmW frequencies, this would pave the way to overcome the main limits of material characterization using conventional S-parameter measurements.

Ellipsometry at microwave frequencies has first been proposed by Stetiu et al. in 2000 [49]. Instead of polarization filters, rotatable rectangular horn antennas are used to transmit a linearly polarized signal and to measure the change of polarization caused by the reflection at the sample under investigation. In the following years, Sagnard et al. used this approach to experimentally demonstrate that reflection ellipsometry can be adopted to microwave systems at fixed frequencies between 10 and 20 GHz [50, 51]. However, the achieved measurement accuracy turned out to be unexpectedly low con-

sidering the high precision known from optical ellipsometry [52]. This is particularly problematic since the material parameters are extracted from the measurement using a multi-parameter optimization algorithm which strongly relies on an accurate measurement of the polarization state of the signal. Furthermore, this first approach to microwave ellipsometry leads to ambiguous results, if there is no prior knowledge on the material properties of the sample that can be used as initial and boundary conditions for the algorithm. In consequence, microwave ellipsometry, as proposed by Stetiu et al, could not compete with conventional free-space methods based on S-parameter measurements. Since then, some effort has been made to improve the measurement accuracy of microwave and millimeter wave ellipsometry. Further investigation of the ellipsometric parameters using numerical simulations [53], a correction method based on Fourier analysis [54] and examination of standing wave effects [55] show promising results. However, the problem seems to be more fundamental so that the method is still inferior compared to more established microwave material characterization.

In summary, there are three critical challenges in successfully realizing ellipsometry at mmW frequencies. First, the measurement accuracy, that has been achieved by Sagnard et al., must be significantly improved and, secondly, ambiguous results from the parameter estimation must be avoided. In addition, ellipsometry involves mechanical rotation of the receiving horn antenna. This reduces measurement speed by several orders of magnitude compared to purely electronic methods such as S-parameter measurements. In this thesis, a novel approach to mmW ellipsometry is presented, that allows for a compact and versatile setup and overcomes all of these three challenges.

Structure of the thesis

Following this introduction, the next chapter 2 briefly discusses the theoretical foundation of dielectric materials and introduces the corresponding material parameters. Subsequently, conventional material characterization in the microwave and millimeter regimes are presented and their applicability to frequencies of 100 GHz and higher is evaluated. It is demonstrated why free-space S-parameter measurements are currently the most established technique, despite of some fundamental limitations. The theoretical framework of microwave ellipsometry is then introduced and it is shown, that this technique can in principle solve some of the main problems of conventional mmW material characterization. Finally, the performance of state-of-the-art microwave ellipsometry is investigated and it is shown that it is inferior to more established methods.
In chapter 3, a novel approach to mmW ellipsometry is presented. Following a detailed description of the experimental setup and a discussion of the influence of several setup related parameters, the achievable measurement accuracy of mmW ellipsometry is evaluated from a theoretical point of view. Based on this information, a novel approach using a strongly reflecting substrate is proposed. Furthermore, an improved, spectroscopic algorithm for parameter estimation is demonstrated and it is shown that it allows for unambiguous results even if there is no prior knowledge on the dielectric properties of the sample under investigation. Subsequently, an approximation method is presented, that significantly reduces measurement time if so called low-loss materials are investigated.

Chapter 4 includes the most important experimental results obtained from the novel mmW ellipsometer. First, a comprehensive analysis of the achievable measurement accuracy is performed. Therefore, possible error sources that result from the new configuration of the mmW ellipsometer are discussed. Based on these considerations, a selection of samples is determined that demonstrates the performance and the limits of the method. Finally, measurements of real and imaginary parts of the dielectric function are presented and discussed for each of the samples.
The final chapter 5 concludes the thesis by summarizing the main findings and pointing out their importance for successful realization of ellipsometry in the mmW regime.

2 Material Characterization using Microwaves

Characterization of dielectrics in the microwave and mmW regime has been an interesting field of research in recent years [56–61]. As mmW sensors and sensor systems become more and more important in industrial applications, the interaction of a wide range of different materials with radiation at frequencies around and beyond 100 GHz is of great importance. Different methods have been developed to characterize the dielectric properties of common plastic and building materials as well as highly specialized composites or laminated multilayer structures. Most of these methods are restricted with respect to their bandwidth or the range of material parameters that can be investigated. In consequence, compared to low-frequent radio bands or the visible spectrum, there still is a distinct lack of precise knowledge on material parameters at mmW frequencies, so that novel measurement concepts are desired. In particular, non-destructive free-space techniques, where the sample under investigation is characterized remotely and in real time, are becoming more and more established in industrial as well as in academic applications. Apart from classical S-parameter measurements, a method known from optical physics shows great potential to overcome some significant limitations of current mmW material characterization: Spectroscopic ellipsometry.

2.1 Electromagnetic materials

The development of modern technology, whether based on optics or electronics, is always closely related to an elementary physical process: The interaction between materials and electromagnetic fields. Since this interaction is, in general, dependent on the frequency of the electromagnetic field, adapting a material characterization method that works well at optical wavelengths to the microwave regime is challenging. Therefore, it is important to understand the structure of different classes of materials and their response to electromagnetic fields on the microscopic and macroscopic scale.

In this section, the basic principles of electromagnetic materials are briefly introduced in order to subsequently derive the fundamental material parameters of dielectrics, an important class of insulating materials which are widely used in mmW applications.

2.1.1 Microscopic scale

The electrical properties of any material are mainly determined by its electron energy bands [62]. According to Bohr's model, atoms are characterized by their discrete energy

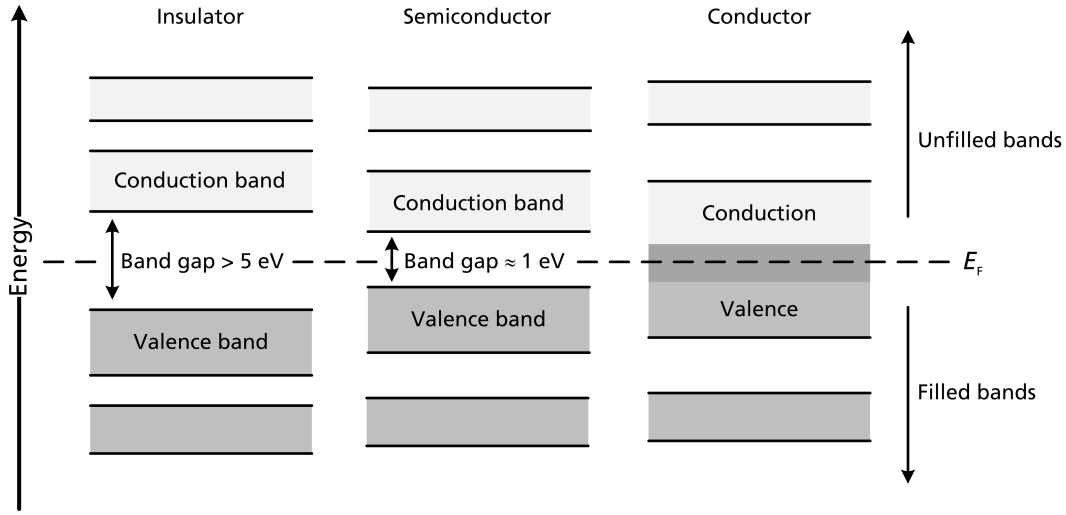

Figure 2.1: Energy band structure of insulators, semiconductors and conductors. At zero temperature, the bands below the Fermi energy E_F are filled with electrons while the higher bands are unfilled. Depending on the gap between valence and conduction band, electrons can occupy higher bands at nonzero temperatures which allows for electric conductance.

levels which combine to form energy bands if multiple atoms are brought together to form a solid [63]. The electron occupancy in these energy bands is given by Fermi-Dirac statistics [64, 65]. At a temperature of $T = 0\,\mathrm{K}$ all quantum states with energy lower than the so called Fermi energy E_F are occupied by electrons, while the quantum states with higher energy remain unoccupied [66]. The highest energy band that is occupied at $T = 0\,\mathrm{K}$ is called valence band. In this state, all electrons are bound to their nuclei. At nonzero temperatures, there exists a probability for electrons to occupy the energy band above the valence band, the so called conduction band. These electrons are denoted as free electrons since they are not bound to their nuclei anymore. The availability and amount of free electrons depends on the energy gap between the valence and conduction band. If this gap is large enough, it is possible that there are no electrons in the conduction band. Therefore, materials with a band gap larger than about 3 eV to 4 eV are classified as electrical insulators [67, 68]. If the band gap is smaller, the free electrons allow for a certain amount of electric conductance and the material is called semiconductor. If valence and conduction bands overlap, the material either provides very high electron mobility or a very large number of free electrons [69]. Since electrical conductivity is proportional to the product of electron mobility and concentration of free electrons, these materials are called conductors. The band structure of insulators, semiconductors and conductors is sketched in Figure 2.1.

A typical example of an insulator is diamond, a form of carbon where the atomic bonding is based on covalent bonds in a way that each carbon atom is connected to eight nearest neighbors [70]. This results in a very strong bonding and therefore in a large band gap between valence and conduction band. In contrast, graphite, another form of carbon is a conductor. Its electrons do not form covalent bonds and the valence band is overlapping with the conduction band. Hence, the electrical properties of materials are not only dictated by their atomic structures but also by the way in which atoms are bound to each other.

2.1.2 Dielectric materials

The interaction between electromagnetic fields and macroscopic, isotropic materials is described by Maxwell's equations:

$$\vec{\nabla} \cdot \vec{D} = \rho \qquad \vec{\nabla} \cdot \vec{B} = 0 \qquad \vec{\nabla} \times \vec{H} = \frac{\partial \vec{D}}{\partial t} + \vec{J} \qquad \vec{\nabla} \times \vec{E} = -\frac{\partial \vec{B}}{\partial t} \tag{2.1}$$

with

$$\vec{D} = \epsilon \vec{E} \qquad \vec{B} = \mu \vec{H} \qquad \vec{J} = \sigma \vec{E} \tag{2.2}$$

where $\vec{E}$ and $\vec{H}$ are the electric and magnetic field vectors, ρ is the charge density and σ is the conductivity of the material. The permittivity $\epsilon = \epsilon' - \mathrm{j}\epsilon''$ and the permeability $\mu = \mu' - \mathrm{j}\mu''$ are complex quantities describing the response of a material to electric and magnetic fields respectively. These parameters are, in general, frequency dependent. Thus, precise knowledge of ϵ, μ and σ is crucial to understand important properties of electromagnetic materials such as their conductance, reflectance or the penetration depth of the electromagnetic field.

Besides semiconductors, one important class of materials for microwave and millimeter wave applications are dielectrics. These materials are insulators (cf. Figure 2.1) that can be polarized if an electric field is applied but will not obtain a significant degree of magnetization in response to a magnetic field. Accordingly, the conductivity and permeability of these materials are approximately constant at $\sigma = 0$ and $\mu = 1$. Consequently, the material properties are fully determined by the dielectric function

$$\epsilon(f) = \epsilon_0 \epsilon_\mathrm{r}(f) = \epsilon_0 \left(\epsilon_\mathrm{r}'(f) - \mathrm{j}\epsilon_\mathrm{r}''(f)\right), \tag{2.3}$$

where f is the frequency of the electromagnetic field, ϵ_0 is the vacuum permittivity and ϵ_r is the relative permittivity of the dielectric material. ϵ_r is mainly related to ionic conduction, dipolar relaxation, atomic polarization and electronic polarization [71]. In the microwave regime, the most dominant effect is dipolar relaxation [30, 72, 73] so that the relative permittivity is typically described by a Debye relaxation model of the form

$$\epsilon_\mathrm{r} = \epsilon_\mathrm{r}^\infty + \frac{\epsilon_\mathrm{r}^0 - \epsilon_\mathrm{r}^\infty}{1 + \mathrm{j}\gamma} \tag{2.4}$$

with

$$\epsilon_\mathrm{r}^\infty = \lim_{f \to \infty} \epsilon_\mathrm{r} \qquad \epsilon_\mathrm{r}^0 = \lim_{f \to 0} \epsilon_\mathrm{r} \tag{2.5}$$

and

$$\gamma = 2\pi f \tau \frac{\epsilon_\mathrm{r}^0 + 2}{\epsilon_\mathrm{r}^\infty + 2} \tag{2.6}$$

where τ is the relaxation time of the dipolar polarization process [70]. At sufficiently low frequencies, the phase difference between the dipole polarization $\vec{P}$ and the applied

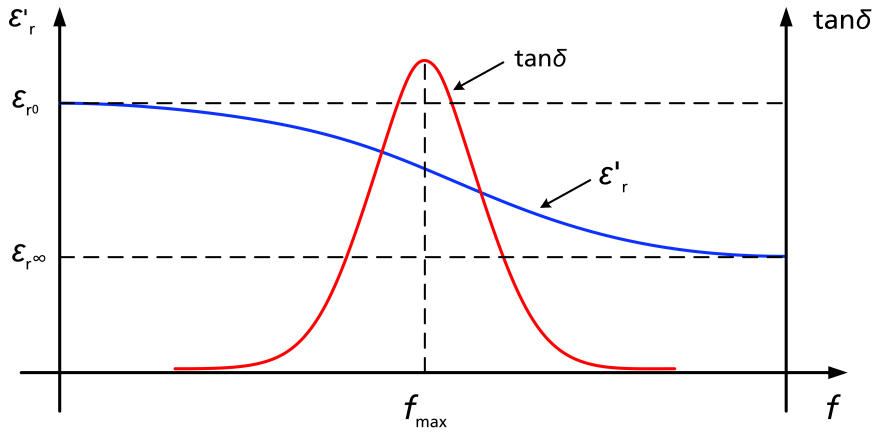

Figure 2.2: Expected frequency dependence of ϵ_r' and $\tan\delta$ at mmW frequencies. While ϵ_r' is monotonically decreasing, $\tan\delta$ has a maximum at f_{max}.

electric field $\vec{E}$ is negligible. At sufficiently high frequencies, the period of $\vec{E}$ is much smaller than the relaxation time τ so that the orientation of the dipoles is not influenced. Hence, ϵ_r^∞ and ϵ_r^0 are both real numbers. Accordingly, the real and imaginary part of the dielectric function can be obtained from equation 2.4:

$$\epsilon_r' = \epsilon_r^\infty + \frac{\epsilon_r^0 - \epsilon_r^\infty}{1+\gamma^2} \qquad \epsilon_r'' = \gamma\frac{\epsilon_r^0 - \epsilon_r^\infty}{1+\gamma^2}. \tag{2.7}$$

ϵ_r' and ϵ_r'' are related to the stored energy and the dissipation of energy within the material respectively [74]. The absorption of microwaves or millimeter waves caused by a dielectric is commonly quantified as the ratio of imaginary and real part of the dielectric function, the so-called loss tangent

$$\tan\delta = \frac{\epsilon_r''}{\epsilon_r'} = \gamma\frac{\epsilon_r^0 - \epsilon_r^\infty}{\epsilon_r^0 + \epsilon_r^\infty\gamma^2}. \tag{2.8}$$

Both ϵ_r' and $\tan\delta$ are functions of the frequency f. Equation 2.4 predicts that the real part of the dielectric function monotonically decreases from ϵ_r^0 to ϵ_r^∞, while the loss tangent has a maximum value of

$$\tan\delta_{max} = \frac{\epsilon_r^0 - \epsilon_r^\infty}{2\sqrt{\epsilon_r^0\epsilon_r^\infty}} \tag{2.9}$$

at a frequency of

$$f_{max} = \frac{1}{2\pi\tau}\cdot\sqrt{\frac{\epsilon_r^0}{\epsilon_r^\infty}}\cdot\frac{\epsilon_r^\infty + 2}{\epsilon_r^0 + 2} \tag{2.10}$$

as sketched in Figure 2.2. This dipolar relaxation model is a good approximation for the dielectric function of homogeneous polymer materials in the microwave and millimeter wave regime [75]. It is a useful tool to investigate the performance of the novel approach

to mmW ellipsometry that will be presented in chapters 3 and 4. From a measurement of ϵ'_r, the Debye parameters ϵ^0_r, ϵ^∞_r and τ can be extracted using equation 2.4. Based on these values, the expected strength of dispersion of the material parameters can be determined and compared to actual measurement.

To be consistent with other publications, the loss tangent $\tan\delta$ and the refractive index $n = \sqrt{\epsilon'_r}$ will be used to describe the dielectric properties of a material throughout this thesis. Since the absorbance of most dielectrics is comparably weak at mmW frequencies, the loss tangent is typically indicated in terms of 10^{-4}.

2.2 Conventional measuring methods

Characterization and qualification of modern plastic and building materials using microwaves was first established in the early 1950s [76]. Since then, along with the remarkable progress in monolithic microwave integrated circuit (MMIC) technology, numerous material characterization methods based on different physical principals have been investigated and developed [32, 77]. Even though, most of these methods are highly specialized with respect to the desired application, they can be generally classified in two categories that are resonant and non-resonant methods. Material characterization using resonators is more accurate but also fundamentally restricted to discrete frequencies. In contrast, non-resonant methods allow for spectroscopic measurements and are preferable if the material parameters must be characterized at different frequency ranges [30]. In general, non-resonant methods are more versatile but less accurate. Accordingly, there is increasing interest in enhancing the measurement accuracy of these methods.

In this section, the most widely used non-resonant techniques based on coaxial air-lines, hollow waveguides and free-space propagation are briefly introduced in order to discuss their suitability for the millimeter wave regime and the achievable measurement accuracy.

2.2.1 Coaxial air-lines

One of the earliest, but still relevant techniques for characterization of the relative permittivity ϵ_r or permeability μ_r at microwave frequencies is based on coaxial transmission lines [78]. A toroidal sample is inserted between the inner and outer conductors of a coaxial air-line so that the S-parameters and thus the electric properties of the probe can be determined [79]. In order to allow for characterization of larger samples and to enhance measurement accuracy, the section of the coaxial line where the sample is placed is usually enlarged as sketched in Figure 2.3. This is particularly beneficial if heterogeneous samples are investigated, where it is important to average over possible fluctuations in the dielectric properties [80]. Coaxial air-lines are typically used if large bandwidths or low frequencies are desired since this method can theoretically be applied down to direct current (DC) frequencies. The maximum frequency and thus the operational frequency range Δf is related to the diameter of the outer conductor D_{out}. A smaller value results in a larger maximum frequency as shown in Table 2.1.

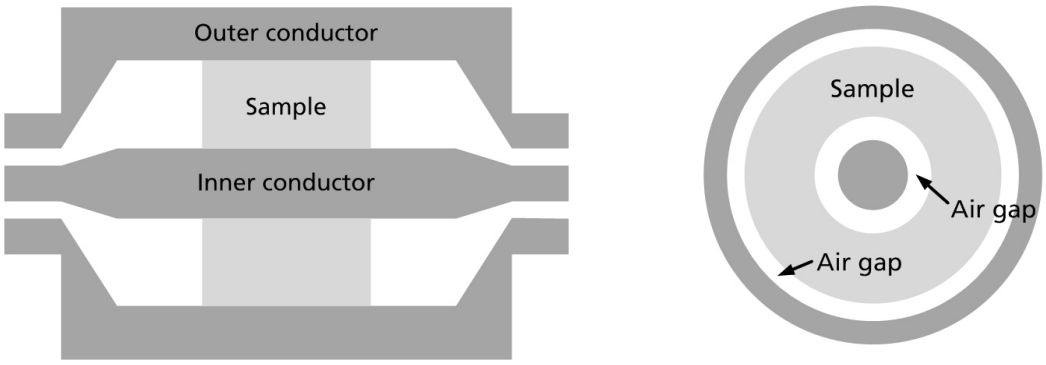

(a) Longitudinal view (b) Cross-section view

Figure 2.3: Sketch of an enlarged coaxial air-line probe. The sample is placed between the inner and outer conductor and must be precisely machined in order to avoid air gaps and asymmetries in the setup.

Apart from algorithm uncertainties, inaccurate sample position and uncertainty on the S-parameter measurement, a significant error source of coaxial air-line methods are air gaps between the sample and the conductors as sketched in Figure 2.3(b). If the air gaps become larger than about 5 % of the wavelength of the signal, the measured material parameters can deviate by more than 30 % from the real value [81]. Thus, more precisely machined samples are required to avoid inaccuracies in the measurement when the conductor diameter is reduced in order to characterize materials at higher frequencies. Furthermore, the minimal diameter of the conductors in coaxial air-lines, that can be used for reliable material characterization, is physically limited. In consequence, this method is, in general, not applicable to millimeter wave systems.

2.2.2 Hollow metallic waveguides

In order to realize measurements of material parameters at frequencies higher than about 35 GHz, hollow metallic waveguides are often used instead of coaxial transmission lines [82]. In most cases rectangular waveguides are designed such that their width d_w and height d_h satisfies $d_h/d_w = 0.5$ [83]. If the wavelength of the transmitted electromagnetic field is larger than d_w but less than $2d_w$, single-mode operation is ensured. Therefore, the minimum and maximum frequencies f_{min} and f_{max} which can be used for

Table 2.1: Operational Frequency ranges of coaxial air-lines with different diameters of the outer conductor [30].

D_{out} [mm]	Δf [GHz]
3.5	0-34.5
7.0	0-18.2
14.0	0-8.6

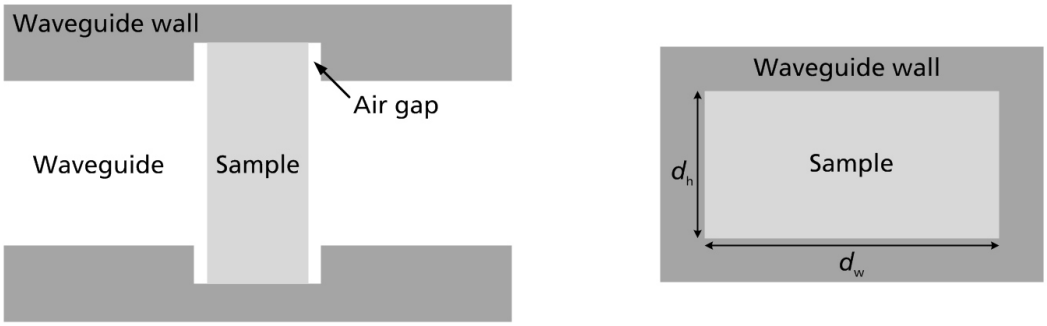

(a) Longitudinal view (b) Cross-section view

Figure 2.4: Sketch of an hollow waveguide used for material characterization. In order to avoid asymmetries in the setup and to minimize the influence of air gaps, the sample is placed in a groove within the hollow waveguide.

material characterization are defined by the geometry of the waveguide. Typically, the operational range of hollow waveguides is restricted to the frequency range between $1.1 \cdot f_{\text{min}}$ and $0.9 \cdot f_{\text{max}}$ to ensure good propagation. The width of waveguides used for material characterization in the frequency range from 75 GHz to 110 GHz, denoted as W-band, is $d_{\text{w}} = 2.54\,\text{mm}$ [84]. Accordingly, machining precision of the samples and air gaps are also limiting factors concerning the achievable measurement accuracy of hollow waveguide methods. Figure 2.4 shows a sketch of an improved waveguide probe, where the sample is placed in a groove within the waveguide walls. Thereby, accurate placement is ensured and the measurement accuracy can be enhanced as long as the sample is not much thinner than the transversal waveguide dimension [85]. In addition, the maximum operational frequency of the hollow waveguide method is significantly higher compared to that of coaxial air-lines. However, there are still significant drawbacks of this technique. The method can not be used for inhomogeneous materials, as long as inclusions are not much smaller than the wavelength [30]. Furthermore, the possible machining precision limits the selection of suitable sample materials and the method is destructive and is therefore not applicable for in situ measurements.

2.2.3 Free-space methods

Among the variety of material characterization methods, free-space techniques have attracted remarkable interest in industrial applications [86, 87]. They are in general contactless, non-destructive and can be used under special conditions such as high temperatures or to investigate fragile samples. Therefore, these methods are ideal for real time manufacturing surveillance or characterization of final products. In consequence, microwave and millimeter wave systems for non-destructive material testing have been continuously developed and improved over the recent two decades [88–92]. While different methods are usually adapted to the requirements of specific applications, the general principle is predominantly based on evaluating the power of the radiation which is reflected or transmitted at the sample under investigation. A typical measurement setup

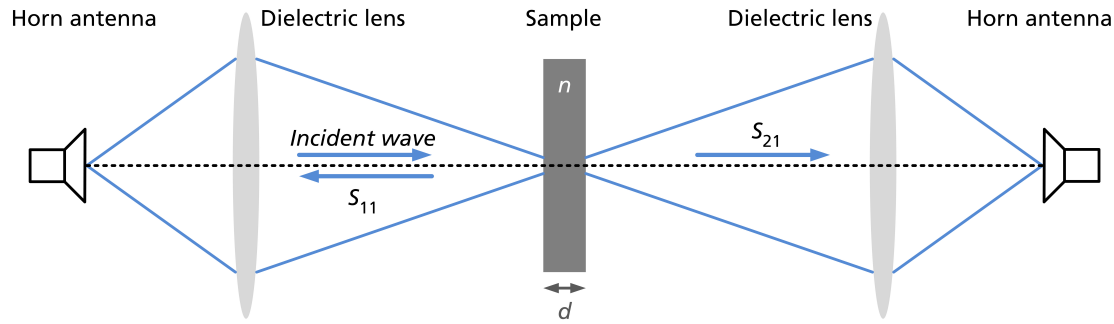

Figure 2.5: Typical setup for free-space measurements of material parameters in the microwave and millimeter wave regime.

is sketched in Figure 2.5. Horn antennas are used to transmit and receive a microwave signal which is focused onto a sample using dielectric, quasi-optical lenses [93]. Thereby, the incident signal is partly transmitted through the sample and partly reflected back to the transmitting (Tx) horn antenna. In order to determine the material parameters of the sample, the corresponding S-parameters S_{11} (reflection) and S_{21} (transmission) are evaluated. It can be shown that the relative permittivity ϵ_r and the sample thickness d are related to the S-parameters by the following equations [94]:

$$S_{11} = \frac{\Gamma(1-T^2)}{1-\Gamma^2 T^2}, \qquad S_{21} = \frac{T(1-\Gamma^2)}{1-\Gamma^2 T^2}, \tag{2.11}$$

where

$$\Gamma = \frac{1-\sqrt{\epsilon_r}}{1+\sqrt{\epsilon_r}} \tag{2.12}$$

and

$$T = \exp\left(-\mathrm{j}\frac{2\pi f d}{c_0}\sqrt{\epsilon_r}\right) \tag{2.13}$$

are the reflection and transmission coefficients at the air-sample interfaces respectively, f is the frequency of the transmitted signal and c_0 is the speed of light in vacuum. Depending on the application, Γ and T can be adjusted, for instance to describe the reflection of multilayer structures or to take a non-perpendicular incident wave into account.

2.2.4 Challenges in modern free-space methods

Even though, modern free-space methods provide decisive advantages over classical non-resonant techniques, such as coaxial air-lines or waveguide probes, there are also significant drawbacks. Only one material parameter, for instance the refractive index n, can be determined per measurement [51]. In consequence, the loss tangent $\tan\delta$ and the geometry of the sample must be well known prior to the measurement. Therefore, conventional S-parameter evaluation is preferably used for low-loss materials where $\tan\delta \approx 0$. If the absorbance of a sample is significant, a series of independent measurements must

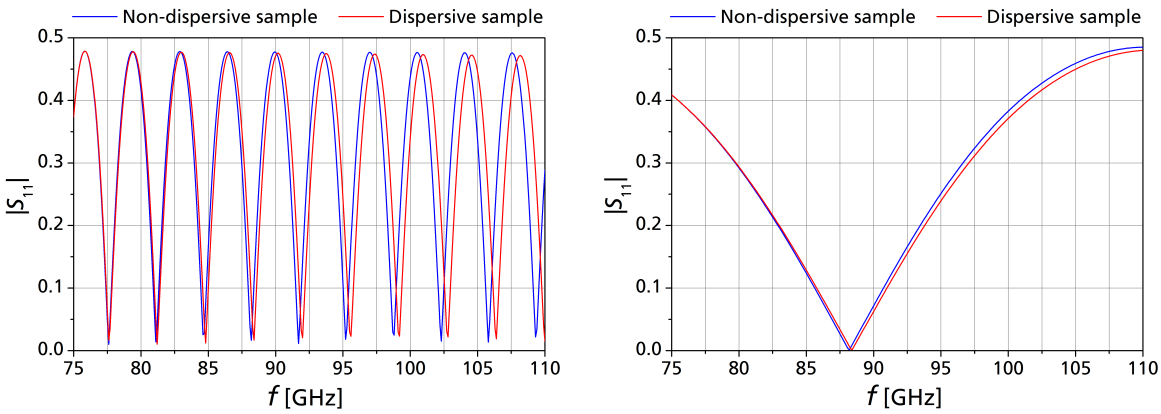

(a) $d = 25\,\text{mm}$ (b) $d = 2\,\text{mm}$

Figure 2.6: Simulated reflectivity of dispersive and non-dispersive samples for characterization using a classical free-space method. In order to measure the dispersion, the sample must be adequately thick and the system must provide a large bandwidth.

be performed. This can be achieved by variation of the incident angle, the frequency of the signal, or a sample related parameter such as its thickness [52]. Since mechanical intervention reduces measurement speed, a spectroscopic approach is often used for modern free-space S-parameter measurements. For this purpose, Fabry-Perot interference, caused by the reflection at the sample interfaces, is evaluated over a preferably wide frequency range [95, 96]. However, this approach leads to reduced measurement accuracy in many cases. This becomes particularly apparent if the dielectric properties of the material under investigation are dispersive. Figure 2.6 shows simulations of the reflectivity $|S_{11}|$ of four hypothetical samples over the frequency range from 75 GHz to 110 GHz. The thickness of the samples is either $d = 25\,\text{mm}$ or $d = 2\,\text{mm}$. In the non-dispersive case, the refractive index is constant at $n = 1.7$, while the refractive index of the dispersive samples decreases linearly from $n = 1.7$ to $n = 1.68$. The non-dispersive, 25 mm thick sample induces a regular periodic reflectivity spectrum. In contrast, the period of the curve corresponding to the dispersive sample is slightly decreasing with frequency. In order to determine the frequency dependent dielectric function of this sample, an according material model, e.g. based on dipolar relaxation (cf. section 2.1.2) can be used to fit the S_{11} measurement. In this case, the achievable measurement accuracy is strongly correlated with the accurateness of the material model. In particular inhomogeneous materials or layered structures such as composites significantly reduce the convergence rate of the optimization algorithm. Alternatively, it is possible to select several small frequency ranges around prominent features of the reflectivity spectrum, such as the minima, and use a non-dispersive model to determine the material parameters within that small frequency range [97]. Both techniques are only feasible, if the system provides enough bandwidth with respect to the sample thickness. Even a bandwidth of 35 GHz is insufficient for precise analysis of the dispersion of a 2 mm thick sample as Figure 2.6(b) indicates.

A further problem of any free-space method is that the electromagnetic field is not limited by a defined boundary. Multi-path reflections and scattering from the environment

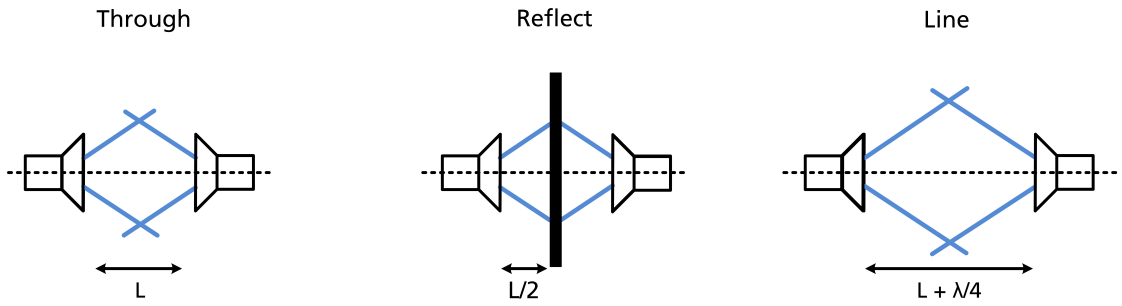

Figure 2.7: TRL calibration standard for a simple free space setup.

decrease measurement accuracy and must be minimized using adequate high frequency absorbers. To avoid scattering at the edges of a sample, the transmitted signal is commonly focused using quasi-optical elements such as dielectric lenses or parabolic mirrors that are placed in the far field of the antenna. In addition, the sample has to be placed in the far field of the focusing elements. If the corresponding aperture size is larger than a half-wavelength of the microwave signal, the far field distance can be estimated by

$$R_\mathrm{f} > \frac{2fD^2}{c_0}, \tag{2.14}$$

where D is the largest dimension of the aperture of the antenna or the focusing element [98]. Since R_f increases quadratically with D, a compact setup based on quasi-optical components is, in general, not feasible at microwave frequencies.

Besides measurements of dispersive or thin materials, a more general challenge of modern free-space S-parameter methods is calibration. S_{11} and S_{21} are complex quantities and are typically measured using a VNA [38]. This is not only cost-intensive, but also disadvantageous regarding the achievable measurement accuracy since, in general, S-parameter measurements need to be calibrated carefully. Even though several calibration standards have been developed, primarily for on-wafer S-parameter measurements, accurate calibration of a free-space VNA setup is challenging or even unfeasible, depending on the exact configuration [30]. One of the most widely used calibration standards is called through-reflect-line (TRL) and can also be applied to simple free-space setups such as a sample placed between two horn antennas [99, 100]. For the through standard, the sample is removed and the face-to-face path of the antennas is measured as sketched in Figure 2.7. The reflection measurement is performed by replacing the sample by a totally reflecting material such as a metal plate. The line standard is similar to the through standard, but the antennas are separated by an additional distance of $\lambda/4$, where λ is wavelength of the microwave signal [101]. Therefore, precise alignment of the antennas and the sample or metal plate is mandatory for accurate calibration. Depending on the material and thickness of the sample, this can be challenging. In addition, multi-path reflections, for instance between the antennas, can not be avoided in free-space microwave measurements and may lead to interference effects that falsify the calibration. Furthermore, long term stability can only be achieved if the setup related parameters

can be precisely controlled. Otherwise, frequent recalibration is required. Accordingly, material characterization using free-space methods involves high efforts and costs and is more suitable to a laboratory environment than to typical industrial demands. Particularly calibration seems to be a limiting factor and is discussed in many current publications concerning microwave and millimeter wave material measurements [102–105].

2.3 Microwave ellipsometry

Since classical S-parameter measurements have been investigated for several decades and are already highly developed [106–108], it seems more favorable to establish a novel method that intrinsically overcomes the challenges described in section 2.2.4 than trying to further optimize S-parameter measurements. A particularly interesting method that could be used for this purpose is reflection ellipsometry, a well-established technique for precise determination of material parameters at optical or infrared wavelengths [48, 109]. A transparent, dielectric sample is illuminated under a non-perpendicular angle using linearly polarized light such that the change of the polarization state, caused by a phase shift between the parallel (p) and perpendicular (s) parts of the electric field within the material, can be measured. For this purpose, a relative power measurement is sufficient so that there is no need for sophisticated calibration of the setup. In addition, a single ellipsometry measurement yields two independent measurands so that two material parameters can be obtained simultaneously. If ellipsometry could also be successfully realized at mmW frequencies, less complex and more cost-efficient setups would be possible and long-term stability of mmW material characterization would be improved. Furthermore, optical ellipsometry is known for providing high sensitivity on measurements of samples that are much thinner than the wavelength. Thus, it can be expected that the accuracy of a mmW ellipsometer outperforms that of conventional S-parameter measurements. Accordingly, reflection ellipsometry is a very promising approach to material characterization in the microwave or millimeter wave regime and has first been proposed by Stetiu et al. in 2000 [49]. Instead of an optical light source combined with polarization filters, a rectangular horn antenna transmits a linearly polarized electromagnetic field onto a dielectric sample. A second, rotatable horn antenna is used to measure the change of polarization caused by the reflection at the sample under investigation. However, the experimental implementation of this technique is demanding so that the measurement accuracy and reproducibility of results which have been previously published are unsatisfying [51, 52, 110].

In this section, the theoretical framework of microwave ellipsometry is presented in order to demonstrate its advantages compared to classical material characterization at mmW frequencies. Previously published methods and algorithms for parameter extraction, as well as the achieved measurement accuracy, are discussed to point out the difficulty of successfully adopting ellipsometry to the mmW regime. Thereby, three key problems are identified that will be solved using the improved method which is presented in this thesis in chapters 3 and 4.

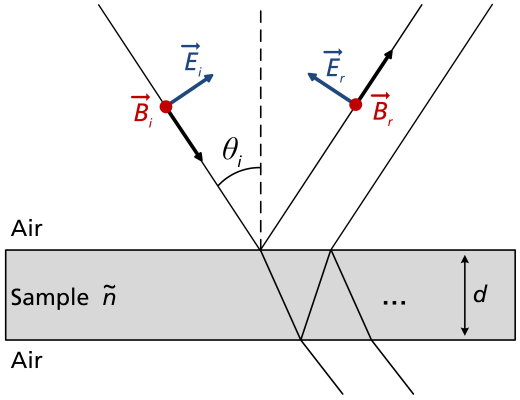

Figure 2.8: The fields which are reflected or transmitted through a single-layer sample depend on the dielectric properties of the material, its thickness as well as the angle of incidence and the surrounding media.

2.3.1 Theoretical framework

The aim of microwave ellipsometry is to measure the change in the polarization state of an electromagnetic wave that is reflected at the air-material interfaces of a single-layer sample, as sketched in Figure 2.8. Therefore, the incident field $\vec{E}_i$ must be linearly polarized. At microwave frequencies, this can be achieved using a rectangular feed horn antenna as transmitter. Within the material, a relative phase shift between the parallel and perpendicular parts of the electric field is induced. In consequence, the polarization of the reflected field $\vec{E}_r$ is, in general, elliptic [46, 109, 111]. The incident and reflected fields are related by a complex reflection coefficient, which depends on the frequency f, the angle of incidence θ, the thickness of the sample d and the complex refractive index $\tilde{n} = n - \mathrm{j}\kappa$:

$$\vec{E}_{\,\mathrm{i}} = \tilde{r}(f, \theta, d, \tilde{n})\vec{E}_{\,\mathrm{r}}. \tag{2.15}$$

The reflection coefficient $\tilde{r}(f, \theta, d, \tilde{n})$ can be calculated separately for the parallel (p) and perpendicular (s) parts of the electromagnetic field:

$$\tilde{r}_{\mathrm{p/s}} = \frac{1 - \exp(-\mathrm{j}2\beta)}{1 - (r'_{\mathrm{p/s}})^2 \exp(-\mathrm{j}2\beta)} \cdot r'_{\mathrm{p/s}}, \tag{2.16}$$

where

$$\beta = \frac{2\pi f}{c_0} d\sqrt{\tilde{n}^2 - \sin^2\theta} \tag{2.17}$$

is the complex propagation factor through the dielectric material, c_0 is the speed of light in vacuum and the coefficients

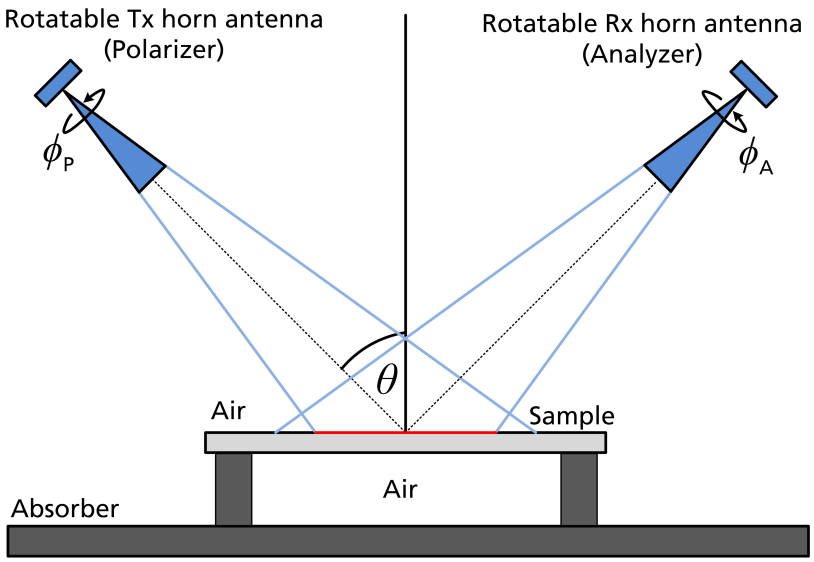

Figure 2.9: Optical ellipsometry can be transferred to the microwave regime by using rectangular horn antennas as polarizer and analyzer. Previous publications have proposed systems for investigation of samples surrounded by air.

$$r'_p = \frac{\sqrt{\tilde{n}^2 - \sin^2\theta} - \tilde{n}^2\cos\theta}{\tilde{n}^2\cos\theta + \sqrt{\tilde{n}^2 - \sin^2\theta}},$$
$$r'_s = \frac{\cos\theta - \sqrt{\tilde{n}^2 - \sin^2\theta}}{\cos\theta + \sqrt{\tilde{n}^2 - \sin^2\theta}} \tag{2.18}$$

describe the reflection of the parallel and perpendicular parts of the electric field at the air-sample interfaces [112]. Accordingly, the polarization of the reflected field is given by the ratio

$$\tilde{\rho} = \frac{\tilde{r}_p}{\tilde{r}_s} \tag{2.19}$$

and depends on the dielectric properties and the geometry of the sample under investigation. In order to determine the refractive index n, the loss tangent $\tan\delta$ (cf. section 2.1.2) or its thickness d, it is beneficial to rewrite the complex quantity $\tilde{\rho}$ in its polar form

$$\tilde{\rho} = \frac{\tilde{r}_p}{\tilde{r}_s} = |\tilde{\rho}| \cdot \exp[j \cdot \arg(\tilde{\rho})] = \tan\Psi \cdot \exp[j\Delta], \tag{2.20}$$

such that

$$\tan\Psi = \frac{|\tilde{r}_p|}{|\tilde{r}_s|} \tag{2.21}$$

and

$$\Delta = \arg(\tilde{r}_p) - \arg(\tilde{r}_s) \tag{2.22}$$

represent the relative amplitude and phase shifts between s-polarized and p-polarized parts of the reflected electromagnetic field. Ψ and Δ are denoted as ellipsometer angles and can be measured using microwave ellipsometry. The corresponding experimental setup is sketched in Figure 2.9. Two rotatable, rectangular horn antennas replace the polarization filters that are used in optical ellipsometry. The Tx antenna (polarizer) transmits a signal with approximately linear polarization. The corresponding polarization angle is defined as ϕ_P. While measuring the power of the reflected signal, the receiving (Rx) antenna (analyzer) is rotated around its axis of symmetry by the angle ϕ_A. Thereby, the polarization of the reflected field can be determined. Consequently, the measured power at the Rx horn antenna P_{Rx} depends not only on the ellipsometer angles Ψ and Δ and the emitted Tx power P_0, but also on the angles ϕ_P and ϕ_A [51, 113]:

$$\begin{aligned} P_{Rx} = P_0[1 &- \cos(2\phi_P)\cos(2\Psi) + \cos(2\phi_A)\left(\cos(2\phi_P) - \cos(2\Psi)\right) \\ &+ \sin(2\Psi)\sin(2\phi_P)\cos(\Delta)\sin(2\phi_A)]. \end{aligned} \tag{2.23}$$

P_0 is the average value of P_{Rx} and can be used for normalization of the measured data to eliminate the influence of the Tx power. Furthermore, by choosing a fixed polarizer angle of $\phi_P = \pm\frac{\pi}{4}$, equation 2.23 can be simplified as follows:

$$\frac{P_{Rx}}{P_0} = 1 - \cos(2\phi_A)\cos(2\Psi) \pm \sin(2\phi_A)\sin(2\Psi)\cos(\Delta). \tag{2.24}$$

Due to the symmetry of this ellipsometer curve, it is sufficient to measure the Rx power over a half rotation from $\phi_A = 0°$ to $\phi_A = 180°$. However, to improve the accuracy of the material parameters estimation, a full rotation of the analyzer antenna is preferable since possible asymmetries in the experimental setup can be averaged. The ellipsometer angles can then be deduced from the measured data. Subsequently, the material parameters n, $\tan\delta$ or d are implicitly derived using equations 2.20, 2.18 and 2.16.

2.3.2 Methodology and parameter extraction

In case of a single-layer sample surrounded by air, the ellipsometer angles Ψ and Δ can either be determined analytically or using a numerical approach. In section 3.2.3 it is shown that uncertainty on the ellipsometer angles greatly influences the outcome of the material parameter estimation. Therefore, the advantages and disadvantages of both methods must be carefully evaluated.

When a linearly polarized microwave signal is reflected at a dielectric sample, its polarization is, in general, elliptic. Figure 2.10(a) shows a sketch of the according polarization ellipsis, which is characterized by two parameters. The azimuth angle γ represents the orientation of the ellipse with respect to the X-axis, which is defined by the (linear) polarization of the transmitted signal. The angle χ between the major half axis a and the

minor half axis b defines the eccentricity of the polarization ellipse such that

$$\tan\chi = \frac{b}{a}. \tag{2.25}$$

Figure 2.10(b) shows two ellipsometer curves which are calculated using equation 2.24 and two arbitrary pairs of ellipsometer angles $(\Psi, \Delta) = (45°, 30°)$ and $(\Psi, \Delta) = (60°, 15°)$. These curves are fully determined by the maximum power P_{max}, the minimum power P_{min} and the analyzer angle corresponding to the maximum power $\phi_{\text{A}}^{\text{max}}$. It can be shown that the azimuth and eccentricity of the polarization ellipse are related to the ellipsometer curve by[51]:

$$\gamma = \phi_{\text{A}}^{\text{max}} \qquad \tan\chi = \sqrt{\frac{P_{\text{min}}}{P_{\text{max}}}}. \tag{2.26}$$

In consequence, the ellipsometer angles Ψ and Δ can be derived from two fundamental relations of ellipsometry [46, 48, 109]:

$$\begin{aligned} \tan(2\gamma) &= \tan(2\Psi)\cos(\Delta) \\ \sin(2\chi) &= \sin(2\Psi)\sin(\Delta) \end{aligned} \tag{2.27}$$

While this method is straight forward and its computational complexity is comparably low, there is a decisive disadvantage for microwave systems. The analytical approach depends on an accurate power measurement in order to precisely calculate $\tan\chi$. Since many dielectric plastic or building materials are fairly transparent for microwaves, it can be expected, that the reflectivity of a typical sample surrounded by air is low. Thus, only a small amount of the signal is reflected to the Rx horn antenna. At mmW frequencies, where the output power of the signal generation chain is limited to a few milliwatts, the values of P_{max} and particularly P_{min} can be in the nanowatt regime. Therefore, the detector must not only provide very high sensitivity, but it is also mandatory that it is well calibrated. Accordingly, one of the main advantages of ellipsometry, compared to conventional S-parameter measurements, is lost. Furthermore, it can be expected that the accuracy on the measurement of the minimum power is low, so that the ellipsometer angles Ψ and Δ can not be precisely determined.

In order to reduce the uncertainty on the ellipsometer angles, a numerical algorithm can be used instead of the analytical method. For this purpose, the measured ellipsometer curve is normalized with respect to its average power P_0. As a result, the detector does not have to be calibrated for absolute measurements and the ellipsometer curve becomes symmetrical around $P_{\text{Rx}}/P_0 = 1$ (cf. equation 2.24). The normalized curve is fully determined by its maximum power P_{max} and the corresponding analyzer angle $\phi_{\text{A}}^{\text{max}}$. It is not necessary to explicitly measure the minimum power P_{min}. Instead, a theoretical power model based on equation 2.24 is used to fit the measured data by minimizing the function

$$F(\Psi, \Delta) = \sqrt{\sum_{\text{A}=1}^{N} \left[\bar{Y}_{\text{A}} - \frac{P_{\text{Rx}}}{P_0}(\phi_{\text{A}}, \Psi, \Delta) \right]^2}, \tag{2.28}$$

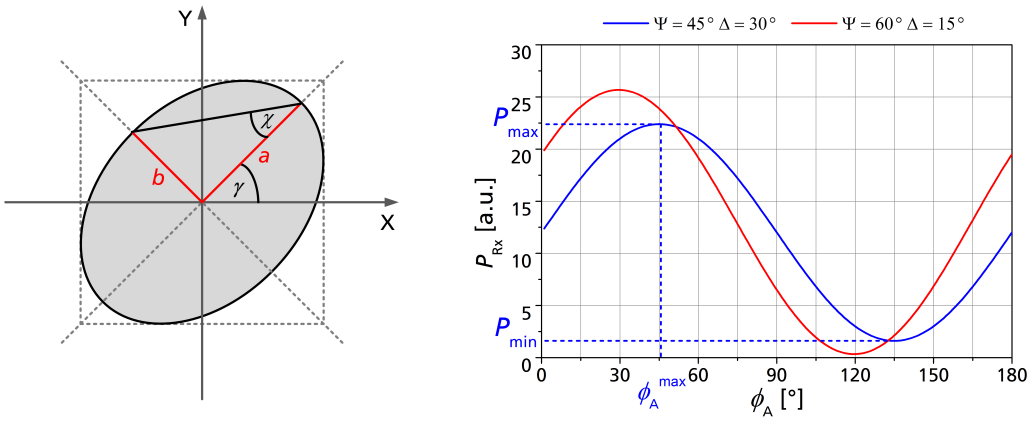

(a) Orientation of the ellipse

(b) Arbitrary ellipsometer curves

Figure 2.10: The polarization change of the reflected signal is defined by the azimuth angle and the ellipticity. Both parameters are related to the ellipsometer curve.

where $\bar{Y}_A$ is the normalized measured value of the power at the analyzer angle ϕ_A and N is the total number of measuring points. This method has an averaging effect and enhances the accuracy of low power measurements. It can be further improved by excluding the regions around the extrema of the ellipsometer curve, where the slope is close to zero and statistical inaccuracies are particularly disadvantageous, from the optimization algorithm.

Once the ellipsometer angles Ψ and Δ are determined from the measurement, analytically or numerically, the material parameters n, $\tan\delta$ and d are estimated using equations 2.21 and 2.22 by global minimization of the function

$$G(n, \tan\delta, d) = \sqrt{A^2 + B^2}, \tag{2.29}$$

where

$$A = \sqrt{\tan^2\Psi - \left[\frac{|\tilde{r}_p|}{|\tilde{r}_s|}\right]^2}, \qquad B = \sqrt{\Delta^2 - [\arg(\tilde{r}_p) - \arg(\tilde{r}_s)]^2} \tag{2.30}$$

and the complex reflection coefficients

$$\tilde{r}_{p,s} = \tilde{r}_{p,s}\,(n, \tan\delta, d) \tag{2.31}$$

are calculated according to equations 2.16, 2.17 and 2.18. This complex multi-parameter optimization algorithm is very sensitive to uncertainties on the ellipsometer angles. It is therefore crucial to measure Ψ and Δ with highest possible precision. Accordingly, numerical determination of the ellipsometer angles is preferable to the analytic approach at mmW frequencies, since the expected reflected power is typically low. If not explicitly states otherwise, the simulations and experimental results presented in this thesis are therefore based on the numerical algorithm presented above.

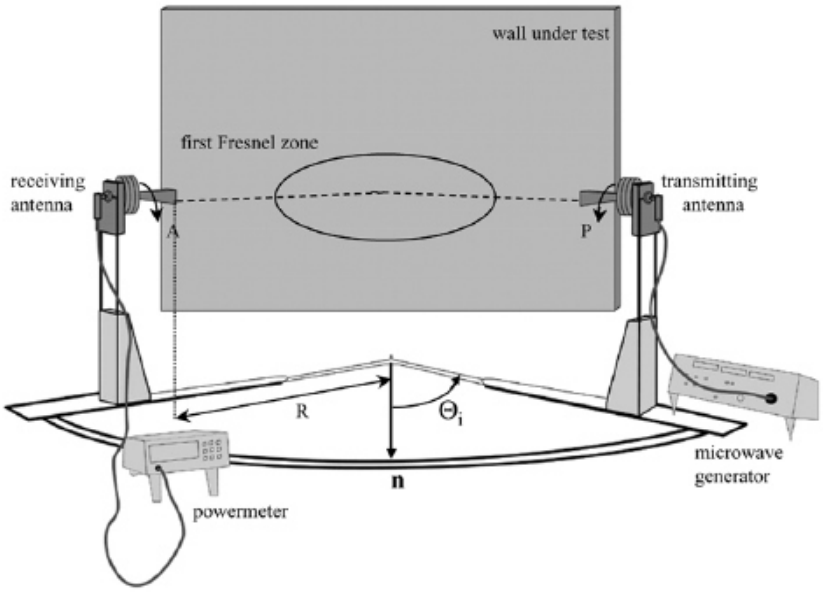

Figure 2.11: Experimental setup of the first microwave ellipsometer. Two rotatable horn antennas transmit and receive the microwave signal. A wall under test, consisting of a dielectric material, is placed in front of the antennas. Source: Sagnard et al. [51].

2.3.3 State-of-the-art microwave ellipsometry

Microwave ellipsometry has first been realized in experiments by Sagnard et al. [51, 52]. The corresponding experimental setup is illustrated in Figure 2.11. Two rotatable horn antennas are used to transmit and receive a microwave signal with a frequency between 10 GHz and 20 GHz. In contrast to most optical ellipsometers, the setup is aligned horizontally. This is due to the comparably large size of the microwave components such as the horn antennas. Accordingly, the system was primarily intended for characterization of larger samples such as walls. An analytical analysis and a numerical approach were used to estimate the material parameters from the measured ellipsometer angles Ψ and Δ. Even at frequencies around 10 GHz, where significantly more output power is available compared to the mmW regime, the analytical approach turned out to be inferior and the numerical method was used for the final analysis. However, interfering factors like multipath reflections, scattering or polarization loss of the antennas significantly influenced the measurement outcome. Consequently, the achieved accuracy of the material parameter estimation was unexpectedly low, considering the high precision known from optical ellipsometry.

Figure 2.12 compares the performance of the microwave ellipsometer to the results from other free-space methods in a similar frequency range. The red data points represent ellipsometer measurements of the refractive index of two samples made from polyvinyl chloride (PVC), a well-known homogeneous polymer material that is used in numerous applications, such as construction of pipes or profile in doors and windows [114, 115]. Both samples have identical properties apart from their thickness. The circles correspond to the measurement of a 10.4 mm thick PVC slab, while the squares

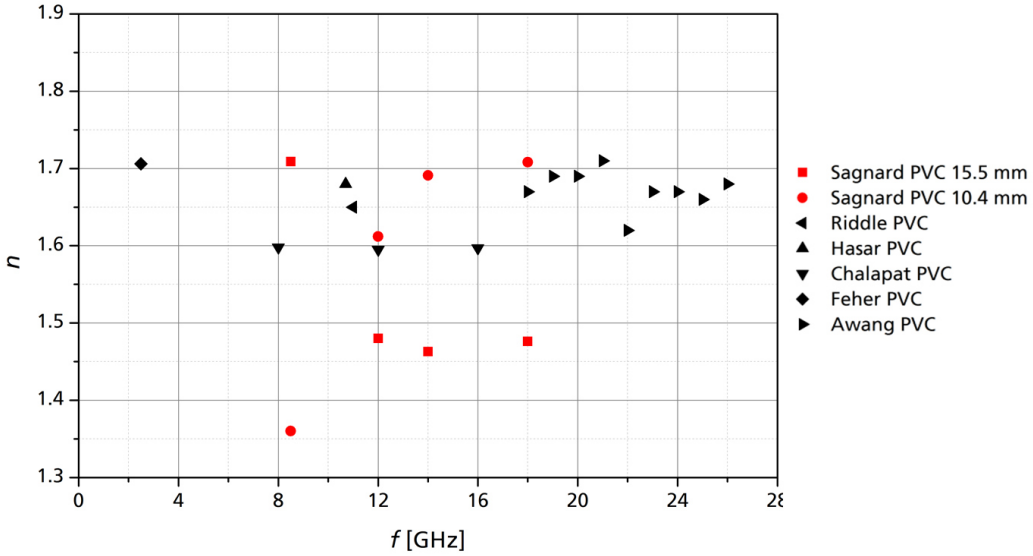

Figure 2.12: Measurements of the refractive index of PVC at microwave frequencies. The measurement accuracy of microwave ellipsometry (red data points) is poor compared to other methods (black data points).

represent the results obtained from a 15.5 mm thick slab. The resulting data was averaged over different angles of incidence to increase accuracy. In addition to the ellipsometer measurements, the black data points show the results of comparable measurements of PVC using conventional free-space methods [116–120]. These measurements suggest that the refractive index of PVC is in the region between $n = 1.6$ and $n = 1.7$ in the corresponding frequency range. There are discrepancies between the data from different measurements, which are symbolized by different triangles, but the single measurements are comparably self-consistent. This indicates that the material properties of the investigated PVC samples were slightly different. In fact, this is a common problem in comparing microwave measurement of industrially produced polymer materials since the exact composition and processing varies from manufacturer to manufacturer [121, 122].

Even in consideration of this disparity, the results from the microwave ellipsometer measurement are predominantly not in accordance with the data from more established free-space measurements. More significantly, the data is not internally consistent. At all of the four frequencies, that were used for the ellipsometer measurement, significantly different values of the refractive index were determined for the 10.4 mm thick and the 15.5 mm thick PVC sample. Since both samples are made from identical material, this can be attributed to low measurement accuracy. Furthermore, neither of the two samples leads to a stable result over frequency. Instead the measured values are clustered into two groups. One in the region from $n = 1.4$ to $n = 1.5$ and another one in the region from $n = 1.6$ to $n = 1.7$. Thus, the material parameter estimation based on the ellipsometer angles Ψ and Δ seems to be ambiguous. This can indeed be shown analytically and will be discussed in more detail in section 3.3.1. If all the measured values are averaged, the refractive index of PVC obtained from microwave ellipsometry is $n = 1.56 \pm 0.13$. This result is not in good accordance with most of the other measurements, despite its large

standard deviation of about 8 %. In comparison to the refractive index, measurement of the loss tangent at mmW frequencies is, in general, considered to be more challenging. This is also true for microwave ellipsometry. The averaged loss tangent corresponding to the ellipsometer measurements shown in Figure 2.12 is $\tan\delta = (3476 \pm 1345) \times 10^{-4}$. This corresponds to a standard deviation of about 38 % and indicates that there was even stronger dispersion in the loss tangent than in the refractive index measurements. Even though there are only few publications including comparable measurements, there is strong evidence that the absorption of the PVC sample was highly overestimated using microwave ellipsometry. According to previously published results, the value of the loss tangent should rather be in the region between $\tan\delta = 50 \times 10^{-4}$ and $\tan\delta = 100 \times 10^{-4}$ at comparable microwave frequencies [123–125].

In summary, there are three decisive problems with state-of-the art microwave ellipsometry. First and most importantly, the achievable measurement accuracy is much lower than expected and can not compete with more established methods, particularly for measurement of the loss tangent. Despite of its theoretical advantages over classical S-parameter measurements, only few effort has been spent to analyze the causes of the unsatisfying performance or to improve the technique [53–55]. Secondly, it is not feasible to obtain unambiguous results, even if the frequency and the angle of incidence are gradually varied throughout several measurements. The third problem is the comparably low measurement speed. Rotation of the analyzer antenna or a change of the angle of incidence involve mechanical interaction and slow down the measurement compared to purely electronic methods.

In the following chapters of this thesis, a novel approach to mmW ellipsometry is presented. Thereby, measurement accuracy is significantly improved and unambiguous analysis of the material parameters is feasible. Furthermore, the configuration allows for an approximation technique that enhances measurement speed by two orders of magnitude in the case of low-loss samples.

3 Spectroscopic Millimeter Wave Ellipsometry

As promising as ellipsometry may seem for mmW material characterization from a fundamental point of view, the problems with its experimental realization, in particular the limited measurement accuracy and ambiguous results, have prevented the method from being competitive with conventional reflectometric S-parameter measurements. In contrast to optical ellipsometry, accurate generation or detection of polarized electromagnetic fields is challenging at microwave frequencies, as their propagation is governed by the principles of reflection, refraction, and diffraction. In addition, the polarization loss of horn antennas limits the achievable measurement accuracy even if parasitic reflections or scattering could be completely avoided. Since precise polarization measurement is a key requirement of ellipsometry, it is particularly challenging to use this method for material characterization at mmW frequencies.

In this chapter, a novel approach to mmW ellipsometry which significantly enhances measurement accuracy and provides unambiguous results is presented. First, the general experimental setup and the influence of different system-related parameters are discussed. Thereby, the critical measurands and their contribution to the achievable measurement accuracy are identified and, as a result, an improved mmW ellipsometer setup using a metallic substrate is proposed. Subsequently, the fundamental methodology and algorithms are presented. It is shown that the measurement accuracy can be significantly increased compared to that of the conventional setup and that unambiguous results are possible using a spectroscopic approach. In addition, an approximation method, that can be used for low-loss samples is derived. It allows to measure the ellipsometer angles Ψ and Δ without continuous rotation of the analyzer antenna and therefore enhances measurement speed.

3.1 Design of a compact millimeter wave ellipsometer

The development of a novel method for mmW material characterization holds great potential, but also involves significant challenges in the design of the experimental setup. In order to compete with or outperform more established methods (see chapter 2.2), the novel mmW ellipsometer must allow for highly resolved measurements of different material parameters over a wide frequency range, while being compact, cost-efficient and versatile.

In this section, the general layout of the mmW ellipsometer is introduced in order to subsequently discuss the critical system parameters and their expected influence on

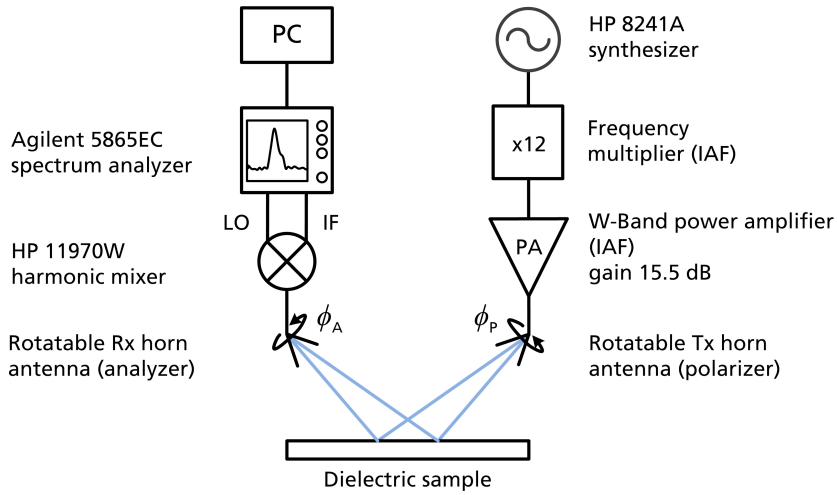

Figure 3.1: Block diagram of the mmW ellipsometer . A frequency multiplier is used instead of a fundamental W-band oscillator in order to provide the maximum possible bandwidth.

the measurements. In conclusion, the final setup and the corresponding mechanical construction are presented.

3.1.1 General layout of the system

The key challenge in spectroscopic mmW ellipsometry can be described in two steps. First, a well-defined mmW signal must be generated, linearly polarized and transmitted onto a sample under investigation. Secondly, the reflected signal must be received and analyzed with respect to expected changes in its polarization state.

A corresponding mmW ellipsometer setup is outlined in the block diagram shown in Figure 3.1. The radio frequency (RF) signal is generated using an HP 8241A synthesizer followed by an x12 frequency multiplier and a W-band medium power amplifier (MPA) which have been designed and fabricated at the Fraunhofer Institute for Applied Solid State Physics (IAF) using an in-house 100 nm indium gallium arsenide (InGaAs) metamorphic high-electron-mobility transistor (mHEMT) technology [126]. Using this setup, any frequency between 75 GHz and 110 GHz, the so called W-band, can be realized. The mmW signal is then transmitted onto a sample stage using an interchangeable and rotatable standard gain horn antenna such that the electromagnetic field, illuminating the sample under investigation, is linearly polarized with respect to a chosen angle. The reflected power is received by another rotatable horn antenna and mixed down using an HP 11970W harmonic mixer. Thus, any change in the polarization state, caused by the reflection at a dielectric material on the sample stage, can be investigated by performing a full rotation of the Rx antenna. By using an Agilent 5865EC spectrum analyzer, the measured power at the Rx antenna is distinctly assigned to the frequency of the 12th harmonic of the transmitted signal. In principle, a conventional W-band power meter can be used instead of the spectrum analyzer to make the overall setup more compact. In this case, the undesired harmonics of the frequency multiplier must be either adequately suppressed or considered in the model parameters for data analysis. This will be discussed in more detail in the following section.

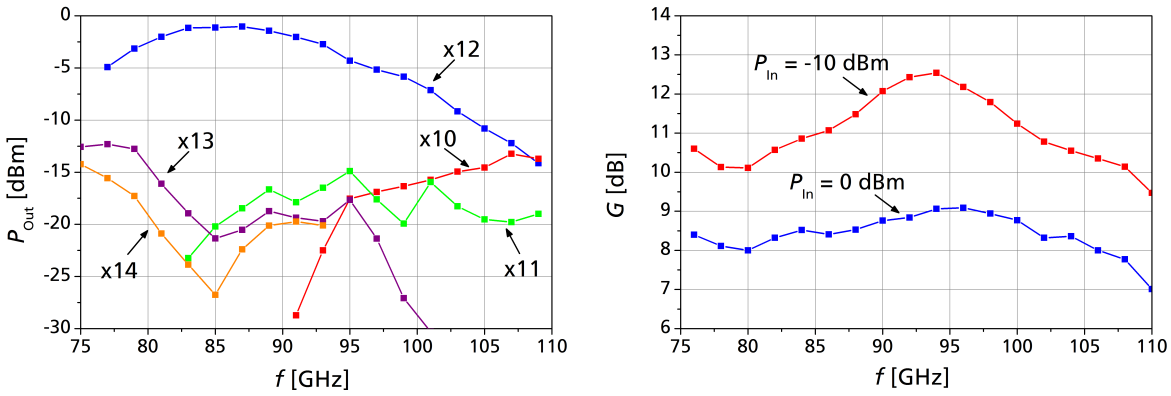

(a) x12 multiplier (input power at 0 dBm)

(b) W-band MPA

Figure 3.2: Measured frequency response of the critical RF-components used in the mmW ellipsometer. Up to a frequency of 105 GHz, the undesired harmonics are adequately suppressed (a).

3.1.2 Signal generation and RF components

Instead of using the signal generation chain shown in Figure 3.1, the RF signal could also be generated using a fundamental W-band voltage-controlled oscillator (VCO). This method has the advantage, that frequency multiplication is not needed and therefore the signal is not superimposed by undesired harmonic frequencies. However, modern W-band oscillator MMICs typically provide a maximum tuning range below 10 GHz [127–130]. Even though there exist single publications demonstrating an ultra-wideband W-band oscillator with a tuning range of 26 GHz based on a 180 nm silicon germanium (SiGe) heterojunction bipolar transistor (HBT) process [131, 132], fundamental W-band oscillators, in general, still seem unfavorable with respect to the desired bandwidth of a mmW ellipsometer. In contrast, using a frequency multiplier, a usable bandwidth of 30 GHz or more can be achieved while the harmonics are adequately suppressed. Consequently, material parameters can be measured over a much broader frequency range without modification of the experimental setup. This is not only beneficial in terms of measurement complexity, but more importantly, plays a decisive role in obtaining unambiguous results as demonstrated in section 3.3.2.

Measurements of the frequency response of the x12 multiplier and the W-band MPA used in the mmW ellipsometer are shown in Figure 3.2. This combination allows to convert an input signal with a power of $P_{In} = 0$ dBm in the frequency range between 6.25 GHz and 9.17 GHz to a W-band signal with a maximum output power of $P_{Out} \approx 7$ dBm at frequencies around 85 GHz. It should be noted that the output power significantly decreases towards the edges of the frequency band, even though the higher gain G of the MPA at lower input power compensates this to a certain extend. However, since the measured ellipsometer curve is typically normalized with respect to its average value for further analysis (cf. section 2.3.2), the measurements are not restricted to the 3 dB bandwidth of the output power spectrum. In general, the full frequency range of the W-band, between 75 GHz and 110 GHz, can be used for ellipsometry with this setup.

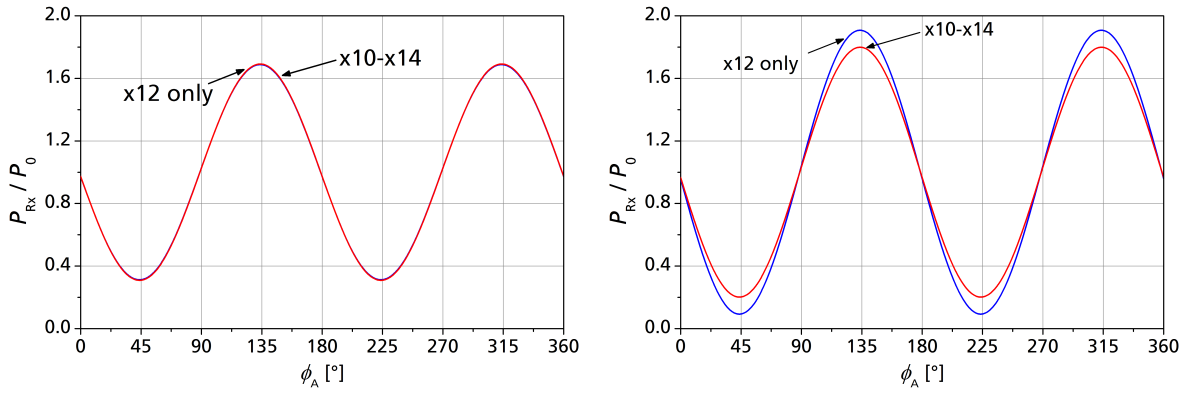

(a) at 91 GHz (b) at 107 GHz

Figure 3.3: Influence of the harmonics generated by the x12 multiplier on a simulated ellipsometer curve corresponding to a 2 mm thick PVC sample. At 91 GHz, the undesired frequencies are adequately suppressed and the curves are virtually indistinguishable. At 107 GHz, the 10th and 11th harmonics are strong enough to clearly influence the ellipsometer curve.

Nevertheless, weak signals decrease the signal-to-noise ratio (SNR), particularly if the material under investigation is strongly absorbing in the mmW regime.

In addition to the power spectrum of the 12th harmonic of the x12 multiplier, the frequency response of the most prominent undesired harmonics are also shown in Figure 3.2(a). Between 80 GHz and 100 GHz they are suppressed by more than 10 dB such that the ellipsometer measurement is not significantly influenced. Below 80 GHz, the 13th harmonic becomes more prominent, but the simulated error on the material parameters is still negligible regarding the expected measurement accuracy of the mmW ellipsometer. In contrast, the power of the 10th harmonic increases considerably at frequencies higher than 100 GHz and even becomes stronger than the 12th harmonic at 110 GHz.

Figure 3.3 shows different simulations of possible mmW ellipsometer measurements at frequencies of 91 GHz and 107 GHz. The normalized power P_{Rx}/P_0 reflected from a 2 mm thick PVC sample is plotted against the rotation angle ϕ_A of the Rx horn antenna. The 12th harmonic of the fundamental signals, 7.58 GHz and 8.92 GHz, as well as a superposition of the 10th to 14th harmonic have been simulated respectively in order to investigate their influence on an actual measurement. While the two ellipsometer curves corresponding to the RF signal at 91 GHz are virtually indistinguishable, there is a significant offset between the curves at 107 GHz. This is most likely caused by the weak suppression of the 10th harmonic. If a conventional W-band power meter is used to measure the reflected signal instead of a spectrum analyzer, there are two ways to address this problem. The first solution is to restrict the measurements to a frequency range, where the influence of the undesired harmonics is negligible, in this case between 80 GHz and 100 GHz. However, this frequency range also depends on the material parameters of the sample which are, in general, not known in advance. For instance, if a material induces a strong resonance at one of the undesired harmonics, a suppression by 10 dB of this specific frequency might not be sufficient. For this reason, it is useful to consider

all the harmonics of the x12 multiplier for data analysis by extending equation 2.24 as follows:

$$\frac{P_{\mathrm{Rx}}}{P_0} = \sum_i a_i \left[1 - \cos(2\phi_{\mathrm{A}})\cos(2\Psi_i) \pm \sin(2\phi_{\mathrm{A}})\sin(2\Psi_i)\cos(\Delta_i)\right]. \tag{3.1}$$

The sum index i represents the harmonic frequencies of the x12 multiplier. Consequently, there exists a distinct set of ellipsometer angles (Ψ_i, Δ_i) that differ depending on the suppression of the respective harmonic i. This is considered in the model using a scaling factor a_i, that can either be calculated based on precise characterization of the RF components used for signal generation, or calibrated using measurements of one or more well-known reference samples.

Therefore, replacing the spectrum analyzer in the setup shown in Figure 3.1 by a more compact W-band power meter has, in principle, no negative impact on the measurement outcome. It also allows for a more cost efficient setup. However, the complexity of the parameterized model used for data analysis increases noticeably, while no additional information is obtained compared to a setup using a spectrum analyzer. In fact, the introduction of a significant number of additional model parameters not only complicates the investigation of the achievable measurement accuracy, but also inhibits to study alternative models e.g. for mmW ellipsometry of multilayer structures. Consequently, using a setup based on a power meter is disadvantageous from an academic point of view. Thus, the measurements which are presented and discussed in this thesis are based on the setup including a spectrum analyzer if not explicitly stated otherwise.

3.1.3 Horn antennas and incident angle

The measurement outcome of mmW ellipsometry does not exclusively depend on the material parameters of the sample under investigation, but also on the specifications of the experimental setup. In particular, the choice of the antennas used as polarizer and analyzer, the resulting illuminated area on the sample as well as the angle of incidence can significantly influence the measured ellipsometer curve. Therefore, these parameters must be well chosen to ensure that the characteristics of the measurement are not dominated by the setup itself, but by the sample-related parameters such as its dielectric properties or geometry.

One of the most significant differences between optical and mmW ellipsometry is the generation, polarization and shape of the beam used for illumination of the sample under investigation. While lasers, in combination with polarization filters, are preferably used in optical ellipsometers, there is no equivalent technology, providing a coherent and collimated beam, in the mmW regime. Instead, the mmW ellipsometer setup includes two pyramidal feed horn antennas which generate a linearly polarized electromagnetic field in the far-field of the antennas [133, 134]. Accordingly, their gain, dimension and position in the experimental setup must be well chosen to avoid near-field effects while keeping the overall system as compact as possible. Figure 3.4 shows a sketch of the beam path of the mmW ellipsometer. A dielectric sample is illuminated under an angle of incidence θ by a pyramidal feed horn antenna with an aperture angle α which is located

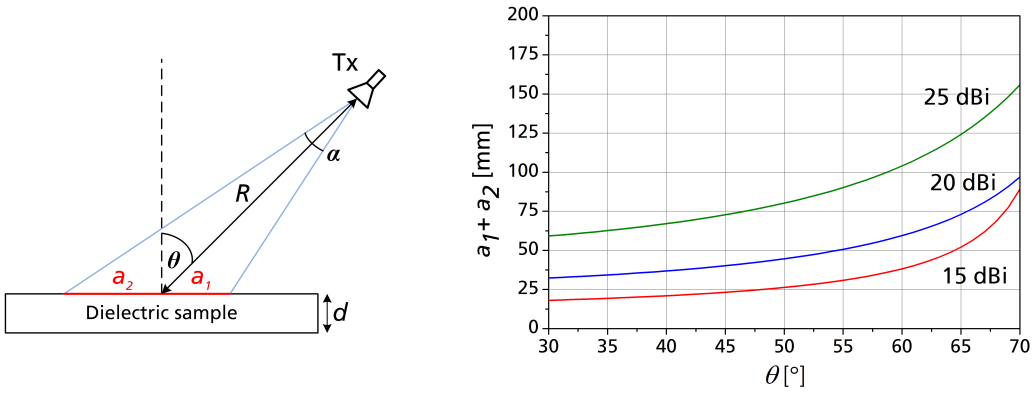

Figure 3.4: The angle of incidence θ, the angular aperture of the horn antenna α and the distance R between sample and antenna influence the illuminated area, represented by $a_1 + a_2$. If the sample is placed in the far-field of the antenna at $R > R_{\text{min}}$, $a_1 + a_2$ increases with the antenna gain and the angle of incidence.

at a distance R from the sample. One limiting factor concerning the total dimensions of the experimental setup is the sample size. It can be estimated using the following trigonometric relation:

$$a_1 + a_2 = R \left[\frac{\sin(\alpha/2)}{\sin(\frac{\pi}{2} - \frac{\alpha}{2} + \theta)} + \frac{\sin(\alpha/2)}{\sin(\frac{\pi}{2} - \frac{\alpha}{2} - \theta)} \right]. \tag{3.2}$$

For $\theta \neq 0$, the illuminated area on the sample becomes asymmetric (i.e. $a_2 > a_1$) and increases with the angle of incidence. Furthermore, it also depends on the antenna gain. While higher antenna gain will, in general, decrease α, the minimum distance R_{min} where the antenna can be placed such that the sample is safely in the far-field of the antenna, is defined by the Fraunhofer distance [133, 135].

$$R_{\text{min}} = \frac{2fD^2}{c_0}. \tag{3.3}$$

It increases quadratically with the maximum dimension D of the antenna aperture. Therefore, higher antenna gain is not necessarily favorable for building a compact mmW ellipsometer setup.

According simulations of the illuminated area depending on the angle of incidence are shown in Figure 3.4 for three different standard gain horn antennas. Consequently, larger antennas with higher gain demand a more extended sample surface as they must be located further away to fulfill the far-field criterion (cf. equation 3.3). Solely based on this consideration, the ideal configuration for building a compact mmW ellipsometer would be to use the 15 dBi antenna at the steepest angle of incidence which the setup allows, in this case $\theta = 30°$. However, a steep angle of incidence as well as low antenna gain reduce the dynamic range of the setup and therefore the measurement accuracy.

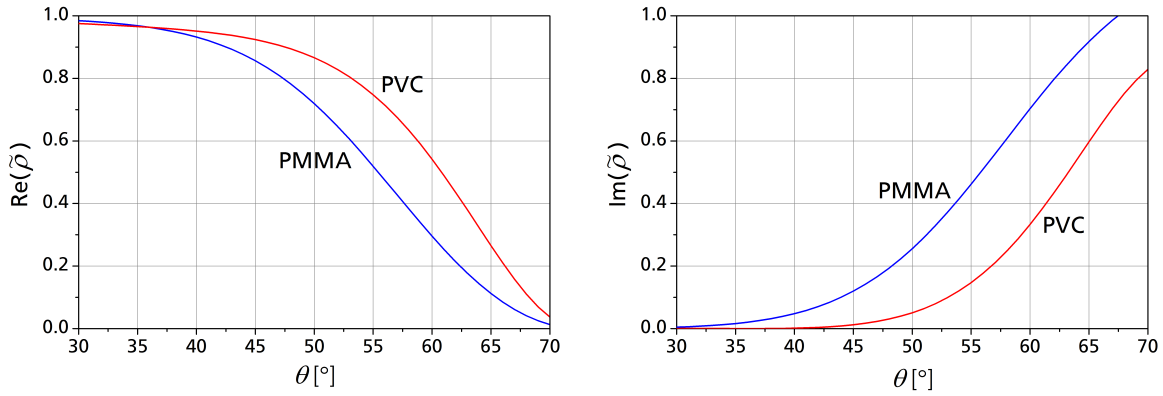

(a) real part (b) imaginary part

Figure 3.5: Influence of the incident angle on the achievable measurement accuracy. In order to clearly distinguish different materials, the incident angle should be as large as possible.

The influence of the incidence angle on the parameter

$$\tilde{\rho} = \frac{\tilde{r}_\mathrm{p}}{\tilde{r}_\mathrm{s}}, \tag{3.4}$$

which represents the ratio of the sample reflectivity for p-polarized radiation and the sample reflectivity for s-polarized radiation (cf. equation 2.20), is shown in Figure 3.5. While the shape of the curves slightly differs between the simulated PVC and polymethyl methacrylate (PMMA) samples, the general behavior is the same. Very steep incident angles up to $\theta = 35°$ result in a real part of $\tilde{\rho}$ close to one and an imaginary part of $\tilde{\rho}$ close to zero. For larger angles, $\mathrm{Re}(\tilde{\rho})$ is significantly decreasing, whereas $\mathrm{Im}(\tilde{\rho})$ is increasing up to angles of about $\theta = 70°$. This is also true for other typical sets of material parameters which are not shown in the graphs. Considering that $\tilde{\rho} = 1$ (that is $\mathrm{Re}(\tilde{\rho}) = 1$ and $\mathrm{Im}(\tilde{\rho}) = 0$) corresponds to a material which does not induce an amplitude shift between p- and s-polarized parts of the reflected electromagnetic field, e.g. a totally reflecting metal surface, it is beneficial to set up the experiment in a way that preferably values of $\mathrm{Re}(\tilde{\rho}) \ll 1$ and $\mathrm{Im}(\tilde{\rho}) \gg 0$ will be measured independently of the sample under investigation. Otherwise, different dielectric materials can not be well separated from each other or even metallic materials. Accordingly, there is a general trade-off between compactness and accuracy of mmW ellipsometry.

In addition, it must be considered, that higher angles of incidence as well as wider antenna patterns (i.e. lower gain) reinforce crosstalk between the antennas, leading to interference effects which falsify the measurement depending on the phase deviation between the line-of-sight path and the intended signal path. The influence of these effects can be determined for the s-polarized and p-polarized parts of the electromagnetic field using the following relation [133]:

$$|C_\mathrm{p,s}|^2 = \frac{G^2(\frac{\pi}{2}-\theta)}{\sin\theta}\left[\frac{G^2(\frac{\pi}{2}-\theta)}{\sin\theta} + 2|\tilde{r}_\mathrm{p,s}|\cos\left(\varphi - \frac{4\pi f R}{c_0}(1-\sin\theta)\right)\right] \tag{3.5}$$

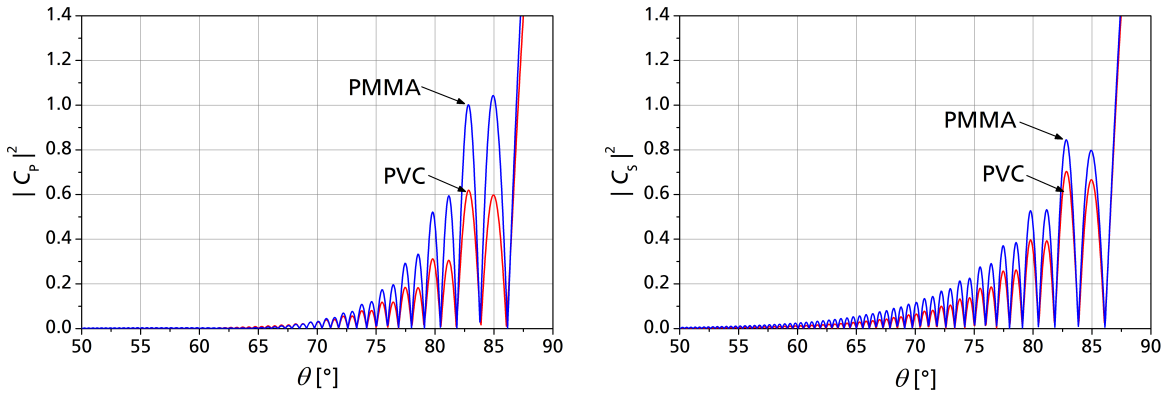

(a) p-polarization (b) s-polarization

Figure 3.6: The of the line-of-sight loss at 94 GHz for p-polarization (a) and s-polarization (b) becomes significant at angles larger than 60°.

where $G(\frac{\pi}{2} - \theta)$ is the gain of the Rx antenna in direction of the Tx antenna, f is the frequency of the signal and

$$\varphi = \frac{2R}{c_0}(\sin\theta - 1) \tag{3.6}$$

is the phase deviation between the line-of-sight and the intended beam path of the signal which is reflected at the sample. Figure 3.6 shows the angular dependence of $|C_p|^2$ and $|C_s|^2$ for 2 mm thick PVC and PMMA samples at a frequency of 94 GHz. In order to reliably exclude line-of-sight effects from the measurements, $|C_p|^2$ and $|C_s|^2$ must be small compared to $|\tilde{r}_p|^2$ and $|\tilde{r}_s|^2$ respectively, that is

$$\frac{|\tilde{r}_p|^2 + |C_p|^2}{|\tilde{r}_s|^2 + |C_s|^2} \approx \frac{|\tilde{r}_p|^2}{|\tilde{r}_s|^2} = |\tilde{\rho}|^2. \tag{3.7}$$

Since $|C_{p,s}|^2$ does not only depend on θ, but also on the frequency and on material parameters, a general statement on the maximum incidence angle which should be used in the setup is not feasible. However, based on further simulations of typical sets of material parameters it can be deduced that by using a setup with an incident angle of 60°, line-of-sight interference can be adequately avoided while $\mathrm{Re}(\tilde{\rho}) \ll 1$ and $\mathrm{Im}(\tilde{\rho}) \gg 0$ are already sufficiently fulfilled at W-band frequencies.

Table 3.1: Setup parameters and recommended operational range of the mmW ellipsometer.

θ [°]	G [dBi]	α [°]	R [mm]
60	20	9	200

f [GHz]	d [mm]	n	$\tan\delta$
75-110	0.5-15	>1.3	> 0.005

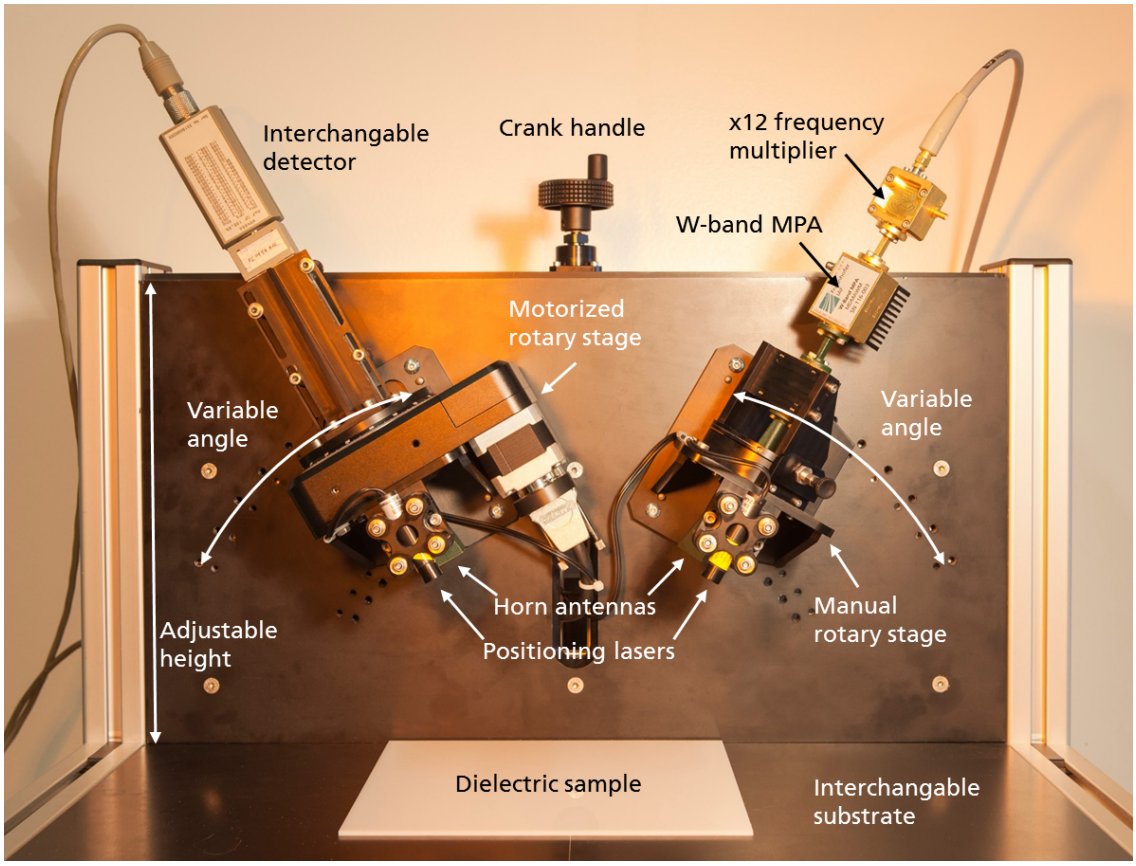

Figure 3.7: Mechanical Construction of the mmW Ellipsometer. The modular design not only allows for variations of the substrate and the incident angle, but also for quick exchange of the signal generation chain and the detector. Furthermore, due to the height-adjustable front panel, samples with a thickness of up to 10 mm can be investigated.

Based on these considerations, the recommended values of the critical setup parameters have been selected for the typical operational range of the mmW ellipsometer that covers the full frequency spectrum of W-band as well as a wide variety of material parameters. These values are summarized in Table 3.1 and define the experimental setup which has been used for all the following measurements if not explicitly stated otherwise.

3.1.4 Mechanical construction

The construction of the final mmW ellipsometer is based on a modular approach in vertical alignment. The setup parameters determined in the previous sections are fully implemented, while it is possible to selectively exchange some of the components, such as the signal generation chain or the power detector, for specific experiments.

Figure 3.7 shows a photograph of the mmW ellipsometer construction. It consists of an interchangeable sample stage that can either be used as a substrate or be replaced by W-band absorbers to investigate a sample surrounded by air as sketched in Figure 2.9. The total dimension of the sample stage is 50 cm $\times$ 32 cm. The actual mmW ellipsometer components are mounted on a front panel which is perpendicular to the sample stage

and can be adjusted in height using a crank handle on top of the construction. The high frequency part of the signal generation chain, consisting of an x12 frequency multiplier, a W-band MPA and the polarizer horn antenna, is mounted to a custom-made, manual rotary stage using hollow waveguides. The rotary stage is, in turn, mounted to the front panel using different threaded holes, such that the angle of incidence can be varied from 30° to 70° in steps if 5°. The Rx antenna and the detector are mounted to a motorized OWIS DRTM-90 rotary stage in order to precisely rotate the analyzer around 360°. The reception angle can be adjusted independently of the incident angle using further threaded holes. In order to keep the distance from the surfaces of samples with different thickness to the polarizer and analyzer antennas constant, the whole front panel can be manually adjusted in height using the crank handle. Two line lasers are mounted to the rotary stages for precise adjustment of the front panel height. In addition, W-band absorbers, which are not shown in Figure 3.7 for the sake of clarity, are used to minimize reflections from the setup components.

The housing of the mmW ellipsometer is based on aluminum profiles and is designed in a way that a phase-locked loop (PLL) based synthesizer board and an HP 437B power meter can be integrated. Thereby, a compact, self-contained system which can be connected to a computer via universal serial bus (USB) can be realized. The total dimension of this compact version of the mmW ellipsometer is $60\,\mathrm{cm} \times 60\,\mathrm{cm} \times 45\,\mathrm{cm}$. However, using this setup implies restrictions from an academic point of view, as illustrated in section 3.1.2, and will therefore not be discussed in more detail in this thesis.

3.2 Millimeter wave ellipsometry on metal substrates

As shown in section 2.3.3, previous microwave ellipsometer measurements suffered from strong deviations in the determined dielectric function, depending on parameters which should not influence the outcome of the measurement that strongly, such as sample thickness or minor variations of the frequency. In this section, the achievable measurement accuracy of microwave ellipsometry is discussed from a fundamental point of view with respect to the critical measurands. Subsequently, it is shown that a novel method, using a strongly reflecting substrate, can significantly enhance the performance of the setup presented in the previous section.

3.2.1 Measurement accuracy and polarization loss

The refractive index of many homogeneous polymers differs only slightly at mmW frequencies and the loss tangent, representing the absorption of millimeter waves, is typically small [12]. Thus, the characterization of these materials in the mmW regime is, in general, challenging. In contrast, another class of materials which is becoming increasingly interesting for mmW applications are composites such as fiber reinforced plastic (FRP). These materials can be very strongly absorbing, depending on their exact composition, so that either high output power or thin samples are required. In order to establish ellipsometry as a reliable material characterization method in the mmW regime, there are several minimum objectives that must be attained. It should not only allow to distinguish

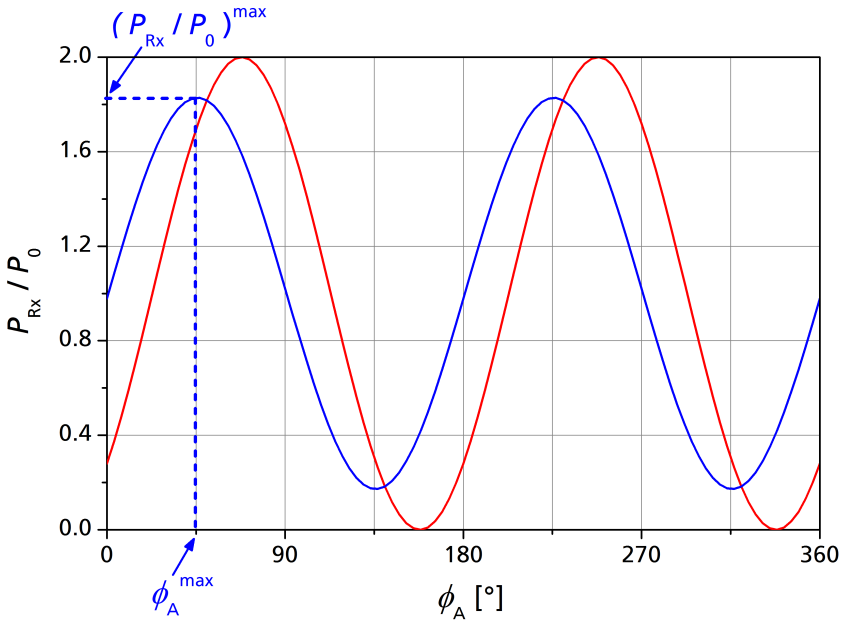

Figure 3.8: Influence of material parameters on two arbitrary simulated ellipsometer curves. The blue curve is compressed around its average value, while the red curve is displaced along the angle axis. In an actual measurement a combination of both effects will most likely be observed. Due to its symmetry, the normalized ellipsometer curve is fully described by the parameters $(P_{Rx}/P_0)^{max}$ and ϕ_A^{max}.

between similar materials, even if their dielectric properties differ only slightly, but also for reliable investigation of strongly absorbing materials. It is shown in section 3.2.3, that these objectives can not be met at frequencies around 100 GHz or higher, if the standard approach is used, that has been proposed by Stetiu et al. [49]. Instead, a novel method with significantly improved measurement accuracy is needed. Therefore, it is useful to first understand how different material parameters influence the actual measurement outcome of mmW ellipsometry.

Figure 3.8 shows two simulated ellipsometer curves. In accordance with equation 2.24, the polarizer antenna is fixed at an angle of 45°. The analyzer antenna is then rotated around 360°, while measuring the received power P_{Rx}. After a full rotation is performed, the measured angular power spectrum is normalized with respect to its average value P_0. Due to the symmetry of the setup, a half rotation of the analyzer is in principle sufficient for further analysis. However, actual measurements typically suffer from slight asymmetries in the setup which can be compensated by performing a full rotation of the Rx antenna. Material parameters such as permittivity and geometry of the sample influence this curve in two different ways. The data can be displaced along the angle axis (red curve in Figure 3.8) or symmetrically compressed with respect to its average value (blue curve in Figure 3.8). In an actual measurement, a combination of both effects will most likely be observed. Since the ellipsometer curve is sinusoidal, the measurement is fully determined by knowledge of the maximum of the normalized amplitude $(P_{Rx}/P_0)^{max}$ and the corresponding analyzer angle ϕ_A^{max}. The achievable measurement accuracy concerning these two parameters is therefore crucial for reliably adopting ellipsometry to the mmW regime. While the detected power can be resolved down to

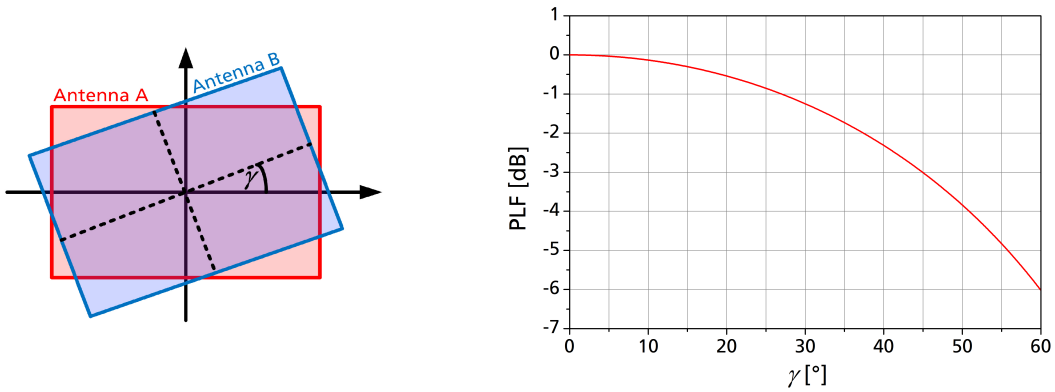

Figure 3.9: Polarization loss of the horn antennas used in the setup. If the Tx antenna A is tilted with an angle γ with respect to the Rx antenna B, the corresponding polarization mismatch leads to a loss of power at the receiver. For small tilting angles, this effects is negligible so that the polarization of a mmW signal can only be measured with an accuracy of up to a few degrees using horn antennas.

nanowatt scales using modern measurement equipment, the polarization at the analyzer antenna can only be assigned to the measured signal with a comparably high uncertainty. Neither does the Tx horn antennas transmit an ideal linearly polarized electromagnetic field, nor is it possible to use the Rx antenna as a perfect polarization filter to analyze the received signal [136]. This becomes particularly apparent by examining the polarization loss factor

$$\mathrm{PLF} = 10 \log_{10} \left[\cos^2 \gamma \right] . \tag{3.8}$$

PLF represents the relative loss of power between an antenna A and an antenna B which are tilted by an angle γ with respect to their polarization plane as shown in Figure 3.9. Even if a perfectly linearly polarized field was transmitted by the polarizer antenna, the loss at the analyzer antenna is negligible while $\gamma < 1\text{-}2°$. Accordingly, there exists a comparably large range of polarization angles which results in indistinguishable Rx power so that the measurement accuracy of the mmW ellipsometer is considerably restricted. Thus, precise measurement of ϕ_A^{max} is much more challenging than precise measurement of $(P_{Rx}/P_0)^{max}$.

3.2.2 Influence of substrates on W-Band ellipsometry

As demonstrated in section 2.3.1, the measured ellipsometer curve, and therefore the parameters $(P_{Rx}/P_0)^{max}$ and ϕ_A^{max}, can be described by the following expression, assuming that the polarizer antenna is fixed at an angle of $\phi_P = 45°$:

$$\frac{P_{Rx}}{P_0} = 1 - \cos(2\phi_A)\cos(2\Psi) + \sin(2\phi_A)\sin(2\Psi)\cos\Delta. \tag{3.9}$$

This curve depends exclusively on the ellipsometer angles Ψ and Δ which in turn are only influenced by the complex reflection coefficients $\tilde{r}_{p,s}$ for p-polarized and s-polarized parts

of the electromagnetic field as the following expressions reveal:

$$\tan\Psi = |\tilde{\rho}| = \frac{|\tilde{r}_\mathrm{p}|}{|\tilde{r}_\mathrm{s}|}, \tag{3.10}$$

$$\Delta = \arg(\tilde{\rho}) = \arg(\tilde{r}_\mathrm{p}) - \arg(\tilde{r}_\mathrm{s}). \tag{3.11}$$

In order to enhance the measurement accuracy of mmW ellipsometry, the influence of important material parameters, such as the refractive index n and the loss tangent $\tan\delta$ on $\tilde{\rho}$ must be investigated in more detail. According to section 2.3.1, the complex refraction coefficients are given by

$$\tilde{r} = \frac{r'_{01} + r'_{12}\mathrm{e}^{\mathrm{j}2\beta}}{1 + r'_{01}r'_{12}\mathrm{e}^{\mathrm{j}2\beta}} \tag{3.12}$$

where

$$\beta = \frac{2\pi f}{c_0} d\sqrt{\tilde{n}^2 - \sin^2\theta} \tag{3.13}$$

is the complex propagation factor through the dielectric material and r'_{01} and r'_{12} are the Fresnel coefficients describing the dependence of the reflection on the corresponding dielectric function [109, 112]. The standard method proposed for microwave ellipsometry makes use of the fact, that the sample under investigation is surrounded by air such that

$$r'_{01} = -r'_{12} = r'. \tag{3.14}$$

In consequence, the only possibility to influence the outcome of the measurement independently of the sample under investigation is to either vary the angle of incidence θ or the frequency f which both will have an impact on β (cf. equation 3.13). The influence of the incident angle on the achievable measurement accuracy has already been discussed in section 3.1.3 and an optimal angle has been determined. Since the frequency dependence of the dielectric function is itself an interesting measurand for many applications, f can not be used for optimization of the measurement accuracy either. Hence, the only possibility to influence the ellipsometer curve or rather $(P_\mathrm{Rx}/P_0)^\mathrm{max}$ and $\phi_\mathrm{A}^\mathrm{max}$ independently of the sample is to use a reflecting substrate for mmW ellipsometry, as shown in Figure 3.7, so that

$$r'_{01} \neq -r'_{12}. \tag{3.15}$$

Thereby, the outcome of the measurement can be specifically adjusted by an adequate choice of r'_{12}.

In principle, two classes of materials can be used as substrates for mmW ellipsometry: Homogeneous dielectrics or metallic materials. The former have the disadvantage, that, in general, their dielectric function is frequency dependent and does not differ much from the dielectric function of the sample. Furthermore, the material parameters of a dielectric substrate must be well known so that the selection of possible substrates is

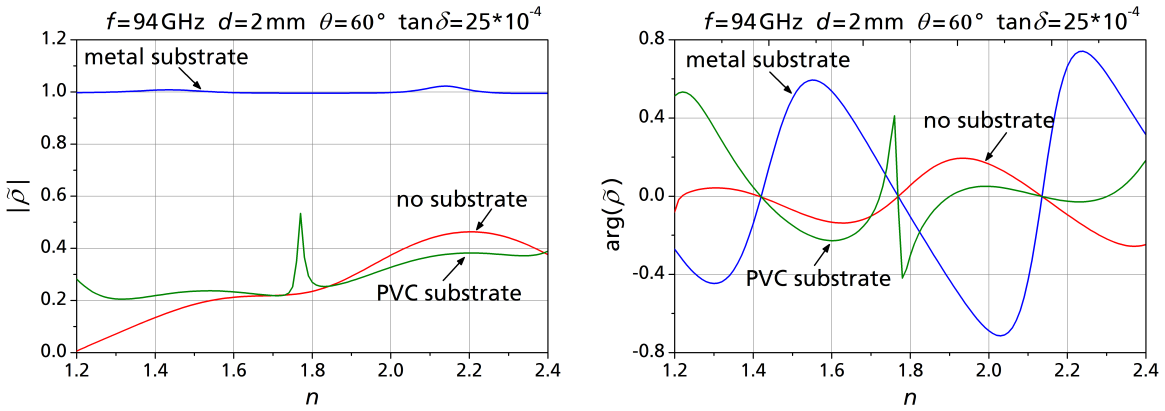

(a) magnitude (b) phase

Figure 3.10: Influence of different substrates on the magnitude and phase of $\tilde{\rho}$. A variation of the refractive index n leads to a nearly constant $|\tilde{\rho}|$ and a strongly varying $\arg(\tilde{\rho})$ if a metal substrate is used and the other material parameters are fixed.

limited. In contrast, metallic materials act as a mirror for mmW radiation. Thus, the reflection at the sample-substrate interface is not frequency dependent, so that dispersive samples can be investigated more reliably. On the other hand, the strong reflection at the metallic substrate dominates the signal and might make the investigation of thin, low loss materials more challenging.

Figure 3.10 shows the influence of a metallic and a dielectric (PVC) substrate on the magnitude and phase of $\tilde{\rho}$, which are directly related to the ellipsometer angles Ψ and Δ (cf. equations 3.10 and 3.11). The response of a 2 mm thick sample with a loss tangent of $\tan\delta = 25 \cdot 10^{-4}$ is simulated at a frequency of $f = 94\,\text{GHz}$ for refractive indices in the range from $n = 1.2$ to $n = 2.4$. This corresponds to the typical parameter range of the low-loss polymers which have been summarized by Lamb et al. [12]. If either no substrate or a dielectric substrate is used, a change in the refractive index influences both magnitude and phase of $\tilde{\rho}$. It should be noted that, in these graphs, a steep slope reflects a strong impact of slight variations of n on the measurands and is therefore desirable. From this point of view, using a PVC substrate is already slightly superior to the standard method. However, the metal substrate shows a remarkably different behavior, that is worth analyzing in more detail. While the $|\tilde{\rho}|$-over-n curve is approximately constant, the $\arg(\tilde{\rho})$-over-n curve exhibits the steepest slopes of all the simulated graphs. In other words, slight variations of n strongly influence one measurand, that is $\arg(\tilde{\rho})$ or Δ, while the other measurand, $|\tilde{\rho}|$ or Ψ, is approximately independent of n. It appears that this corresponds to less information that can be extracted from the measurement, but in contrast, it is the main reason why using a metal substrate is greatly advantageous to the conventional method. This becomes particularly apparent when the same curves are simulated for a sample with fixed refractive index as a function of the loss tangent as shown in Figure 3.11.

Neither of the simulated $\arg(\tilde{\rho})$-over-$\tan\delta$ curves has a significant slope up to a loss tangent of $\tan\delta = 500 \times 10^{-4}$. Accordingly, the ellipsometer angle Δ can not be used to reliably measure the absorption of a dielectric low loss sample. The same also holds for

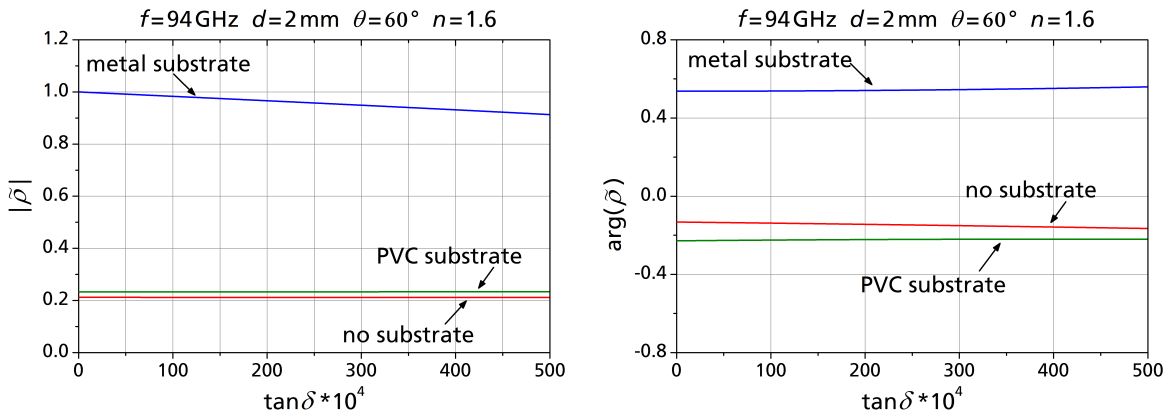

(a) magnitude (b) phase

Figure 3.11: In contrast to the refractive index n, a variation of the loss tangent $\tan\delta$ induces a change in $|\tilde{\rho}|$ while $\arg(\tilde{\rho})$ is kept constant if a metal substrate is used and the other material parameters are fixed. Thus, a metallic substrate can be used to decouple the influence of real and imaginary parts of the dielectric function of a sample on the measurands.

the $|\tilde{\rho}|$-over-$\tan\delta$ curves corresponding to the standard method and the PVC substrate. Neither of those two methods is suitable for investigation of the absorption of low loss polymers in the mmW regime. In contrast, using a metal substrate induces a decreasing $|\tilde{\rho}|$-over-$\tan\delta$ graph. Therefore, sample materials with different strength of absorption lead to a difference in ellipsometer angle Ψ, while Δ is constant.

As a result, using a metallic substrate for mmW ellipsometry decouples the influence of real and imaginary parts of the dielectric function of a sample on the measurands. While the refractive index of a dielectric sample only influences the ellipsometer angle Δ, the absorption of the sample is exclusively reflected in a change of the ellipsometer angle Ψ. In addition, the impact of small variations of n and $\tan\delta$ on the measurands is significantly enhanced compared to the standard method.

3.2.3 Improvement of measurement accuracy

Using a metal substrate for mmW ellipsometry, it can be assumed that for any material with $\tan\delta < 50 \times 10^{-4}$ (cf. Figure 3.11) the magnitude of $\tilde{\rho}$ is approximately constant at

$$|\tilde{\rho}| = \tan\Psi \approx 1 \tag{3.16}$$

and therefore

$$\Psi \approx 45° \tag{3.17}$$

so that equation 3.9 can be simplified to

$$\frac{P_{Rx}}{P_0} \approx 1 + \sin(2\phi_A)\cos\Delta. \tag{3.18}$$

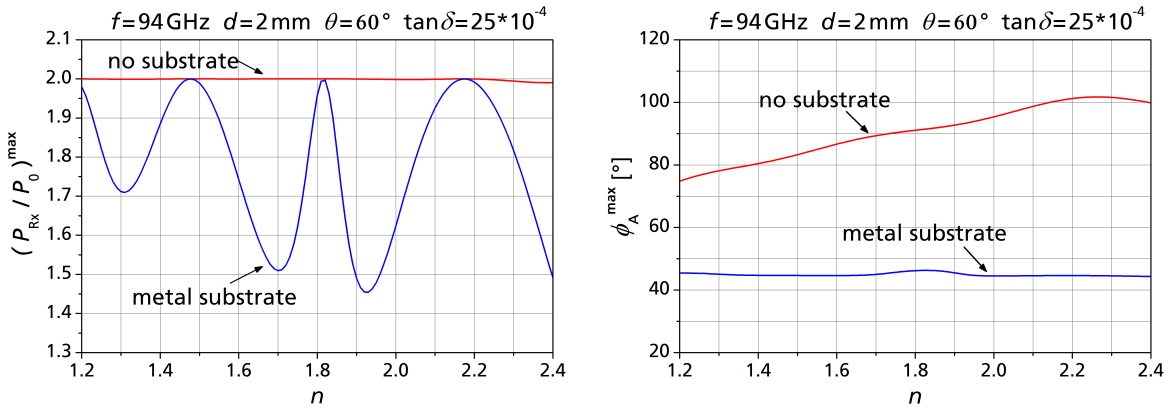

Figure 3.12: Influence of the refractive index n on the normalized maximum power $(P_{Rx}/P_0)^{max}$ (a) and the corresponding analyzer angle ϕ_A^{max} (b). If the sample is surrounded by air, different refractive indices are exclusively reflected in different ϕ_A^{max}. Using a metal substrate, the refractive index mainly influences $(P_{Rx}/P_0)^{max}$.

This equation describes a sinusoidal relationship with a fixed maximum at $\phi_A^{max} = 45°$, which is stretched by a factor $\cos\Delta$ depending on the refractive index n of the sample. Since there is no offset along the angle axis in the ellipsometer curve described by equation 3.18, it is sufficient to measure the maximum power of the ellipsometer curve to determine the refractive index of low loss samples, whose absorption is too weak to be measured using a mmW ellipsometer. If, in contrast, the same sample is surrounded by air, the phase of $\tilde{\rho}$ is small and

$$\cos\Delta \approx 1 \tag{3.19}$$

so that equation 3.9 can be approximated by

$$\frac{P_{Rx}}{P_0} \approx 1 - \cos(2\phi_A)\cos(2\Psi) + \sin(2\phi_A)\sin(2\Psi) = 1 - \cos(2\phi_A - 2\Psi). \tag{3.20}$$

This equation describes a sinusoidal with fixed amplitude that is displaced along the ϕ_A-axis depending on the ellipsometer angle Ψ. In order to determine the refractive index of a sample using this method, the displacement of the curve must be measured. Figure 3.12 shows the dependence of the normalized maximum power $(P_{Rx}/P_0)^{max}$ and the corresponding analyzer angle ϕ_A^{max} on the refractive index n for an arbitrary low loss sample. As expected, $(P_{Rx}/P_0)^{max}$ is constant if no substrate is used, while ϕ_A^{max} depends on n. The metal substrate reverses this behavior. The $(P_{Rx}/P_0)^{max}$-over-n curve is strongly oscillating, whereas the ϕ_A^{max}-over-n curve is approximately constant. In section 3.2.1, it has been shown that $(P_{Rx}/P_0)^{max}$ can be measured much more precisely than ϕ_A^{max} due to the polarization loss of horn antennas. Accordingly, using a metal substrate for mmW ellipsometry not only has the advantage that small variations of the material parameters

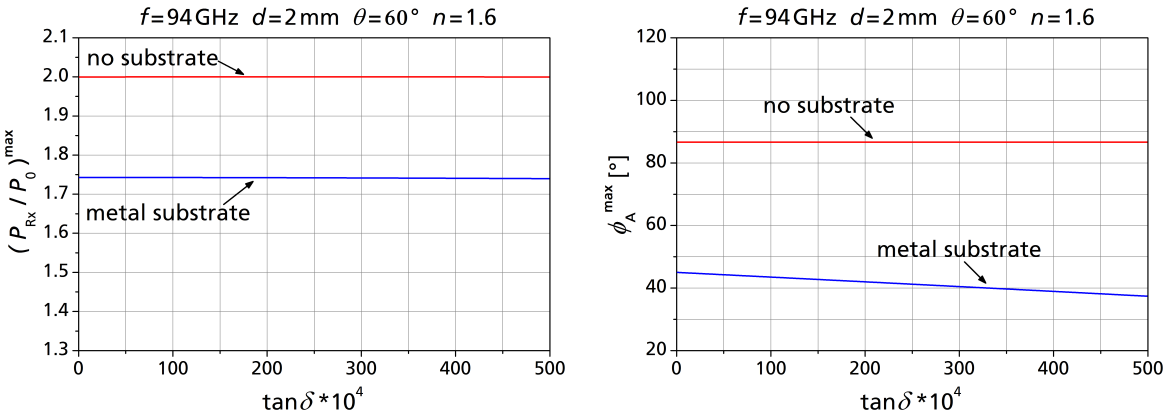

Figure 3.13: Influence of the loss tangent $\tan\delta$ on the normalized maximum power $(P_{Rx}/P_0)^{max}$ (a) and the corresponding analyzer angle ϕ_A^{max} (b). If the sample is surrounded by air, its absorption can not be measured reliably using mmW ellipsometry. In contrast, the $\tan\delta$ of a sample placed on a metal substrate influences ϕ_A^{max}.

influence the measurands more strongly, but also allows for a more accurate measurement of the refractive index of low loss samples.

One of the main drawbacks of the standard approach on microwave ellipsometry is that the loss tangent of the samples is greatly overestimated compared to values that have been published based on other characterization methods (cf. section 2.3.3). Considering the above, the reason for this inaccuracy might be that absorption of a sample only slightly influences the measurands of the ellipsometer. Figure 3.13 shows how $(P_{Rx}/P_0)^{max}$ and ϕ_A^{max} evolve, when the loss tangent of an arbitrary simulated polymer is increased. If the sample is surrounded by air, both curves are constant as long $\tan\delta < 500 \times 10^{-4}$. Further simulations reveal that there is no significant improvement up to $\tan\delta \approx 2500 \times 10^{-4}$, before the slopes of the curves become more significant. Thus, this value can be understood as an approximate lower limit for the loss tangent that can be measured using conventional mmW ellipsometry. However, the absorbance of most plastic and building materials is much lower. In contrast, ϕ_A^{max} decreases with $\tan\delta$, if the sample is placed on a metal substrate. Thus, significant absorption of a dielectric sample, that is $\tan\delta = 50 \times 10^{-4}$, leads to a measurable influence on the ellipsometer curve. Since $(P_{Rx}/P_0)^{max}$ is constant using a metal substrate, the influence of the refractive index and the loss tangent on the measurement is decoupled. By considering this effect for data analysis, measurement accuracy can be increased.

Figure 3.14 shows exemplary mmW ellipsometer measurements of four dielectric samples at a frequency of $f = 94$ GHz and an incidence angle of $\theta = 60°$. If the standard method is used, the curves are barely distinguishable from each other. In contrast, if the samples are placed on a metal substrate, the curves differ in their amplitudes and also slightly in their relative offset. The different materials, as well as the different thicknesses of the samples are clearly distinguishable. By fitting equation 3.9 to this data, the ellipsometer angles and their corresponding uncertainties can be determined for both methods. The results are summarized in Table 3.2, where Ψ_{air} and Δ_{air} correspond to the

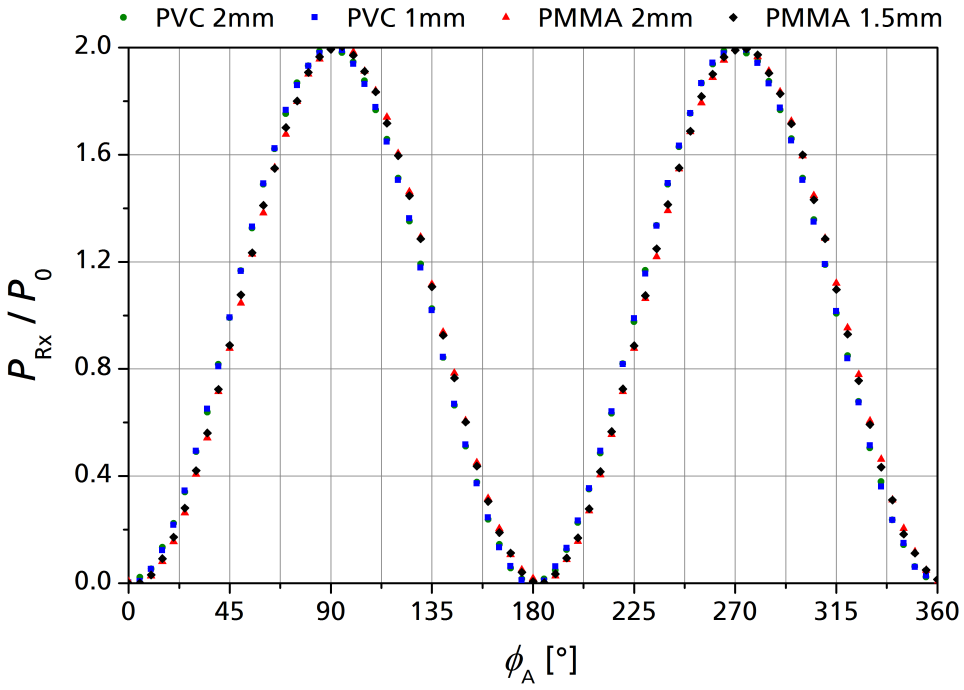

(a) Standard method without substrate

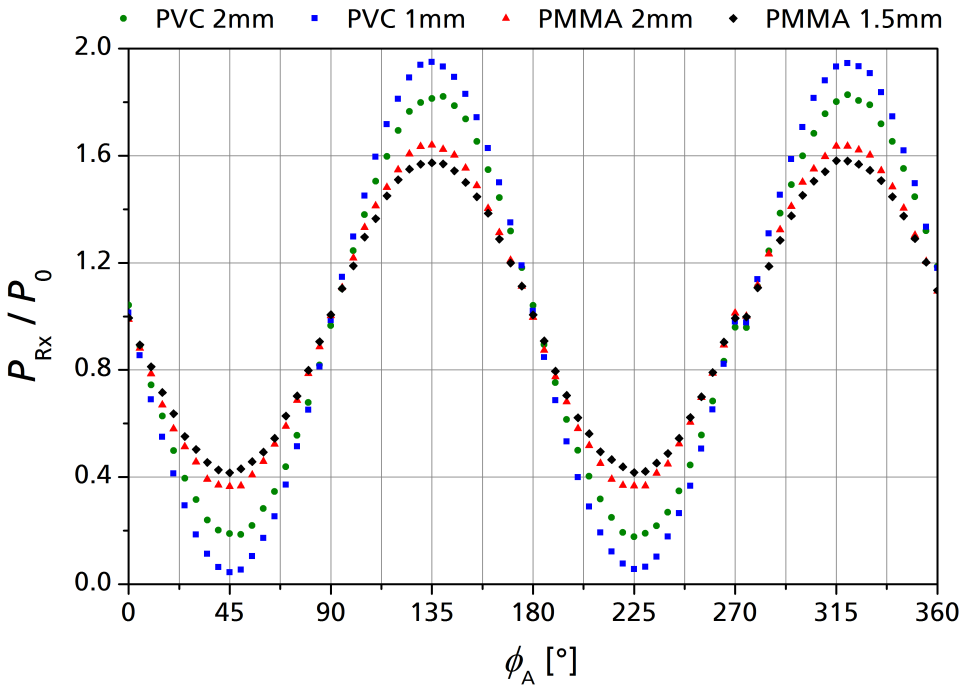

(b) Metal substrate

Figure 3.14: Measured ellipsometer curves of four dielectric samples. Using the standard method, the curves are barely distinguishable from each other. If the samples are placed on a metal substrate, not only the different materials, but also the difference in the sample thickness becomes apparent.

Table 3.2: Ellipsometer angles corresponding to different PMMA and PVC samples, measured at a frequency of 94 GHz. Ψ_{air} and Δ_{air} correspond to the curves in Figure 3.14(a), whereas Ψ_{met} and Δ_{met} correspond to the curves in Figure 3.14(b).

Material	d [mm]	Ψ_{air} [°]	Δ_{air} [°]	Ψ_{met} [°]	Δ_{met}[°]
PMMA	2	86.4 ± 0.8	162.5 ± 11.9	45.1 ± 0.1	57.2 ± 0.2
PMMA	1.5	86.8 ± 0.9	179.6 ± 11.4	45.3 ± 0.1	53.8 ± 0.2
PVC	2	89.3 ± 5.7	179.9 ± 141.0	46.1 ± 0.1	35.3 ± 0.3
PVC	1	87.9 ± 1.5	106.4 ± 12.6	46.2 ± 0.1	16.7 ± 0.1

ellipsometer measurements shown in Figure 3.14(a), and Ψ_{sub} and Δ_{sub} are obtained by fitting the data shown in Figure 3.14(b). The optimization procedure used for this purpose is based on a damped least-squares method [137]. While convergence is generally achieved within a few iterations for all the data sets, the errors on the fitting parameters in Table 3.2 vary significantly. Overall, the uncertainty on Ψ_{air} and particularly Δ_{air} is much higher compared to those of Ψ_{met} and Δ_{met}. This is caused by the fact that the ellipsometer angle Ψ_{air} is close to 90° independently of the sample. The theoretical ellipsometer curve (cf. equation 3.9) basically consists of the two oscillating terms

$$\begin{aligned} T_1 &= \cos(2\phi_A)\cos(2\Psi), \\ T_2 &= \sin(2\phi_A)\sin(2\Psi)\cos\Delta. \end{aligned} \tag{3.21}$$

Since the first-order Taylor series expansion of $\cos x$ at $x = 90°$ is constant, small variations of Ψ_{air} do not have a significant impact on the first term T_1. In addition,

$$\lim_{\Psi \to 90°} T_2 = 0, \tag{3.22}$$

so that the influence of Δ_{air} on the ellipsometer curve becomes negligible as $\Psi_{air} \to 90°$ and the corresponding error on the measurement increases drastically. This is particularly apparent for the 2 mm thick PVC sample. As expected from equations 3.16 and 3.17, Ψ_{met} is always close to 45° so that T_1 is negligible and T_2 approximately only depends on Δ_{met}. In consequence, the ellipsometer angles of the four samples can be clearly distinguished from each other.

In summary, using a metal substrate for mmW ellipsometry has two decisive advantages. The measurands are not only more sensitive to small changes in the materials parameters but also decoupled with respect to different variables. Changes in the refractive index n mainly express themselves in a compression of the ellipsometer curve with respect to its average value, while the absorption of a dielectric sample leads to a measurable offset of the ellipsometer curve along the ϕ_A^{max} axis. Therefore, the corresponding ellipsometer angles can be measured with significantly higher accuracy. However, as already apparent in Figure 3.12, these measurements are, in general, ambiguous so that a single set of ellipsometer angles is not sufficient for reliable material analysis. This will be discussed in more detail in section 3.3.

3.2.4 Parameter limits

Every material characterization technique induces requirements for the samples under investigation with respect to their geometry or dielectric properties. The possible parameter range, where a material can be investigated, is typically limited. Thus, samples have to be carefully chosen to fit within that range in order to obtain optimal results. On the other hand, to establish a novel material characterization method, such as mmW ellipsometry on metal substrates, it is important to particularly investigate the performance of the method for non-ideal cases. Therefore, the selection of samples which are presented in this thesis were chosen in a way to demonstrate cases where solid results are expected, as well as cases which push the method to its limits. In the following, the limits on geometry and dielectric properties of materials which can be used for mmW ellipsometer are determined based on simulations. In chapter 4, it is shown how approaching or exceeding these limits influences actual measurements.

The achievable measurement accuracy of mmW ellipsometry is strongly related to the normalized amplitude of the ellipsometer curve (P_{Rx}/P_0) (c.f. section 3.2.3). It depends on the thickness of the sample d, its refractive index n and its loss tangent $\tan\delta$. For $(P_{\mathrm{Rx}}/P_0)^{\max} \to 2$, different dielectric materials can not be reliably distinguished from each other or even metals anymore so that the measurement accuracy decreases significantly. Therefore, it is important to understand how different material parameters influence the ellipsometer curve, particularly in extreme cases. Figure 3.15(a) shows the influence of the sample thickness d on $(P_{\mathrm{Rx}}/P_0)^{\max}$. The simulated sample has a refractive index of $n = 1.6$, a loss tangent of $\tan\delta = 50 \times 10^{-4}$ and is illuminated under an angle of $\theta = 60°$ at a fixed frequency of $f = 94\,\mathrm{GHz}$. While the curve is oscillating strongly between $(P_{\mathrm{Rx}}/P_0)^{\max} = 2$ and $(P_{\mathrm{Rx}}/P_0)^{\max} \approx 1.5$, its general behavior does not significantly change if the thickness of the sample is increased. This is also true for other parameter combinations corresponding to samples which are not explicitly shown in Figure 3.15. According to the above considerations, there exists an unlimited number of sample thicknesses, where $(P_{\mathrm{Rx}}/P_0)^{\max} \to 2$ so that the method is not reasonably applicable. However, by using a novel, spectroscopic approach, which will be discussed in section 3.3, this limitation can be overcome. The measurement accuracy is then basically limited by the minimal value of $(P_{\mathrm{Rx}}/P_0)^{\max}$ over a specific thickness range. Therefore, the thickness limit for spectroscopic mmW ellipsometer can be characterized by the envelope of the $(P_{\mathrm{Rx}}/P_0)^{\max}$ over d curve, which is shown as dashed line in Figure 3.15(a). Since it is nearly constant up to $d = 15\,\mathrm{mm}$, there is no upper limit for sample thickness within the range which is defined by the mechanical construction of the ellipsometer setup (cf. Table 3.1). According to Figure 3.15(a), the lower limit is $d_{\min} \approx 0.1\,\mathrm{mm}$. However, this simulation does not consider possible errors due to air gaps between a very thin sample and the substrate. In section 4.1, it is shown that this effect is significant and that the minimal thickness for reliable material characterization should rather be $d_{\min} \approx 0.5\,\mathrm{mm}$.

Assuming a circular sample, there exists a minimal diameter $D_{\min}$, below which a substantial amount of the incident radiation hits the area outside of the sample. According to section 3.1.3, the illuminated area on the sample and therefore the minimal sample

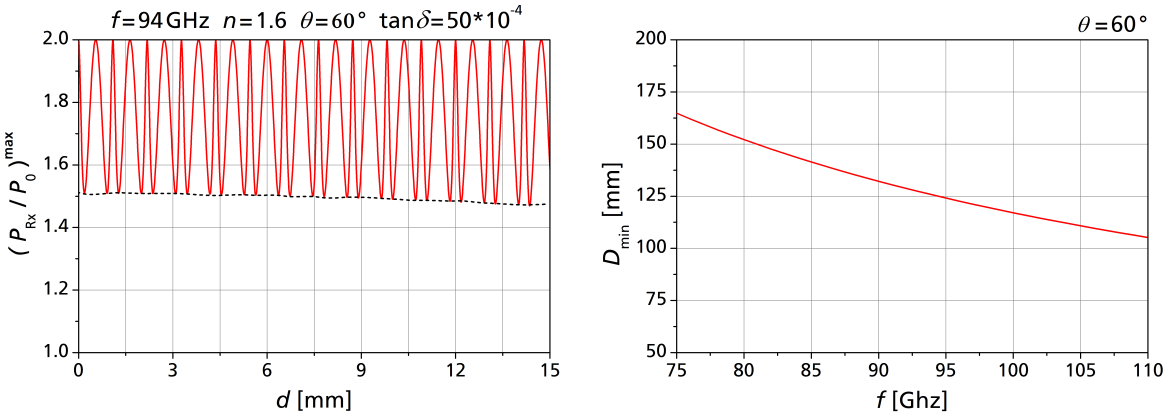

(a) Sample thickness

(b) Minimum sample size

Figure 3.15: Limits of the sample geometries that can be used for mmW ellipsometry. The thickness should be larger than about 0.1 mm but is not fundamentally limited up to 15 mm which is the mechanical limit of the experimental setup. The minimal diameter of the samples depends on the frequency since the beamwidth of the transmitted decreases with the wavelength.

diameter can be determined as follows:

$$D_{\text{min}} = R\left[\frac{\sin(\alpha/2)}{\sin(\frac{\pi}{2}-\frac{\alpha}{2}+\theta)}+\frac{\sin(\alpha/2)}{\sin(\frac{\pi}{2}-\frac{\alpha}{2}-\theta)}\right], \tag{3.23}$$

where R is the distance between the antenna and the sample, θ is the incident angle and α is the aperture angle of the rectangular Tx horn antenna. In general, α depends on the wavelength and the size of the antenna. The 3 dB aperture angle of a rectangular horn antenna can be estimated as

$$\alpha_{3\,\text{dB}} \approx \left(0.886\times\frac{\lambda}{b}\right)\text{rad} = \left(50.8\times\frac{\lambda}{b}\right)^{\circ}, \tag{3.24}$$

where b is the length of the larger side of the rectangle defining the antenna aperture [133]. Previous measurements of the radiation pattern of the 20 dBi antenna used in the mmW ellipsometer verify this approximation [138]. However, half of the radiated power is transmitted into the area outside of this angle. Therefore, an estimation of D_{min} by inserting equation 3.24 into equation 3.23, will most likely lead to unphysical results. A better approach is to use the 10 dB aperture angle instead of $\alpha_{3\,\text{dB}}$. Since the shape of the transmitted signal can be approximated using Gaussian beam theory [93], $\alpha_{10\,\text{dB}}$ can be obtained by transformation from the full width at half maximum (FWHM) to the full width at tenth of maximum (FWTM) of a Gaussian function [139]:

$$\alpha_{10\,\text{dB}} = \sqrt{\frac{\ln 10}{\ln 2}}\times\alpha_{3\,\text{dB}}. \tag{3.25}$$

Figure 3.15(b) shows the frequency dependence of D_{min}, with respect to $\alpha_{10\,\text{dB}}$, between 75 GHz and 110 GHz. As expected, the minimal diameter decreases with the frequency. The shortest dimension of a suitable sample for measurements using the full bandwidth

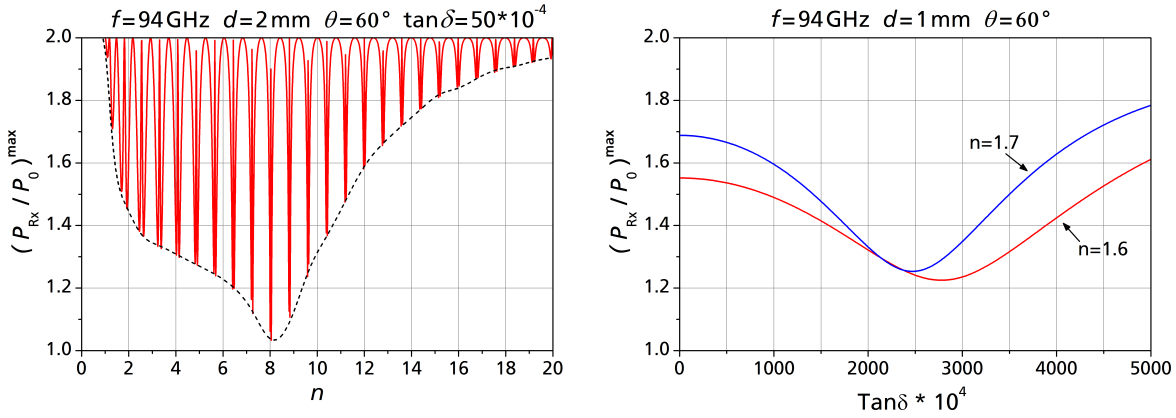

(a) Refractive index (b) Loss tangent

Figure 3.16: Influence of the dielectric function on the measurement accuracy. While the minimum refractive index and loss tangent are about $n = 1.25$ and $\tan\delta = 50 \times 10^{-4}$ respectively, there are, in principal, no relevant upper limits on these parameters.

must not be smaller than 165 mm. The validity of this estimation can be confirmed by comparing the results from measurements of samples with $D > D_{\text{min}}$, $D = D_{\text{min}}$ and $D < D_{\text{min}}$ respectively (cf. section 4.1).

Most of the established mmW material characterization methods provide satisfying results for common, homogeneous plastic materials with refractive indices in the range $n = 1.5$-1.8 [12]. Typically the more challenging cases are non-homogeneous structures such as composites [140, 141] or materials with high refractive indices [142–144] where specialized methods have been developed. While it is not feasible to generally simulate the influence of inhomogeneous materials on mmW ellipsometry, the optimal parameter range of the refractive index can be estimated by investigation of the expected measurement accuracy. Therefore, in analogy to the optimal thickness estimation (cf. Figure 3.15(a)), the influence of n on $(P_{\text{Rx}}/P_0)^{\text{max}}$ must be simulated. The resulting curve for a hypothetical sample with a thickness of $d = 2$ mm and a loss tangent of $\tan\delta = 50 \times 10^{-4}$ is shown in Figure 3.16(a). Again, the envelope of the strongly oscillating curve is sufficient to estimate the possible measurement accuracy if a spectroscopic algorithm is used for data processing. It decreases from $(P_{\text{Rx}}/P_0)^{\text{max}} = 2$ at $n = 1$ to $(P_{\text{Rx}}/P_0)^{\text{max}} \approx 1.05$ at $n = 8$. Accordingly, the possible measurement accuracy is increasing with the refractive index in this range. From $n = 8$ to $n = 20$, $(P_{\text{Rx}}/P_0)^{\text{max}}$ increases again so that the expected measurement accuracy decreases. However, at refractive indices that are much higher than what is typically considered as a high refractive material for millimeter waves such as silicon ($n = 3.2$-3.4) [145, 146], measurement accuracy is still sufficient. While the turning point, in this case at $n = 8$, depends on the other material parameters, the general course of the curve is always similar. In this behavior mmW ellipsometry on metal substrates differs from most other material characterization techniques at mmW frequencies. There is no relevant upper limit for the refractive index of samples that can be used for this methods. In contrast, low refractive samples are the more challenging cases. The simulations shown in Figure 3.16(a) and Figure 3.12(a) suggest that the

Table 3.3: Classes of samples used to demonstrate the performance of mmW ellipsometry on metal substrates

	n	$\tan\delta \times 10^{-4}$	d [mm]	D [mm]
Optimal samples	> 1.5	$100 - 500$	> 1	≥ 175
Challenging samples	$1.3 - 1.5$	$50 - 100$	$0.5 - 1$	$100 - 175$
Unsuitable samples	< 1.3	< 50	< 0.5	< 100

minimum refractive index that still provides adequate measurement accuracy is $n_{\text{min}} \approx 1.25$.

Figure 3.16(b) shows the influence of the loss tangent on the maximum normalized amplitude of the ellipsometer curve. Unlike the sample thickness or the refractive index, the loss tangent does not induce a strongly oscillating curve with steep slopes in the desired parameter range. An increasing loss tangent does not significantly influence $(P_{\text{Rx}}/P_0)^{\text{max}}$ unless the absorption of the sample is adequately strong. The exact value depends on the other material parameters, but further simulations show that a good estimation generally is $\tan\delta \approx 500 \times 10^{-4}$. Higher loss tangents have a significant impact on $(P_{\text{Rx}}/P_0)^{\text{max}}$. In consequence, one of the main advantages of mmW ellipsometry on metal substrates, the decoupling of the measurands Ψ and Δ (cf. section 3.2.3), is lost. This will also induce higher uncertainties on the measurement of the other material parameters. The optimal parameter range for the loss tangent is therefore between $\tan\delta \approx 100 \times 10^{-4}$ and $\tan\delta \approx 500 \times 10^{-4}$. Previous measurements of the loss tangent of FR-4, a composite material that is typically considered as strongly absorbing at mmW frequencies, indicate that high-loss materials should fit within that range [147]. In contrast, the loss tangent of some low-loss materials is smaller than $\tan\delta \approx 50 \times 10^{-4}$, so that these materials can not be reliably characterized with respect to their loss tangent using mmW ellipsometry on metal substrates.

These estimations on the optimal working range and limits of mmW ellipsometry on metal substrates also define the sample selection which is investigated in this thesis. Three classes of samples are used to demonstrate the full potential of this novel method. First, samples that fit well within the optimal working range of the mmW ellipsometer demonstrate the maximum possible measurement accuracy. Secondly, samples that are close to or slightly beyond the estimated limits of the method are used to investigate how much performance is lost if the method is used under non-ideal conditions. Finally, there are samples with parameters well beyond the expected limits which are unsuitable for the presented method. The respective parameter ranges are summarized in Table 3.3. The final selection of samples is presented in section 4.2.

3.3 Spectroscopic approach

Using a metallic substrate on which the dielectric samples are placed solves one of the three crucial issues (cf. section 2.3.3) in the implementation of ellipsometry at mmW

frequencies: The achievable measurement accuracy of the ellipsometer angles Ψ and Δ is significantly improved. The second challenge is to overcome ambiguities in the parameter estimation algorithms. Therefore, two or more independent measurements of the same sample under modified measurement parameters are required. One can either change a sample specific parameter, such as its thickness, or a setup specific parameter, such as the angle of incidence or the frequency, throughout various measurements. Changing the sample in a series of measurements is in general unfavorable and is therefore not considered in this thesis. In section 3.1.3, it has been shown that the range of incident angles that allow for adequate sensitivity of the mmW ellipsometer, while suppressing line-of-sight interference, is limited and not suitable for overcoming ambiguities. Furthermore, variation of the angle of incidence involves mechanical intervention and therefore slows down the measurements. In contrast, sweeping the frequency is not only time-efficient but also favorable from another point of view. Using modern fractional-n PLL synthesizers, the frequency resolution of a mmW ellipsometer is, in principle, not limited for most practical applications, so that even weak dispersion effects can be measured in narrow frequency bands. This is particularly beneficial and allows, for instance, to investigate the influence of dispersive materials on quasi-optical elements [148].

In this section, it is demonstrated that a spectroscopic algorithm not only allows for unambiguous results in mmW ellipsometry, but also further improves the performance of the method with respect to measurement accuracy. In addition, dispersive samples can be investigated over a wide frequency range and in more detail than it is possible with conventional free-space methods.

3.3.1 Ambiguities in millimeter wave ellipsometry

According to section 2.3.1, the ellipsometer angles Ψ and Δ are related to the material parameters of the sample under investigation by the complex ratio $\tilde{\rho}$. Using equations 2.19 and 2.20, it can be shown that for a sample placed on a metallic substrate $\tilde{\rho}$ is given by

$$\tilde{\rho} = \tan\Psi \cdot \exp[\mathrm{j}\Delta] = \frac{r_\mathrm{p}' - r_\mathrm{p}' r_\mathrm{s}' \exp[-\mathrm{j}2\beta] - \exp[-\mathrm{j}2\beta] + r_\mathrm{s}' \exp[-\mathrm{j}2\beta]^2}{r_\mathrm{s}' - r_\mathrm{p}' r_\mathrm{s}' \exp[-\mathrm{j}2\beta] - \exp[-\mathrm{j}2\beta] + r_\mathrm{p}' \exp[-\mathrm{j}2\beta]^2}. \tag{3.26}$$

Equation 3.26 describes a complex, periodic function depending on the material parameters n, $\tan\delta$ and d. Thus, there exists an infinite number of equivalent sets of material parameters $(n', \tan\delta', d')$ such that the right-hand side of equation 3.26 remains unchanged and

$$\tilde{\rho}(n', \tan\delta', d') = \tilde{\rho}(n, \tan\delta, d). \tag{3.27}$$

In consequence, one set of ellipsometer angles (Ψ, Δ) corresponds to an infinite number of material parameters. Most of these parameter combinations are unphysical and can be identified and ignored using appropriate algorithms. Nevertheless, without prior knowledge on the sample under investigation, a single-frequency mmW ellipsometer measurement does not lead to unambiguous results.

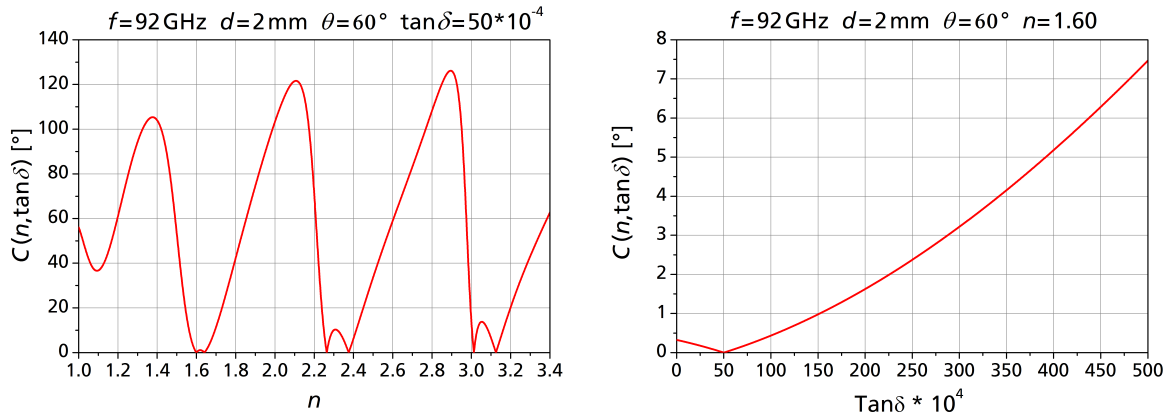

(a) Refractive index (b) Loss tangent

Figure 3.17: Ambiguities in mmW ellipsometry. There exist multiple values for the refractive index that result in the same ellipsometer angles Ψ and Δ. In contrast, the value of the loss tangent is unambiguous.

Assuming a sample with refractive index $n = 1.6$, loss tangent $\tan\delta = 50 \cdot 10^{-4}$ and thickness $d = 2\,\text{mm}$, the corresponding ellipsometer angles at a frequency of 92 GHz and an incident angle of $\theta = 60°$ can be determined using equations 3.26, 2.17 and 2.18:

$$\Psi_0 = 45.27°, \qquad \Delta_0 = 56.22°. \tag{3.28}$$

These values can be used to find the equivalent material parameters n_i' and $\tan\delta_i'$ that lead to identical measurement results. Therefore, the comparison function $C(n, \tan\delta)$ is defined as:

$$C(n, \tan\delta) = |\Psi(n, \tan\delta) - \Psi_0| + |\Delta(n, \tan\delta) - \Delta_0|\,, \tag{3.29}$$

If the material parameters are equivalent so that $(\Psi, \Delta) = (\Psi_0, \Delta_0)$, the comparison function yields zero, i.e. $C(n_i', \tan\delta_i') = 0$. In any other case, the function is positive. Figure 3.17(a) shows the dependence of $C(n, \tan\delta)$ on the refractive index from $n = 1$ to $n = 3.5$ while the other parameters are kept constant. Apart from $n = 1.6$, the real refractive index of the hypothetical sample, the function has zeros at

$$n_1' = 1.65, \qquad n_2' = 2.27, \qquad n_3' = 2.39, \qquad n_4' = 3.01, \qquad n_5' = 3.13. \tag{3.30}$$

In particular, the value of n_1' is very close to the real refractive of the sample. Even if the expected parameter range can be restricted due to basic knowledge of similar materials, it is most likely not feasible to unequivocally identify the real value of the refractive index of the sample. In contrast, the corresponding curve for varying the loss tangent only has a single zero at the real value of $\tan\delta = 50 \times 10^{-4}$, as shown in Figure 3.17(b). Accordingly, the mmW ellipsometer measurement of the loss tangent is unambiguous at fixed frequencies. However, the average slope of the curve depending on $\tan\delta$ is much flatter than the curve depending on n. Therefore, small variations of the loss tangent

only induce a small deviation of the ellipsometer angles with respect to Ψ_0 and Δ_0. Consequently, the expected measurement accuracy is insufficient.

In summary, single-frequency mmW ellipsometer measurements of the refractive index are comparably precise but ambiguous, while measurements of the loss tangent are unambiguous but measurement accuracy is limited, even if a metallic substrate is used.

3.3.2 Algorithm improvement

Millimeter wave ellipsometry can be further improved by combining its major strength with proven concepts of established free-space methods for material characterization in the mmW regime. At fixed frequencies, ellipsometry is in principle superior to methods based on evaluation of S-parameters since it allows to measure an additional physical quantity, the polarization of the electromagnetic signal. On the other hand, it is inferior to classical microwave reflectometry, that takes advantage of effects that are sensitive to small changes in material parameters such as Fabry-Perot interference [149]. As demonstrated in section 3.1, the experimental setup allows for measurements over a wide range of frequencies between 75 and 110 GHz. Therefore, it is possible to not only measure the classical ellipsometer parameters but also interference effects caused by the sample. By using a spectroscopic algorithm for data analysis, ambiguities of the refractive index can be eliminated and the measurement accuracy concerning the loss tangent can be increased.

Figure 3.18 shows the evolution of the normalized maximum amplitudes $(P_{\mathrm{Rx}}/P_0)^{\max}$ of a mmW ellipsometer measurement of a 2 mm thick PMMA sample over the frequency range from 80 to 105 GHz. The measured data is clearly superimposed by Fabry-Perot interference (cf. also Figure 2.6). In addition to the measurement, theoretical models based on equations 3.26 and 2.24 are shown for the refractive indices

$$n_1 = 1.60, \qquad n_2 = 1.65, \qquad n_3 = 2.27, \qquad n_4 = 2.39. \tag{3.31}$$

All of the four curves describe the data point at 92 GHz equally well. A single-frequency analysis of this data point will therefore lead to ambiguous results. However, Fabry-Perot interference induces an individual and unequivocal power spectrum for each of the four possible refractive indices. By evaluation of the additional data, measured over the full frequency range, the real refractive index of the PMMA sample can be unequivocally identified to be close to $n = 1.6$.

In section 3.2.3 it has been shown that, at fixed frequencies, the refractive index of a dielectric material mainly influences the maximum power of the reflected signal, while the loss tangent mainly influences its polarization. Depending on the frequency, the influence of the loss tangent on the polarization is hardly measurable using rotatable horn antennas (cf. Figure 3.17(b)). However, the change of the polarization state caused by the dielectric is frequency dependent. This allows a spectroscopic analysis of the polarizer angle corresponding to the maximum of the ellipsometer curve $\phi_{\mathrm{A}}^{\max}$ in addition to the $(P_{\mathrm{Rx}}/P_0)^{\max}$ over f curve.

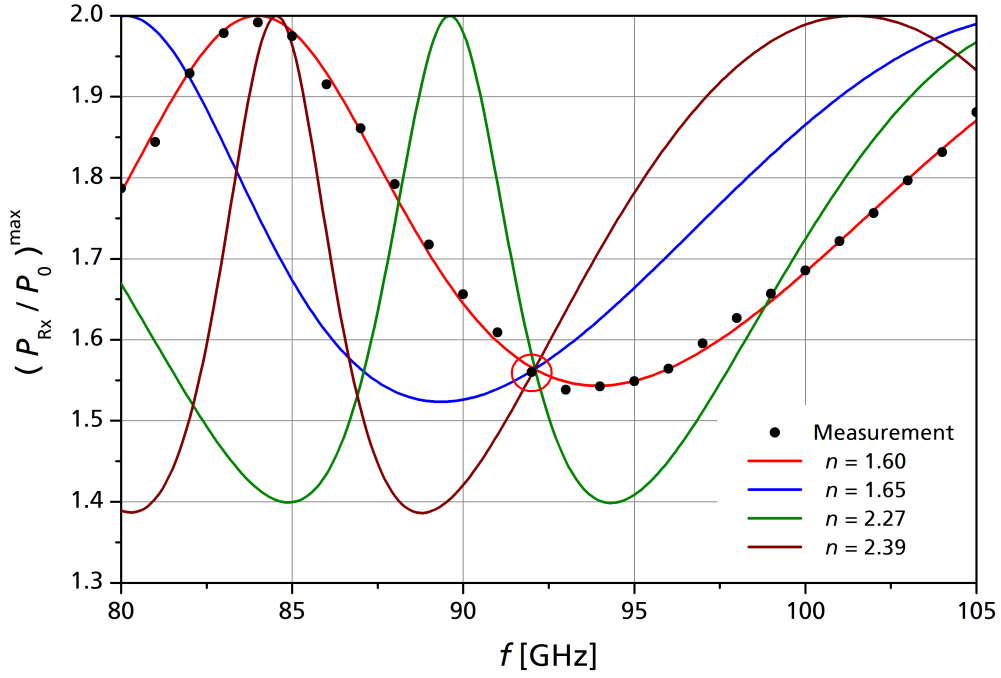

Figure 3.18: Measurement of the maximum reflected power of a 2 mm thick PMMA sample and corresponding simulated curves based on different refractive indices. The data point at $f = 92\,\mathrm{GHz}$ is described equally well by any of the models, while a full spectrum analysis clearly identifies the real value of the refractive index.

Figure 3.19(a) shows a simulation of the maximum normalized power and the corresponding analyzer angle of three different 2 mm thick samples over a frequency range between 80 and 105 GHz. The dielectric properties of these hypothetical samples are only slightly different. The $(P_{\mathrm{Rx}}/P_0)^{\mathrm{max}}$ over f curves corresponding to materials with $\tan\delta = 50 \times 10^{-4}$ and $\tan\delta = 100 \times 10^{-4}$ are virtually indistinguishable. In contrast, a variation in the refractive index from $n = 1.60$ to $n = 1.61$ results in a unique power spectrum. Accordingly, from analysis of a measured $(P_{\mathrm{Rx}}/P_0)^{\mathrm{max}}$ over f curve, only the refractive index can be precisely determined.

The analyzer angle spectra shown in Figure 3.19(b) indicate that spectroscopic analysis of the polarization of the reflected signal is a promising approach to enhance the measurement accuracy concerning the loss tangent. A variation from $\tan\delta = 50 \times 10^{-4}$ to $\tan\delta = 100 \times 10^{-4}$ has a significant influence on the simulated curve, while a deviation of $\Delta n = 0.1$ in the refractive index is visible but can most likely not be resolved using the rectangular horn antennas of the mmW ellipsometer . Accordingly, the decoupling of the measurands, which is caused by the metallic substrate (cf. section 3.2.3), remains valid even if mmW ellipsometry is combined with spectroscopy. The evaluation of the refractive index is not significantly influenced by a strong frequency dependence in the loss tangent and vice versa. Consequently, this method allows for more detailed dispersion measurements than conventional free-space material characterization methods at mmW frequencies. In addition, the refractive behavior and absorption of a material can

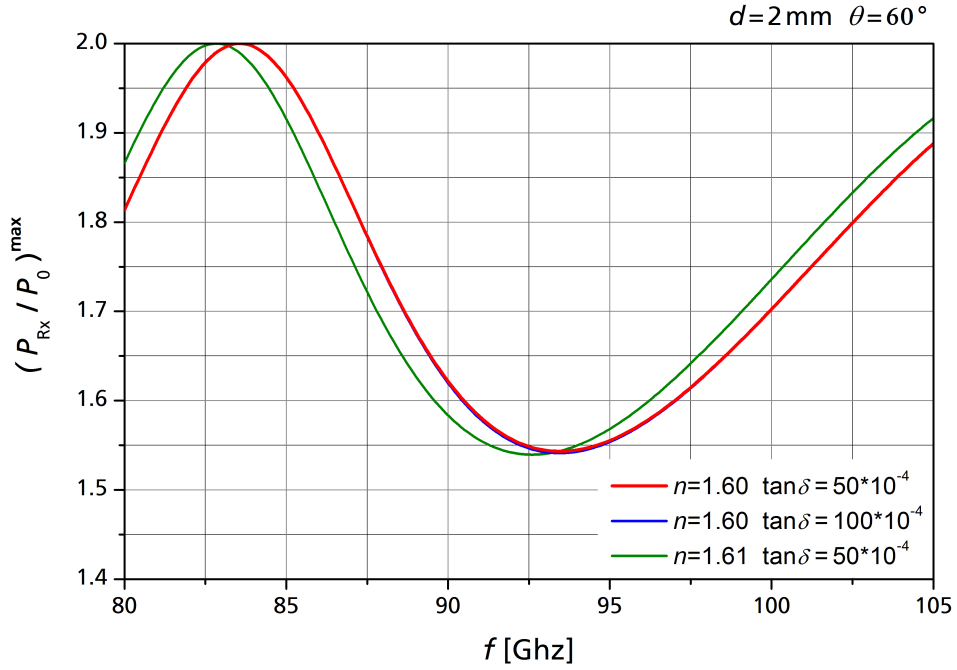

(a) Normalized maximum power

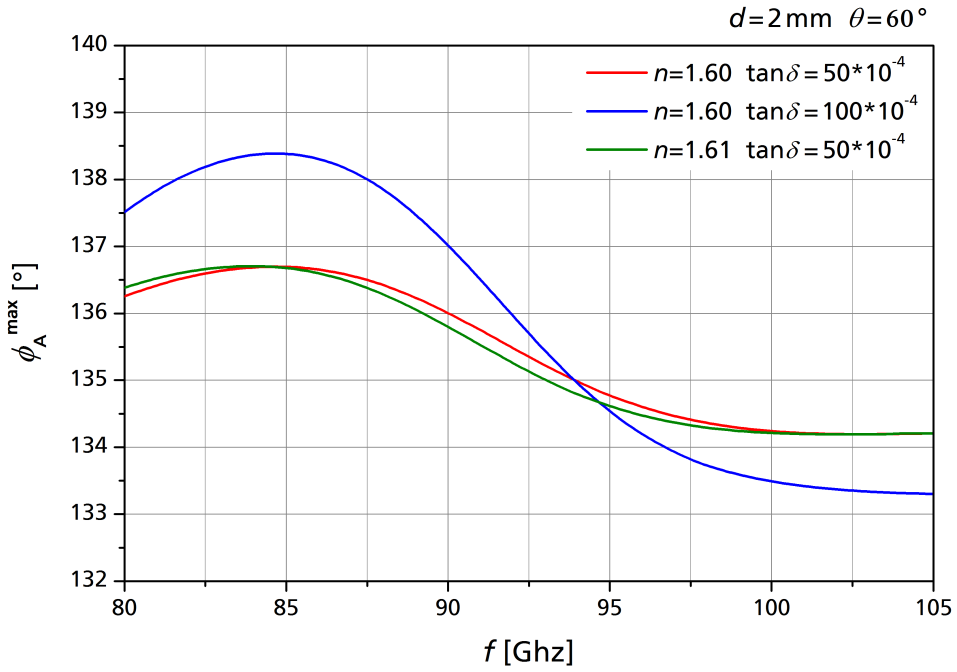

(b) Corresponding analyzer angle

Figure 3.19: A slight variation of the loss tangent leads to virtually indistinguishable $(P_{Rx}/P_0)^{max}$ over f curves, while a slight variation of the refractive index is measurable. In contrast, the ϕ_A^{max} over f curve can only be significantly influenced by a difference in the loss tangent of a sample.

be independently estimated by qualitative analysis of the $(P_{Rx}/P_0)^{max}$ over f and the ϕ_A^{max} over f curves without complex data processing.

In conclusion, the following procedure for material characterization using mmW ellipsometry on metal substrates is proposed. First, the ellipsometer curves of a sample are measured over a wide range of frequencies in order to plot the $(P_{Rx}/P_0)^{max}$ over f and ϕ_A^{max} over f curves. Subsequently, a model is used to fit the data in each case by optimizing the material parameters n and $\tan\delta$ respectively. If the refractive index and the loss tangent are not dispersive over the relevant frequency range, this step will most likely already result in a good first estimation. This method makes use of Fabry-Perot interference and is commonly used in microwave and millimeter wave reflectometry. However, in general, dielectric samples are dispersive over a bandwidth of several GHz, particularly if the materials are inhomogeneous or consist of several different layers. In this case, the optimized parameter set, obtained from the reflectometric analysis, is used as starting point for the ellipsometric analysis. The ellipsometer angles Ψ and Δ are separately determined at each frequency of the measurement as described in section 2.3.2. Sensible boundary conditions on the model parameters, based on the information obtained from the spectroscopic analysis, are used to eliminate ambiguities. Furthermore, comparison of the material parameters, that are evaluated at each frequency, to the spectroscopic result identify statistical errors in the measurement. Thereby, the dispersion curve of a dielectric sample can be measured in great detail over a desired frequency range using mmW ellipsometry.

3.3.3 Characterization of dispersive materials

Detailed characterization of dispersive materials is one of the major challenges in modern microwave and millimeter wave material parameter measurements. A wide bandwidth as well as high frequency resolution are required to resolve the dispersion of common dielectrics, such as homogeneous plastics or laminated building materials at mmW frequencies. From evaluation of dipolar relaxation models (cf. section 2.2), it can be expected that, for instance, the refractive index of a typical homogeneous dielectric will not vary by more than 1 % to 2 % over the full W-band. Therefore, measurement precision is a critical factor and statistical as well as system related error sources must be minimized for reliable dispersion measurements. The achievable measurement accuracy of classical S-parameter methods is typically insufficient, since it depends strongly on the calibration of the setup which is difficult for free-space measurements (cf. section 2.2.4). Thus, dispersion effects are usually not measured directly in mmW bands. Instead, the frequency dependence of the dielectric function is parameterized using a material model (cf. equation 2.4) that is fitted to the measured data. However, the convergence rate of these algorithm is insufficient if the complexity of the material model increases. Therefore, dispersion of inhomogeneous or layered materials can not be reliably investigated using conventional free-space methods at mmW frequencies. These materials are particularly interesting for many industrial application, since they provide significantly enhanced stability at moderate weight. Accordingly, there is an increasing demand for improved material characterization, that can be used for investigation of dispersive, non-homogeneous dielectrics. As shown in the previous sections, the achievable

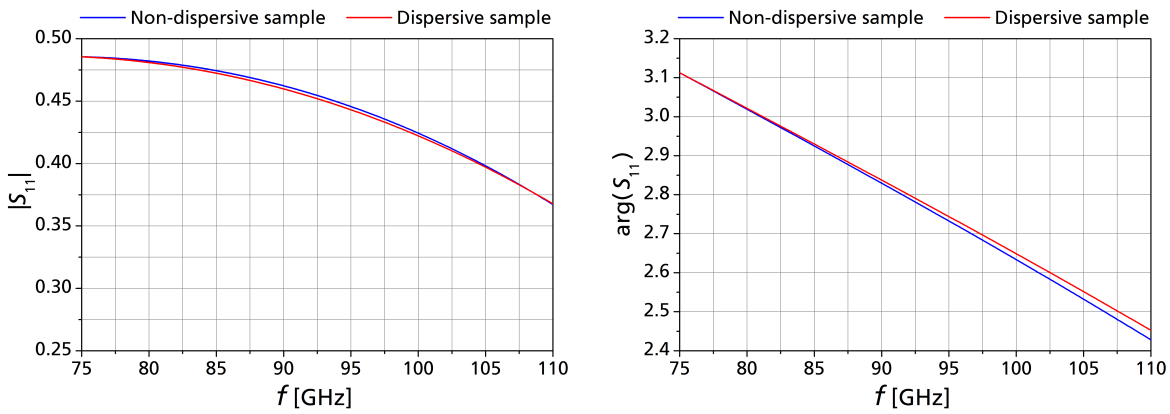

(a) Conventional S-parameter evaluation

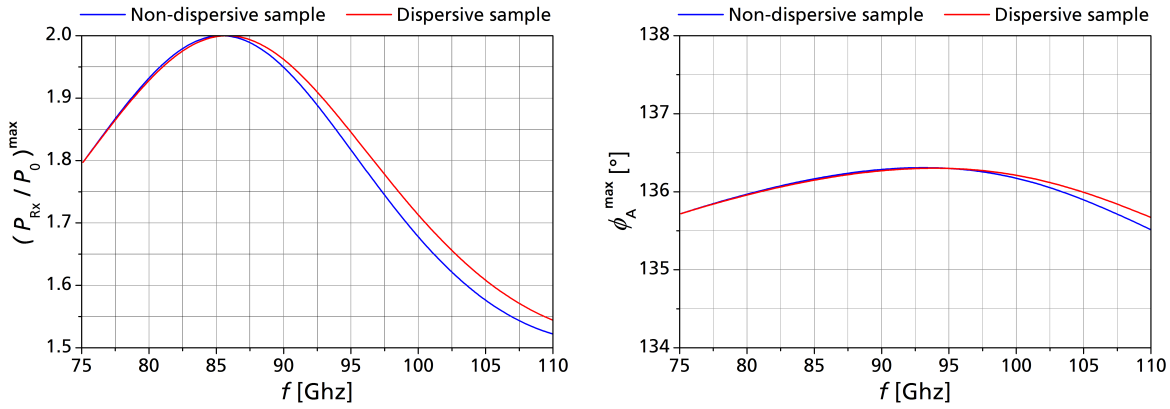

(b) mmW ellipsometry

Figure 3.20: Comparison of a weakly dispersive and a non-dispersive thin low-loss sample used for mmW material characterization. A conventional S-parameter evaluation results in a negligible deviation of the measurands while the difference between the samples is more clearly visible using mmW ellipsometry.

measurement accuracy of mmW ellipsometry is significantly enhanced if a metallic substrate is used. In addition, there is no need for calibration, and frequency resolution for spectroscopic measurements is virtually not limited, so that even weak dispersion effects are, in theory, detectable using spectroscopic mmW ellipsometry on metal substrates.

Figure 3.20(a) shows a simulation of the influence of a thin and weakly dispersive sample on a classical reflection S-parameter measurement. The absolute value and the argument of the complex scattering parameter S_{11} are plotted vs. the frequency for a dispersive and a non-dispersive sample. It is assumed that the refractive index of the dispersive material decreases linearly from $n = 1.70$ to $n = 1.68$, while the loss tangent is constant at $\tan\delta = 50 \times 10^{-4}$. The thickness of the sample is $d = 600\,\mu\text{m}$ and the angle of incidence is $\theta = 60°$. Accordingly, this thin and dispersive low-loss sample represents a very challenging case for material characterization at mmW frequencies. In comparison to a similar sample with constant refractive index at $n = 1.70$, the variation in both $|S_{11}|$ and $\arg(S_{11})$ is negligible with respect to expected measurement accuracy. Thus, the

frequency dependence of the refractive index of the dispersive sample is most likely not detectable using classical free-space methods.

If a mmW ellipsometer is used to investigate the two samples, there is a more significant deviation in the corresponding measurement curves as shown in Figure 3.20(b). The difference in the maximum angle $\phi_{\mathrm{A}}^{\max}$ can not be resolved due to the polarization loss of the horn antennas (cf. section 3.2.1). However, in chapter 4 it is shown that the deviation of the $(P_{\mathrm{Rx}}/P_0)^{\max}$ over f curves is just about measurable considering the achievable measurement accuracy of the presented setup. Accordingly, the sample thickness of $d = 600\,\mu\mathrm{m}$ represents a limit case for investigation of weakly dispersive materials where the refractive index does not change by more than $\delta n = 0.0005/\mathrm{GHz}$. This limit is already beyond the capabilities of conventional mmW material characterization. In consequence, mmW ellipsometry is superior for investigation of thin dispersive materials. If the sample thickness or the amount of dispersion δn is increased, the difference between dispersive and non-dispersive samples becomes more distinct in the ellipsometer curves as well as in the S-parameter measurements.

3.4 The two-point approximation method

In the previous sections, it has been shown that measurement accuracy of mmW ellipsometry can be significantly enhanced by using a metal substrate. In addition, using a spectroscopic approach, ambiguities can be avoided and dispersive samples can be characterized more detailedly compared to S-parameter measurements. However, reflection ellipsometry involves mechanical rotation of the analyzer around at least 180° and is therefore disadvantageous with respect to the achievable measurement speed. In fact, it is advantageous to perform a full rotation of the analyzer antenna around 360° in order to average possible asymmetries in the setup. Using a metal substrate for mmW ellipsometry results in an additional significant improvement of the method if the sample under investigation consists of a low-loss material. Due to the decoupling of the influence of real and imaginary parts of the dielectric function on the ellipsometer angles Ψ and Δ, it is sufficient to measure the maximum and minimum power instead of the full ellipsometer curve. Therefore, mechanical movement of the antennas can be reduced in order to enhance measurement speed.

In this section, an approximation method based on the symmetry of the ellipsometer curve is presented. The theoretical formalism is derived in order to discuss the algorithm and its performance as well as the limits of the approximation.

3.4.1 Theory

The field confinement and absorption of most of the common plastic and building materials ($n < 2$ and $\tan\delta < 0.01$) is fairly low in the mmW regime so that only a small amount of energy is left in the material. Using a metal substrate for these materials enhances field confinement and therefore reinforces the influence of the material properties on the measurement. It can be assumed that the reflection at the metal interface is very strong

compared to the reflection at the material under investigation. Therefore, the relative amplitude shift between p- and s-polarized radiation caused by the material is small since the overall signal is dominated by the metal reflection. In this case, equation 2.21 yields

$$\tan\Psi = \left|\frac{\tilde{r}_\mathrm{p}}{\tilde{r}_\mathrm{s}}\right| \approx 1 \quad \Rightarrow \quad \Psi \approx \frac{\pi}{4}. \tag{3.32}$$

Using this approximation, equation 2.23 can be simplified so that the power at the receiver is given by

$$P_\mathrm{Rx} = P_0[1 + \cos(2\phi_\mathrm{P})\cos(2\phi_\mathrm{A}) + \sin(2\phi_\mathrm{P})\cos(\Delta)\sin(2\phi_\mathrm{A})]. \tag{3.33}$$

Due to symmetry, the maxima and minima of the ellipsometer curve are always separated by $\Delta\phi_\mathrm{A} = \pm\frac{\pi}{2}$. The corresponding analyzer power at the extrema depend on the polarizer angle ϕ_P and the analyzer angle at the maximum $\phi_\mathrm{A}^\mathrm{max}$ and minimum $\phi_\mathrm{A}^\mathrm{min}$:

$$P_\mathrm{Rx}^\mathrm{max} = P_0[1 + \cos(2\phi_\mathrm{P})\cos(2\phi_\mathrm{A}^\mathrm{max}) + \sin(2\phi_\mathrm{P})\cos(\Delta)\sin(2\phi_\mathrm{A}^\mathrm{max})], \tag{3.34}$$

$$P_\mathrm{Rx}^\mathrm{min} = P_0[1 + \cos(2\phi_\mathrm{P})\cos(2\phi_\mathrm{A}^\mathrm{min}) - \sin(2\phi_\mathrm{P})\cos(\Delta)\sin(2\phi_\mathrm{A}^\mathrm{min})]. \tag{3.35}$$

If the values of $\phi_\mathrm{A}^\mathrm{max}$ and $\phi_\mathrm{A}^\mathrm{min}$ are known prior to the measurement, $P_\mathrm{Rx}^\mathrm{max}$ and $P_\mathrm{Rx}^\mathrm{min}$ can be measured directly without a full rotation of the analyzer. Thereby, measurement time can be significantly reduced since only two data points need to be measured instead of the full ellipsometer curve. Superposition of equations 3.34 and 3.35 yields the following relation:

$$P_\mathrm{Rx}^\mathrm{max} + P_\mathrm{Rx}^\mathrm{min} = 2P_0[1 + \cos(2\phi_\mathrm{P})\cos(2\phi_\mathrm{A}^\mathrm{max})]. \tag{3.36}$$

Since the ellipsometer curve is symmetric with respect to P_0, equation 3.36 implies that

$$\cos(2\phi_\mathrm{P})\cos(2\phi_\mathrm{A}^\mathrm{max}) = 0 \tag{3.37}$$

for all polarizer angles ϕ_P. Consequently, the analyzer angles corresponding to the maximum and minimum power of the ellipsometer curve corresponding to a low-loss sample, which fulfills equation 3.32, are constant at

$$\phi_\mathrm{A}^\mathrm{max} = \frac{\pi}{4} \quad , \quad \phi_\mathrm{A}^\mathrm{min} = \frac{3\pi}{4}. \tag{3.38}$$

By fixing the polarizer angle at $\phi_\mathrm{P} = +\frac{\pi}{4}$, the ellipsometer angle Δ can be determined analytically:

$$\cos(\Delta) = \frac{2P_\mathrm{Rx}^\mathrm{max}}{P_\mathrm{Rx}^\mathrm{max} + P_\mathrm{Rx}^\mathrm{min}} - 1. \tag{3.39}$$

Since the ellipsometer angle Ψ is approximately constant so that $\tan\Psi \approx 1$, the material parameters of a low-loss sample can be determined from a measurement of the reflected power at only two analyzer angles, which are known in advance. Accordingly,

the measurement speed of mmW ellipsometry, which is essentially limited by the mechanical rotation of the Rx horn antenna, can be significantly improved using this method. However, it is important to estimate the validity and limits of the approximation in order to select appropriate samples.

3.4.2 Algorithm and performance

As shown in section 3.3.2, a key part of the algorithm, which is used to determine the material parameters from mmW ellipsometer measurements, is the evaluation of the $(P_{\mathrm{Rx}}/P_0)^{\max}$ over f curve. Thereby, a first estimation on the thickness, the dielectric function and the strength of dispersion of a material is obtained. This is an important step since it is crucial to specify sensible starting points and boundaries for the optimization procedure that is used for the material parameter estimation. The $(P_{\mathrm{Rx}}/P_0)^{\max}$ over f curve is generally obtained by normalization of the full ellipsometer curve with respect to its average value. If the two-point approximation is used, the curve can be approximated using only the minimum and maximum power:

$$\left(\frac{P_{\mathrm{Rx}}}{P_0}\right)^{\max} \approx \frac{P_{\mathrm{Rx}}\left(\frac{\pi}{4}\right)}{P_0} \approx \frac{2P_{\mathrm{Rx}}\left(\frac{\pi}{4}\right)}{P_{\mathrm{Rx}}\left(\frac{\pi}{4}\right) + P_{\mathrm{Rx}}\left(\frac{3\pi}{4}\right)} \,. \tag{3.40}$$

Accordingly, the measurement can be simplified in the following way. The analyzer antenna is first fixed at $\phi_{\mathrm{A}} = \frac{\pi}{4}$ while the power is measured over the full frequency band. Subsequently a single rotation of the antenna to $\phi_{\mathrm{A}} = \frac{3\pi}{4}$ and another measurement of the power spectrum is sufficient to obtain the $(P_{\mathrm{Rx}}/P_0)^{\max}$ over f and to calculate the ellipsometer angles Ψ and Δ according to equations 3.32 and 3.39. In contrast, if the two-point approximation can not be used, a full rotation of the Rx antenna must be performed at any frequency.

The performance of the approximation algorithm can be investigated using simulated ellipsometer curves corresponding to hypothetical, homogeneous samples with a refractive index of $n = 1.71$ and a thickness of $d = 2\,\mathrm{mm}$ over the frequency range from 75 GHz to 110 GHz. The loss tangent of these samples varies from $\tan\delta = 25 \times 10^{-4}$ to $\tan\delta = 200 \times 10^{-4}$. This corresponds, in average, to the data of most of materials summarized by Lamb et al. [12]. The simulated ellipsometer curves are then analyzed in two different ways: First the full datasets are evaluated to obtain the ellipsometer angles by fitting the model described by equation 2.24 (360° analysis) and secondly using the two-point approximation algorithm presented above. The results of both methods are compared to the simulated value of $n = 1.71$ in Figure 3.21.

If the loss tangent of the sample is small ($\tan\delta = 25 \times 10^{-4}$ and $\tan\delta = 50 \times 10^{-4}$), the two-point approximation is only slightly more imprecise compared to the standard method. There even exist ellipsometer curves (at 85 GHz) where the two-point approximation is superior. This is most likely due to bad convergence of the optimization parameters using the 360° method. In general, also the 360° analysis does not perfectly reproduce the initial simulation, since it is based on multi-parameter optimization. In these cases, the theoretical additional error caused by the approximation is small enough

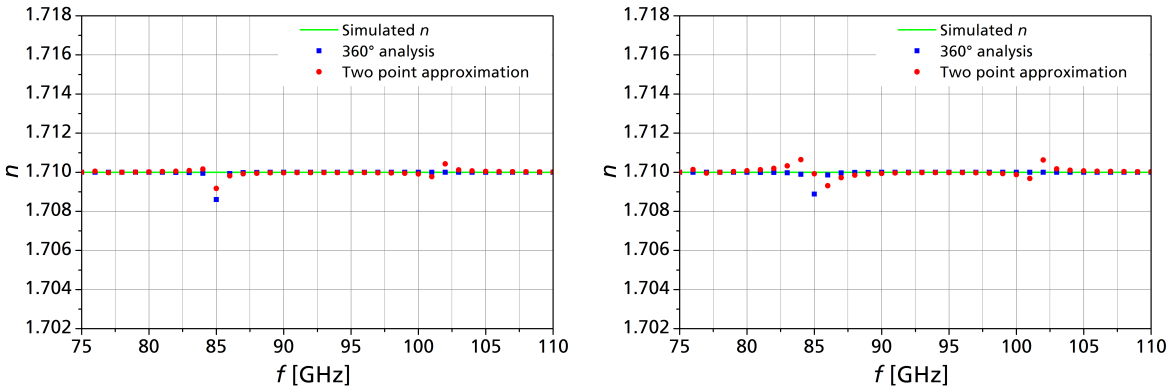

(a) $\tan\delta = 25 \times 10^{-4}$

(b) $\tan\delta = 50 \times 10^{-4}$

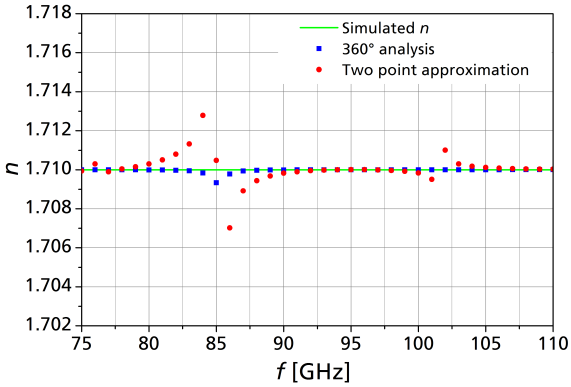

(c) $\tan\delta = 100 \times 10^{-4}$

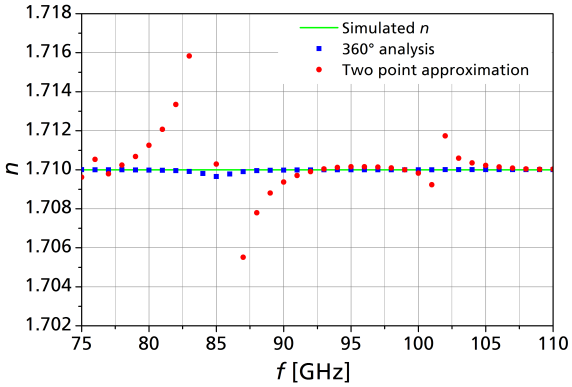

(d) $\tan\delta = 200 \times 10^{-4}$

Figure 3.21: Theoretical performance of the two-point approximation method. Neither the 360° analysis nor the two-point approximation are able to perfectly reproduce the initial simulated refractive index. The difference between both methods becomes more significant if the loss tangent of the sample is increased.

to take full benefit of the enhanced measurement speed. For higher loss tangents, the deviation between both methods becomes more significant so that the benefit of increased measurement speed must be evaluated against loss of precision considering the specific application.

3.4.3 Limits of the method

Figures 3.21(a)-(d) indicate, that the performance of the mmW ellipsometer algorithms are frequency dependent. The two-point approximation and, to a smaller degree, also the 360° analysis are particularly imprecise at a frequency of $f = 85\,\mathrm{GHz}$. This behavior is related to the $(P_{\mathrm{Rx}}/P_0)^{\max}$ over f curve and depends on the material parameters on the samples. The non-dispersive sample shown in Figure 3.20(b), which is similar to the sample shown in Figure 3.21(b), induces a maximum in the $(P_{\mathrm{Rx}}/P_0)^{\max}$ over f

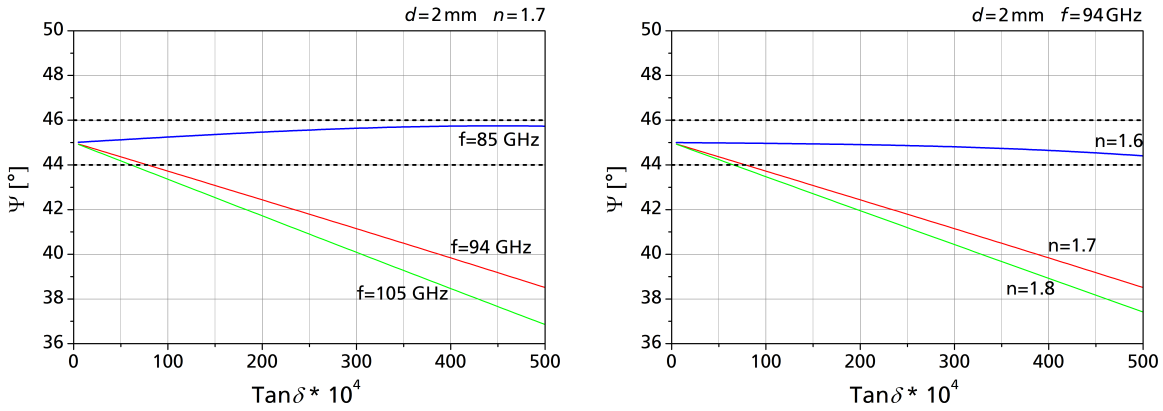

(a) Frequency (b) Refractive index

Figure 3.22: Influence of different frequencies and refractive indices on the ellipsometer angle Ψ depending on the loss tangent. As long as Ψ is close to 45°, the two-point approximation can be used to increase measurement speed.

curve at $f = 85\,\text{GHz}$ with $(P_{\text{Rx}}/P_0)^{\text{max}} = 2$. According to equations 2.24 and 2.22, this indicates that $\Delta \approx 0$. Thus, there exist combinations of material and setup related parameters in a way that there is no significant phase deviation between p-polarized and s-polarized parts of the reflected electromagnetic field. In these cases, small changes in the ellipsometer angle Ψ, which are neglected in the two-point approximation, are particularly important for accurate results. In consequence, the performance of the approximation method is significantly decreased. Once again, the $(P_{\text{Rx}}/P_0)^{\text{max}}$ over f is an important tool for evaluating the performance of mmW ellipsometry if the sample parameters are unknown. If there exists one or more maxima with $(P_{\text{Rx}}/P_0)^{\text{max}} = 2$, then the two-point approximation will most likely lead to inaccurate results in the frequency ranges around the maxima if the loss tangent of the sample is high enough.

The limit value of the loss tangent does not only depend on the frequency, but also on the refractive index of the sample, its thickness and the angle of incidence of the mmW ellipsometer. In addition, polarization loss of the horn antennas influences the method. A quantitative analysis or a binding recommendation on the validity of the approximation is therefore not meaningful. However, a qualitative estimation is feasible by individual investigation of the respective parameters. The angle of incidence in the mmW ellipsometer setup is optimized with respect to measurement accuracy (cf. section 3.1.3) and can be treated as constant. If the thickness of the sample is decreased, the influence of the strong reflection at the metallic substrate is even more dominant. Accordingly, the approximation $\tan\Psi \approx 1$ is valid for more lossy materials as well. In order to estimate the maximum loss tangent which allows to use the two-point approximation in a typical mmW ellipsometer measurement, the influence of frequency and refractive index of a 2 mm thick sample on the ellipsometer angle Ψ is shown in Figure 3.22. As long as $\tan\Psi \approx 1$, the two-point approximation can be safely used for evaluation of the measurements. Considering the achievable measurement accuracy of the mmW ellipsometer, this implies that the value of Ψ should be within the range from 44° to 46°.

Figure 3.22(a) shows the dependence of Ψ on the loss tangent for three different frequencies at $f_1 = 85\,\text{GHz}$, $f_2 = 94\,\text{GHz}$ and $f_3 = 105\,\text{GHz}$, assuming that the refractive index is constant at $n = 1.7$. It is noteworthy that there is only a weak dependence on the loss tangent if the frequency is 85 GHz so that $\Psi \approx 45°$. This appears inconsistent with the simulated performance of the two-point approximation shown in Figure 3.21, which is particularly low at exactly that frequency. However, as discussed above, the maximum power corresponding to the simulated sample at $f_1 = 85\,\text{GHz}$ is $(P_{\text{Rx}}/P_0)^{\text{max}}(f_1) \approx 2$. This implies not only $\Psi \approx 45°$, but, more importantly, also $\Delta = 0°$ such that the two-point approximation is generally disadvantageous at frequencies close to $f_1 = 85\,\text{GHz}$. In contrast, the curves corresponding to f_2 and f_3 significantly decrease with the loss tangent so that $\Psi < 44°$ for $\tan\delta > 75 \times 10^{-4}$.

A similar diagram can be obtained by fixing the frequency at 94 GHz and varying the refractive index as shown in Figure 3.22(b). If the refractive index of the sample is $n_1 = 1.6$, the ellipsometer angle Ψ remains within the range between 44° and 46°. It can be shown, that this configuration also induces a maximum in the corresponding $(P_{\text{Rx}}/P_0)^{\text{max}}$ over f curve so that is unsuitable for the two-point approximation. The curves corresponding to $n_2 = 1.7$ and $n_3 = 1.8$ are decreasing with the loss tangent. Again, the approximation is valid up to a loss tangent of $\tan\delta \approx 75 \times 10^{-4}$.

In summary, the two-point method is preferable to the 360° analysis if the sample is not thicker than 2 mm and consists of a material with a loss tangent up to $\tan\delta = 75 \times 10^{-4}$. It should be noted, that the two-point approximation works best if the slopes in Figure 3.22 are as flat as possible and if there is no maximum in the $(P_{\text{Rx}}/P_0)^{\text{max}}$ over f curve. However, the weak dependence of the ellipsometer angle Ψ on the loss tangent induces low measurement accuracy with respect to the imaginary part of the dielectric function. Therefore, samples which are suitable for fast analysis of the refractive index are in general challenging cases if the loss tangent is the main measurand of interest. In this case the two-point approximation should not be used in order to optimize measurement accuracy.

3.5 Summary of methodology

In section 2.3.3, three fundamental problems of microwave ellipsometry have been identified: Insufficient measurement accuracy, ambiguous results and slow measurement speed. Since optical ellipsometry does, in general, not suffer from such limitations, these problems must be related to the microwave regime. The previously proposed method involves an angle and a power measurement. In this chapter, it has been shown that the angle measurement is much more imprecise than the power measurement, due to the polarization loss of the rectangular horn antennas. It has further been demonstrated, that the material parameters influence the angle measurement more strongly than the power measurement. Accordingly, the accuracy of conventional microwave ellipsometry is intrinsically limited. Based on these findings, a novel approach to mmW ellipsometry has been presented. A strongly reflecting substrate decouples the influence of the material parameters on the measurement. Real quantities, such as the refractive index or the thickness of the sample, mainly influence the power measurement, but not the angle

measurement. Therefore, the accuracy with respect to these parameters is significantly increased. In contrast, the absorption of a sample, a complex quantity, is exclusively reflected in the angle measurement. Combined with a spectroscopic approach, this decoupling also leads to an improvement of the measurement accuracy concerning the loss tangent and to unambiguous results for the refractive index, independently of the thickness. Furthermore, it has been demonstrated that the new configuration allows for an approximation method in the case of low loss samples. Thereby, the measurement speed can be reduced for a wide selection of materials.

4 Experimental Results

Spectroscopic mmW ellipsometry on a metal substrate is a very promising approach to overcome the main problems with conventional microwave ellipsometry: Accuracy, ambiguity and measurement speed. The novel method is predestined for characterization of thin dielectric sheets, such as varnish layers or laminated building materials. Furthermore, ellipsometry does not rely on precise calibration and a compact, versatile setup is feasible at mmW frequencies around 100 GHz. Thus, from a theoretical point of view, spectroscopic mmW ellipsometry on a metal substrate is suitable to a wide variety of applications. However, there are several challenges in the actual experimental realization, that can only be roughly estimated based on simulation. A detailed experimental verification of the simulation results, based on an appropriate selection of sample materials, is mandatory to verify the enhancement of performance, that is expected from this novel approach to mmW ellipsometry.

In this chapter, first possible error sources that may falsify the ellipsometer measurements are identified and discussed from an experimental point of view. Then, a range of dielectric samples is selected to demonstrate the performance of mmW ellipsometry under optimal conditions but also in more challenging cases, where measurements are superimposed by interfering effects. For this purpose, the refractive index and loss tangent of numerous samples are determined over a wide frequency range between 85 GHz and 105 GHz. The achieved measurement accuracy is discussed with respect to statistical reproducibility, frequency and sample related parameters such as thickness and lateral dimension.

4.1 Possible error sources in millimeter wave ellipsometry

Spectroscopic mmW ellipsometry on a metal substrate brings many advantages over the conventional approach, but also new possible sources for systematic errors. If the samples are placed on a strongly reflecting substrate instead of being surrounded by air, small gaps between the material and the sample stage might be created. Furthermore, the strongly reflecting substrate is problematic if small samples are investigated since this enhances the influence of line-of-sight interference caused by antenna crosstalk.

In this section, the most significant error sources related to the novel method are discussed based on exemplary measurements. This allows for an appropriate selection of samples for the refractive index and loss tangent measurements which are presented in the following sections.

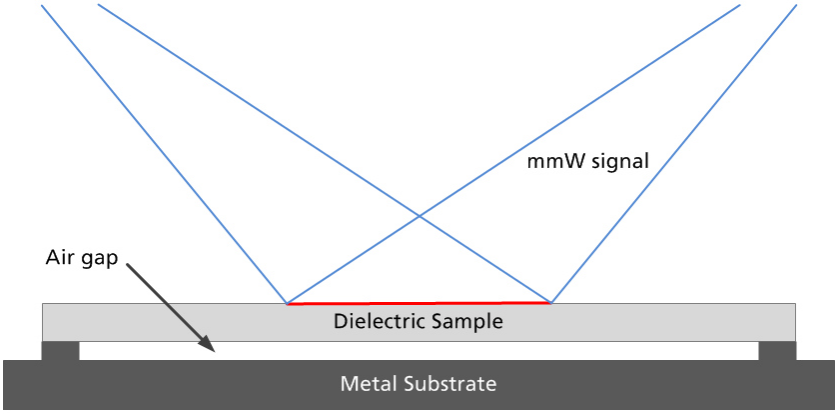

Figure 4.1: Exaggerated sketch of a possible air gap between a dielectric sample and the metal substrate used in the improved mmW ellipsometer setup.

4.1.1 Air gaps

Whenever a sample used for microwave or millimeter wave material characterization is not surrounded by air, such as in hollow waveguide methods, small air gaps between the sample and its environment are one of the main error sources of the measurement (cf. section 2.2). Depending on the thickness of the unintentional air layer relative to the wavelength of the electromagnetic field, interference and scattering effects distort the signal and lead to falsified results. While a metal substrate has decisive advantages for mmW ellipsometry from a theoretical point of view, it also allows for small air gaps between the sample and the substrate as sketched in Figure 4.1. Consequently, their experimental influence on must be investigated in order to ensure that the increased measurement accuracy using a metal substrate is not compensated by losses due to an unintentional air layer.

Using a transfer-matrix formalism, the reflectivity of a sample-substrate configuration including an air gap can be derived for s-polarized and p-polarized parts of the electromagnetic field [112, 150, 151]:

$$\tilde{r}_{\mathrm{p/s}} = \frac{e^{\mathrm{j}\beta_{\mathrm{air}}}\left(r'_{\mathrm{p/s}}e^{\mathrm{j}\beta} - r'_{\mathrm{p/s}}e^{-\mathrm{j}\beta}\right) - e^{-\mathrm{j}\beta_{\mathrm{air}}}\left(e^{-\mathrm{j}\beta} - r'^{2}_{\mathrm{p/s}}e^{\mathrm{j}\beta}\right)}{e^{\mathrm{j}\beta_{\mathrm{air}}}\left(e^{\mathrm{j}\beta} - r'^{2}_{\mathrm{p/s}}\mathrm{e}^{-\mathrm{j}\beta}\right) - \mathrm{e}^{-\mathrm{j}\beta_{\mathrm{air}}}\left(r'_{\mathrm{p/s}}e^{-\mathrm{j}\beta} - r'_{\mathrm{p/s}}e^{\mathrm{j}\beta}\right)}, \tag{4.1}$$

where $r'_{\mathrm{p/s}}$ and β are defined according to equations 2.18 and 2.17 respectively and

$$\beta_{\mathrm{air}} = \frac{2\pi f}{c_0} d_{\mathrm{air}} \sqrt{1 - \sin^2\theta} \tag{4.2}$$

is the propagation factor through the air gap, d_{air} is the thickness of the air gap, c_0 is the speed of light in vacuum and θ is the angle of incidence. Using the ellipsometer equation

$$\frac{\tilde{r}_{\mathrm{p}}}{\tilde{r}_{\mathrm{s}}} = \tan\Psi \times \exp[\mathrm{j}\Delta], \tag{4.3}$$

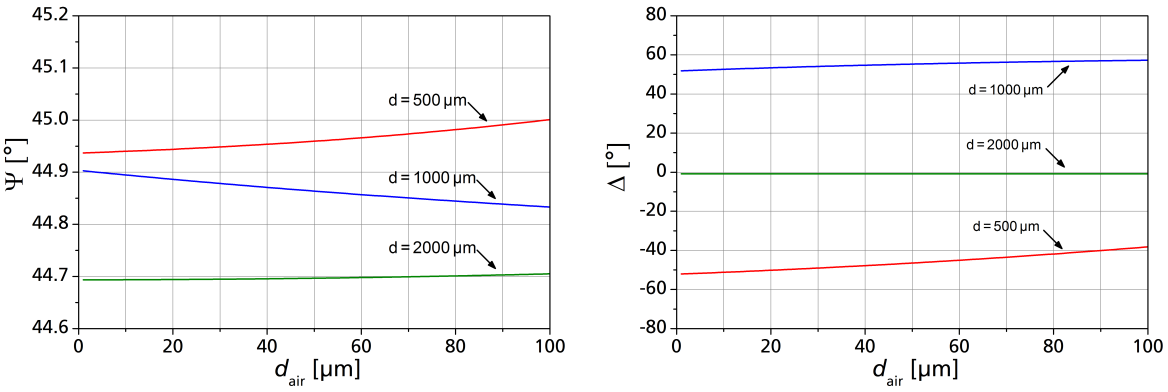

(a) (b)

Figure 4.2: Simulated influence of an air gap on hypothetical samples with $n = 1.6$ and $\tan\delta = 50 \times 10^{-4}$ at a frequency of $f = 94\,\text{GHz}$. As the sample thickness approaches the thickness of the air gap, the measurement error increases.

the influence of the air gap thickness d_{air} on the ellipsometer angles Ψ and Δ can be determined. Figure 4.2 shows according simulations of the ellipsometer angles corresponding to hypothetical samples with $n = 1.6$ and $\tan\delta = 50 \times 10^{-4}$ at a frequency of $f = 94\,\text{GHz}$. As expected, the influence of the air gap increases as the sample thickness is decreased. However, the deviation of the ellipsometer angle Ψ is comparably small. Even the 500 µm thick sample does only induce a change of $\delta\Psi \approx 0.05°$ for a 100 µm thick air gap. Compared to the achievable measurement accuracy of the ellipsometer angle, this is negligible (cf. Table 3.2). In contrast, in the worst case, the ellipsometer angle Δ is falsified by more than $\delta\Delta \approx 15°$. This would lead to significant errors in the estimation of the corresponding material parameters. In the actual experimental setup, a 100 µm thick air gap would be visible with the naked eye and a 50 µm thick imperfection should at least lead to a notable reduction of fraction between the substrate and the sample. If there exists an air gap in the mmW ellipsometer setup, it is most likely thinner than 50 µm. However, according to Figure 4.2, even a small air gap of 20 µm to 30 µm falsifies the outcome of the measurement in case of the 500 µm thin sample.

In order to estimate the probability of creating a significant air gap when placing the sample onto the metallic substrate, the ellipsometer curves of a 2 mm thick and a 1 mm thick PMMA plate were consecutively measured ten times. After each measurement, the samples were removed and put back to the mmW ellipsometer by hand. The average ellipsometer curves are shown in Figure 4.3. Both measurements were highly reproducible, so that error bars corresponding to the standard deviation are not visible. In addition, the samples were placed on frames made from 50 µm and 100 µm thick sheets to force an air gap between sample and substrate as sketched in Figure 4.1. The reproducibility of these measurements was also high, so that the statistical deviation can again be neglected. However, the air gaps lead to a measurable deviation of the ellipsometer curve in both cases. While the measurements corresponding to the 50 µm thick air gap are close to the measurements without a forced air gap for both samples, the 100 µm thick air gap results in a significant falsification of the ellipsometer curve. In case of the 2 mm thick

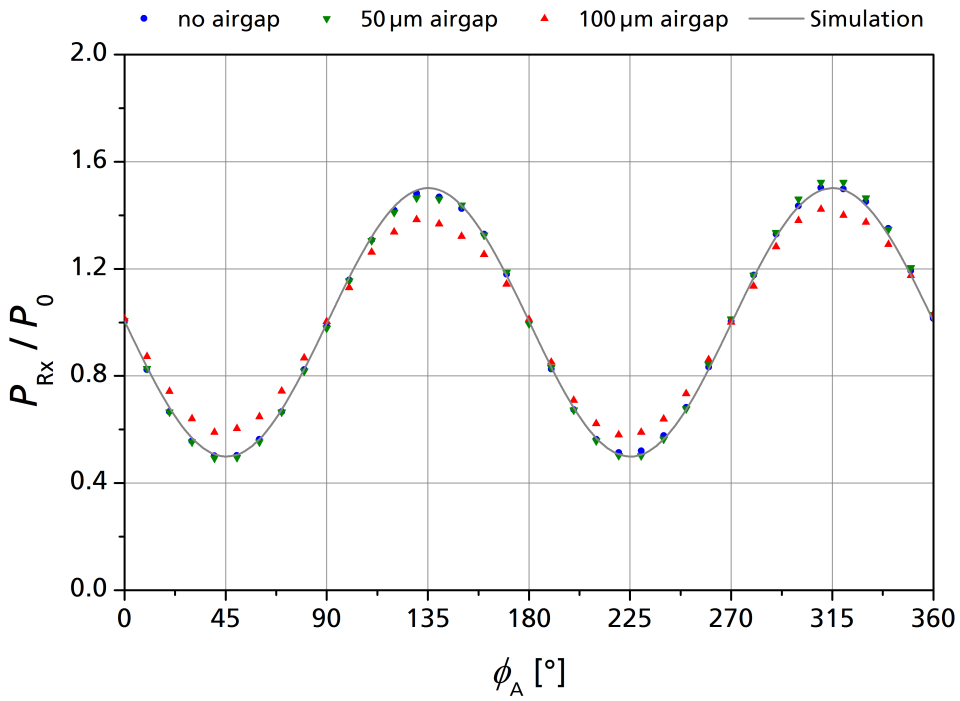

(a) 2 mm thick PMMA sample

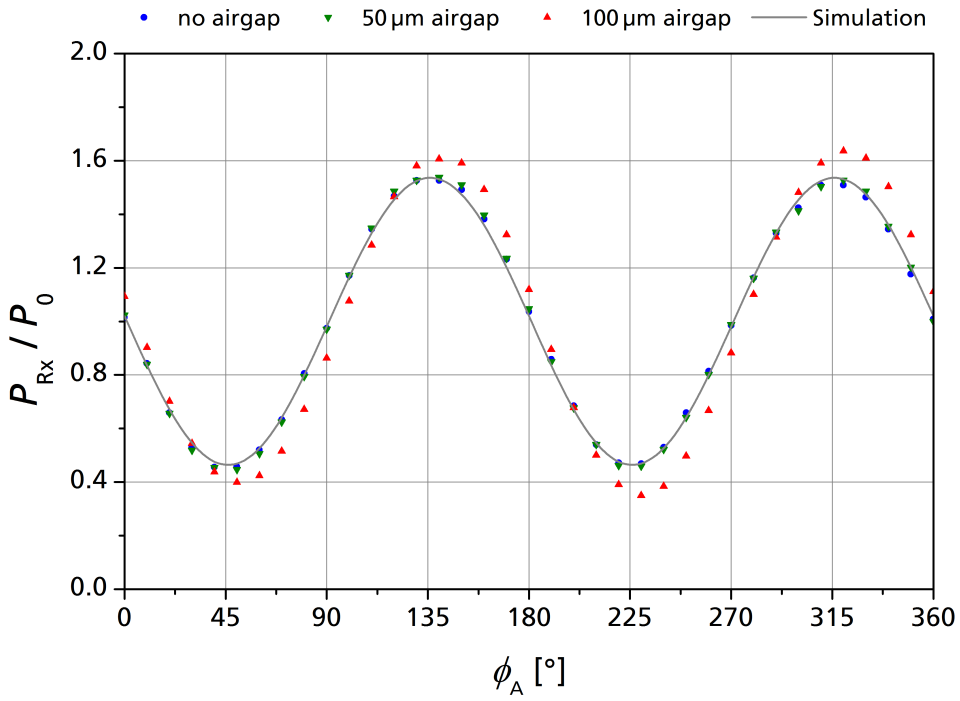

(b) 1 mm thick PMMA sample

Figure 4.3: Measurements and simulations of the ellipsometer curve corresponding to two PMMA samples. Using a frame made of thin sheets, air gaps have been forced to investigate their influence on the measurement.

sample, the ellipsometer curve is compressed compared to the measurements without an air gap. According to section 3.2.3, this is caused by a deviation of the ellipsometer angle Δ. Thus, the measurement results are in accordance with the simulations shown in Figure 4.2(b) for the 2 mm thick sample. In contrast, the ellipsometer curve, measured for the configuration with a 100 µm air gap between the substrate and a 1 mm thick sample, has a higher amplitude and is shifted along the angular axis compared to the other measurements. While the amplitude change is again caused by a deviation of the ellipsometer angle Δ, the shift along the angular axis is related to the ellipsometer angle Ψ. It is significantly larger, than expected from the simulations shown in Figure 4.2(a). This is most likely due to higher order interference effects, within the material and the air gap, that are not considered in the model described by equation 4.1.

Nevertheless, air gaps are comparably unproblematic for mmW ellipsometry on metal substrates considering their significance for other material characterization methods, such as hollow waveguide techniques (cf. section 2.2). Using the setup presented in section 3.1.4, it is unlikely that an air gap of more than 30 µm to 50 µm remains unnoticed. However, the influence of air gaps depends on the sample thickness, the specific material and also slightly on the frequency. Simulations using a transfer matrix formalism can be used to estimate, whether or not a thin sample is particularly prone to error caused by air gaps, but might underestimate the influence on the ellipsometer angle Ψ. In result, the loss tangent measurement could be falsified by small air gaps even if simulations predict a negligible influence. This effect will be discussed in more detail in section 4.3.2.

4.1.2 Sample size

Apart from the thickness, also the lateral size of the samples used for mmW ellipsometry must be considered. If their dimension is small enough, the mmW signal illuminates its edges or even the strongly reflecting substrate on which the sample is placed. Scattering and refraction effects superimpose the measurement in this case. In section 3.2.4, it has been shown that the minimal sample size depends on the frequency of the mmW signal. Using equations 3.23-3.25, the theoretical minimal diameter of a sample can be calculated. At a frequency of 92 GHz it is $D_{\mathrm{min}} \approx 125\,\mathrm{mm}$. However, the illuminated area on the sample stage of the mmW ellipsometer is asymmetric for non-perpendicular incidence (cf. Figure 3.4). Therefore, exact positioning of the sample, with respect to the illuminated area, is challenging so that it is unlikely that samples where $D = D_{\mathrm{min}}$ lead to satisfying results. Furthermore, the 10 dB aperture angle, which is used in equation 3.23, is only an approximation for the beam path. Consequently, there is still a small amount of radiation that hits the area around a sample with $D = D_{\mathrm{min}}$, even if the sample is perfectly positioned. It is therefore important to experimentally investigate the influence of a small samples size in order to make a more reliable statement on the minimal sample dimension that is suitable for mmW ellipsometry.

Figure 4.4 shows ellipsometer measurements of six square-shaped polycarbonate (PC) platelets with identical thickness of $d = 2.5\,\mathrm{mm}$ at a frequency of $f = 92\,\mathrm{GHz}$. The side length of the samples varies from $D = 250\,\mathrm{mm}$ to $D = 75\,\mathrm{mm}$. For better clarity, the data points have been interpolated using a spline model. While the impact of the de-

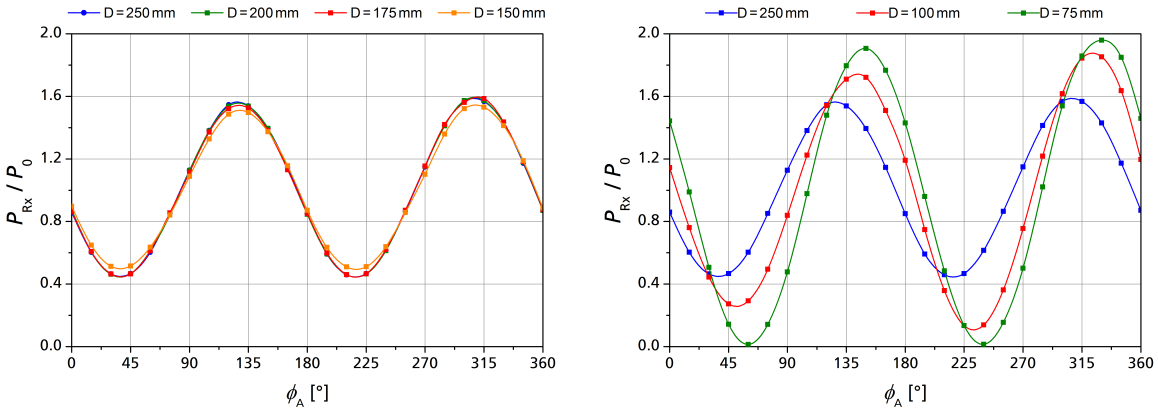

(a) adequate sample size (b) small samples

Figure 4.4: Ellipsometer measurements of six 2.5 mm thick PC plates at a frequency of 92 GHz. If the side length of the sample is smaller than 150 mm, the ellipsometer measurement is strongly falsified.

creasing sample size on the ellipsometer curve is small for $D \geq 150\,\text{mm}$ (Figure 4.4(a)), the measurement is significantly falsified in case of the smaller samples (Figure 4.4(b)). Here, the amplitude of the ellipsometer curve approaches $(P_{Rx}/P_0) = 2$ and the angle of the maximum increases. Accordingly, the reflection and absorption of the sample are overestimated. In addition, the ellipsometer curve becomes asymmetric, which is most likely caused by scattering effects at the edges. Accordingly, the theoretic prediction, that samples with $D_{\text{min}} < 125\,\text{mm}$ will lead to unphysical results, is true. However, as Figure 4.4(a) indicates, there is also a recognizable deviation in the $D = 150\,\text{mm}$ measurement, compared to the larger samples. Further measurements show that the minimal sample size, that can be reliably used for mmW ellipsometry, is about 10 % to 20 % larger than equation 3.23 suggests, depending on the material and the precision of the alignment on the sample stage. In particular optically transparent materials, where the use of the positioning lasers of the mmW ellipsometer is limited, should have an adequate safety margin with respect to D_{min}.

4.1.3 Antenna crosstalk

While the influence of small samples and air gaps can be minimized with an appropriate experimental setup, it is not possible to completely avoid direct crosstalk between the antennas. In section 3.1.3, it has been shown that steep angles of incidence, with less crosstalk, are unfavorable with respect to the achievable measurement accuracy. On the other hand, simulations show that crosstalk between the antennas disrupts the measurement, if the incident angle is flat enough (cf. Figure 3.6). While it is clear that $\theta > 70°$ leads to strong interference effects, the influence of crosstalk at steeper angles on an actual measurement is not that obvious. In particular, the validity of the approximation in equation 3.7 is hard to determine based on simulations. While an incident angle of $\theta = 60°$ is considered to be a good compromise between accuracy and line-of-sight loss, it is important to experimentally verify this assumption.

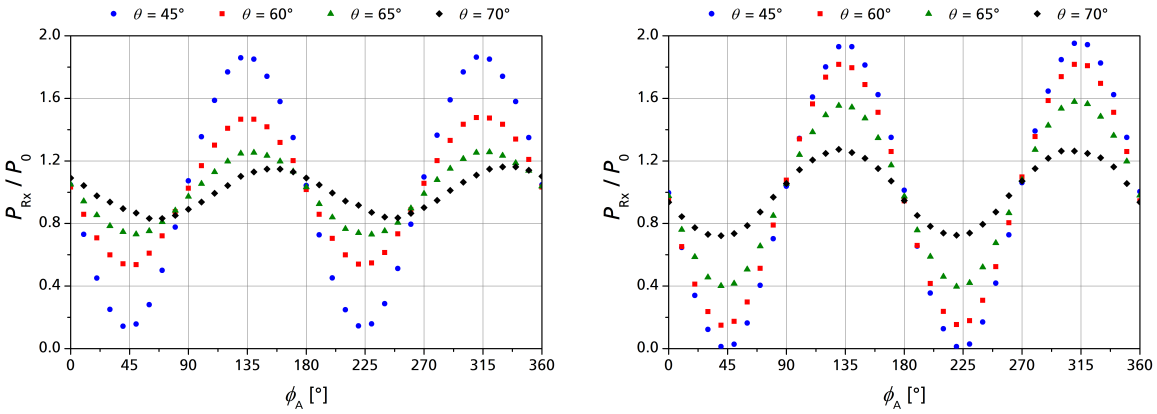

(a) 2 mm thick PMMA sample

(b) 2 mm thick PVC sample

Figure 4.5: Ellipsometer measurements in dependence of the incidence angle θ. At first glance, it is not clear whether or how the measurements are influenced by crosstalk between the antennas. There are no obviously inconsistent data points or asymmetries in the ellipsometer curves.

Figure 4.5 shows measurements of two 2 mm thick samples made from PMMA and PVC at different angles of incidence. At $\theta = 45°$, the amplitude of the ellipsometer curve is close to $(P_{Rx}/P_0) = 2$, independently of the sample. Thus, precise material parameter estimation is not feasible. However, at such a steep angle of incidence crosstalk between the antennas can be safely neglected. This measurement is therefore a good reference to investigate the influence of line-of-sight interference on the ellipsometer curve for flat angles of incidence. Compared to $\theta = 45°$, the ellipsometer curves of the flatter angles of incidence are compressed around their average value or displaced along the angular axis. There are no obviously inconsistent values or significant asymmetries in the ellipsometer curve so that there is no clear indication, whether or how the measurement was superimposed by crosstalk between the antennas.

To analyze the data more quantitatively, equation 2.24 was fitted to the ellipsometer measurements shown in Figure 4.5. This allows to determine the maximum normalized power $(P_{Rx}/P_0)^{max}$ and the corresponding analyzer angle ϕ_A^{max} for each angle of incidence. The corresponding data is shown in Figure 4.6. In addition to the measured values, which are represented by circles, corresponding simulations of $(P_{Rx}/P_0)^{max}$ and ϕ_A^{max} are plotted as solid lines vs. the incidence angle. The measured maximum normalized power is in good accordance with the simulations for all of the four incidence angles and both samples. In contrast, the measured analyzer angles of the maxima only agree with the theoretical curves if the angle of incidence is not larger than 60°. For $\theta = 65°$ and $\theta = 70°$, the measurement overestimates ϕ_A^{max} with respect to the simulations in case of both samples. Since there is no physical reason why the model should get inaccurate at higher incidence angles, this effect is attributable to line-of-sight interference caused by crosstalk between the antennas.

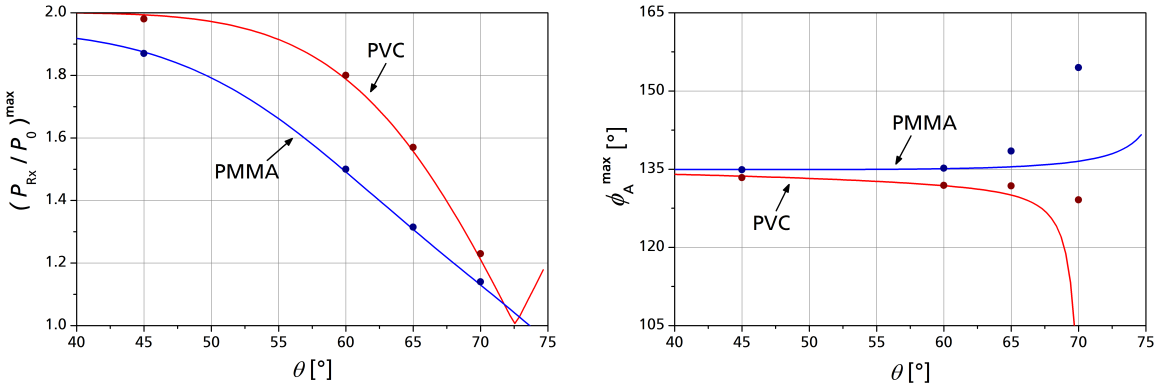

(a) Maximum power (b) Analyzer angle

Figure 4.6: Maximum power and corresponding analyzer angle of the ellipsometer curves shown in Figure 4.6. In addition to the measurement results (circles), according simulations are shown for each case (solid lines).

4.1.4 Summary

There are three significant setup-related error sources in spectroscopic mmW ellipsometry if a metal substrate is used. Small samples influence both of the ellipsometer angles Ψ and Δ and therefore lead to falsification of the refractive index and the loss tangent. Accordingly, the dimension of the samples should be at least 150 mm, preferably more. However, the fabrication of some interesting materials, such as ceramics that can be used for high frequency applications, does not allow for arbitrary large samples. In this case, the measurements shown in Figure 4.4 are a good basis for estimating the error caused by the insufficient sample size.

In contrast to small samples, air gaps and crosstalk between the antenna predominantly influence the analyzer angle corresponding to the maximum of the ellipsometer curve. This results in an overestimation of the loss tangent so that the material appears to be more strongly absorbing than it actually is. While small samples can in principle be avoided, small air gaps and particularly crosstalk between the antennas fundamentally limit the measurement. Samples can not be thinner than about 500 mm and the angle of incidence can not be larger than 60°.

4.2 Determination of the refractive index

For many mmW applications, low-loss materials are preferably used to minimize the attenuation of high-frequency signals. Therefore, absorption is typically negligible and the refractive behavior of a material is the main property of interest. As shown in chapter 3, mmW ellipsometry is particularly promising for measurements of the refractive index of low-loss samples at mmW frequencies. From a theoretical point of view, the improved method significantly enhances the achievable measurement accuracy with respect to the ellipsometer angles Ψ and Δ. In addition, as demonstrated in the previous section, the

most prominent setup related error sources mainly influence the loss tangent measurement. If the sample dimension is larger than about 150 mm and the material under investigation fits within the range of optimal samples (cf. Table 3.3), a low systematic error on the refractive index measurement is expected.

In this section, mmW ellipsometer measurements of the refractive index are presented for a selection of different samples. The corresponding materials were chosen in a way to demonstrate the performance of the mmW ellipsometer for optimal conditions as well as for challenging tasks. Thereby, the influence of the sample thickness, the reproducibility of the measurements and the validity of the two-point approximation are emphasized. The achieved measurement accuracy is then discussed and compared to the conventional approach to microwave ellipsometry.

4.2.1 Sample selection

As illustrated in section 2.2.4, measurement of the dielectric properties of plastic and building materials at frequencies around 100 GHz is, in general, challenging. Accordingly, the selection of materials which are already well characterized is limited. Reliable material parameters, which have been verified throughout several independent measurements are only rarely available. In most cases, homogeneous low-loss polymers have been investigated. The most extensive overview on material parameters at microwave and mmW frequencies can be found in the work of Lamb et al. [12]. These materials are a good reference to classify the performance of mmW ellipsometry. In particular, the refractive index of polymethyl methacrylate (PMMA), polycarbonate (PC), polyvinyl chloride (PVC), polyoxymethylene (POM) and high-density polyethylene (HDPE) is comparably well known at mmW frequencies [152–161]. Since the actual values are all within the range between $n = 1.5$ and $n = 1.8$, these materials are good references for mmW ellipsometry if the sample dimensions are chosen according to Table 3.3. Thus, these materials are used to demonstrate the accuracy of the mmW ellipsometer in an optimal case. The final selection of samples and their properties are summarized in Table 4.1.

In contrast, there is only little or no knowledge on the refractive index of more complex materials, such as laminates, inhomogeneous plastics or ceramics at mmW frequencies. The characterization of these materials is, in general, more difficult compared to that of homogeneous polymers. In addition, Figures 3.16 indicates that low refracting materials are particularly challenging for mmW ellipsometry, as well as thin or small samples. Thus, these cases must be investigated to demonstrate the performance of ellipsometry for non-optimal scenarios. A corresponding selection of samples is shown in Table 4.2. FerroA6M-E is a homogeneous ceramic which is only available as thin sheets with a thickness of less than 1 mm and a maximum diameter of $D = 175$ mm. Accordingly, the sample geometry is not ideal for mmW ellipsometry. There is no available data on the refractive index of FerroA6M-E in the frequency range around 100 GHz, but low-frequency measurements indicate that it is comparably high and values in the range of $n \approx 2.5$ can be expected [162]. According to Figure 3.16, this allows for high measurement accuracy. Thus, FerroA6M-E is a good choice to investigate the accuracy of mmW ellipsometry for unfavorable sample dimensions.

Table 4.1: Selection of optimal samples for mmW ellipsometry measurements.

Material	n previously published	d [mm]	D [mm]
Polyoxymethylene (POM)	1.75-1.77 [158]	2	200
Polyvinyl chloride (PVC)	1.65-1.71 [163, 164]	1;2	200
Polycarbonate (PC)	1.55-1.68 [155–157]	2.5	250
Polymethyl methacrylate (PMMA)	1.60-1.61 [152–154]	1.5;2	200
High-density polyethylene (HDPE)	1.52-1.56 [159–161]	1	220

Table 4.2: Selection of challenging samples for mmW ellipsometry measurements.

Material	n previously published	d [mm]	D [mm]
Ceramic FerroA6M-E	2.4-2.5 [162]	0.5;0.9	175
Glass-reinforced laminate FR-4	2-2.2 [147, 165]	1	300
3D-printed polylactic acid (PLA)	N/A	2.4	200
Polytetrafluoroethylene (PTFE)	1.40-1.44 [166–168]	1	210

Another class of materials, which is becoming increasingly important for mmW applications, is that of glass-fiber reinforced plastics (GFRPs) [169–171]. Since they are made of laminated layers of glass fibers, high stability is obtained at minimized weight. FR-4 is one of the most widely used GFRPs for microwave applications at frequencies up to 5 GHz. From measurements in this frequency range it can be expected that the refractive index at mmW frequencies is in the range around $n = 2$ [147, 165]. Thus, FR-4 is well suited to demonstrate the ability of mmW ellipsometry to characterize laminated materials. The sample size of $D = 300\,\text{mm}$ is adequately large to guarantee that possible inaccuracies are predominantly related to the structure of the material.

As shown in section 3.2.4, mmW ellipsometry works best if the refractive index of a sample is larger than $n \approx 1.5$ (cf. Figure 3.16). Polytetrafluoroethylene (PTFE) is a low refracting homogeneous polymer that is comparably well characterized at mmW frequencies, with an expected refractive index in the range between $n = 1.4$ and $n = 1.44$ [166–168]. Accordingly, an adequately large PTFE sample is a good reference for evaluation of the performance of mmW ellipsometry for low refracting materials. Apart from PTFE, another interesting low refractive material is polylactic acid (PLA). If fabricated as filament wire, it can be used for 3D printing and is therefore promising for mmW applications to reduce fabrication costs [172, 173]. However, depending on the exact configuration, the air content in 3D-printed material can be relevant with respect to its average dielectric properties. Therefore, the refractive index of a 3D-printed sample is not predictable, but it can be assumed that it is low due to air inclusions. Thus, the 3D-printed PLA sample is a good choice to investigate inhomogeneous, low refracting samples. To avoid further possible inaccuracies, its thickness and dimension have been chosen to be $d = 2.4\,\text{mm}$ and $D = 200\,\text{mm}$ respectively.

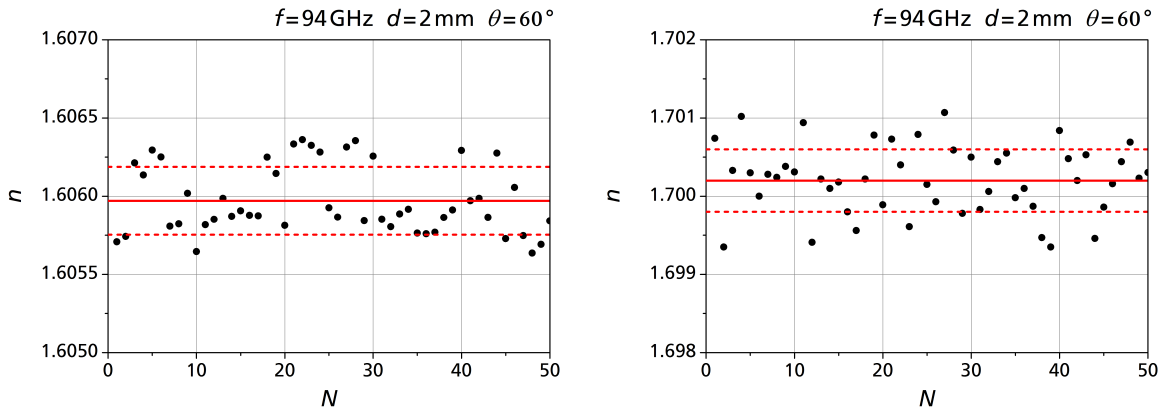

(a) PMMA sample (b) PVC sample

Figure 4.7: Average value and standard deviation corresponding to 50 identical mmW ellipsometer measurements.

4.2.2 Reproducibility of measurements

Before presenting the results of the refractive index measurements for all the samples listed in Tables 4.1 and 4.2, it is useful to investigate the statistical reproducibility of these measurements. For this purpose, the refractive index of each sample has been measured $N = 50$ times under identical conditions. The samples have been removed and put back to the sample stage after each measurement. Figure 4.7 shows according measurements for the 2 mm thick PMMA and PVC samples at a frequency of 94 GHz. From these data, the arithmetic average $\overline{n}_{94\text{GHz}}$ and the corresponding standard deviation

Table 4.3: Statistical uncertainties on the measured refractive index.

Material	d [mm]	$\overline{n}_{94\text{GHz}}$
Ceramic FerroA6M-E	0.9	2.4782 ± 0.0003
Ceramic FerroA6M-E	0.5	2.4804 ± 0.0003
Glass-reinforced epoxy laminate FR-4	1	1.9808 ± 0.0002
Polyoxymethylene (POM)	2	1.7619 ± 0.0002
Polyvinyl chloride (PVC)	2	1.7002 ± 0.0004
Polyvinyl chloride (PVC)	1	1.7024 ± 0.0003
Polycarbonate (PC)	2.5	1.6562 ± 0.0003
Polymethyl methacrylate (PMMA)	2	1.6059 ± 0.0002
Polymethyl methacrylate (PMMA)	1.5	1.6038 ± 0.0003
High-density polyethylene (HDPE)	1	1.5224 ± 0.0004
3D-printed polylactic acid (PLA)	2.4	1.4441 ± 0.0003
Polytetrafluoroethylene (PTFE)	1	1.4070 ± 0.0003

are calculated in order to estimate the reproducibility of the mmW ellipsometer measurements. The corresponding values are summarized for all of the samples in Table 4.3. The PMMA and PVC measurements shown in Figure 4.7 represent the lowest and highest statistical uncertainty of these measurements respectively. In general, the refractive index measurement is precise up to the fourth decimal for all of the samples. Consequently, statistical deviations are most likely negligible with respect to the systematic, setup related error sources. This is also true for measurements at other mmW frequencies that are not listed in Table 4.3 for the sake of clarity. Thus, the mmW ellipsometer allows for high statistical reproducibility of the measured values, so that it is not necessary to average over numerous measurements to obtain reliable results and data acquisition time can be reduced.

4.2.3 Influence of the sample thickness

Apart from insufficient measurement accuracy, another major problem of conventional microwave ellipsometry is that the measured material parameters strongly depend on the sample thickness (cf. Figure 2.12). According to section 3.3.1, this can be attributed to the periodicity of the material model which leads to ambiguous results. Using a strongly reflecting substrate to decouple the measurands and a spectroscopic approach, unambiguous measurements are possible with mmW ellipsometry (cf. Figure 3.18). In consequence, samples made from identical materials but with different thickness should lead to similar results.

Figure 4.8 shows ellipsometer measurements of the refractive index of two FerroA6M-E samples with $d = 0.5\,\mathrm{mm}$ and $d = 0.9\,\mathrm{mm}$, as well as two PVC samples with $d = 1\,\mathrm{mm}$ and $d = 2\,\mathrm{mm}$. Thus, the ceramic samples represent a challenging case, while the PVC samples are within the optimal range of operation of the mmW ellipsometer. In contrast to conventional microwave ellipsometry, the sample thickness only slightly influences the measured dispersion curves in both cases. In order to analyze the deviation more quantitatively, the relative difference between both samples, normalized with respect to the corresponding mean value, can be determined and averaged over the full frequency range for each material:

$$\overline{\sigma} = \frac{1}{N} \sum_{\mathrm{i}} \frac{\sqrt{Y_{\mathrm{i},1}^2 - Y_{\mathrm{i},2}^2}}{\overline{Y_{\mathrm{i}}}}. \tag{4.4}$$

$Y_{\mathrm{i},1}$ and $Y_{\mathrm{i},2}$ are the measured refractive indices at the frequency i, where the subscripts 1 and 2 represent the thickness of the sample. $\overline{Y_{\mathrm{i}}}$ is the corresponding mean value and N is the number of measurement points at different frequencies. In percentage terms, the deviation between the measurements shown in Figure 4.8(a) and (b) is given by:

$$\overline{\sigma}_{\mathrm{Ferro}} = 0.05\,\% \tag{4.5}$$

$$\overline{\sigma}_{\mathrm{PVC}} = 0.11\,\%. \tag{4.6}$$

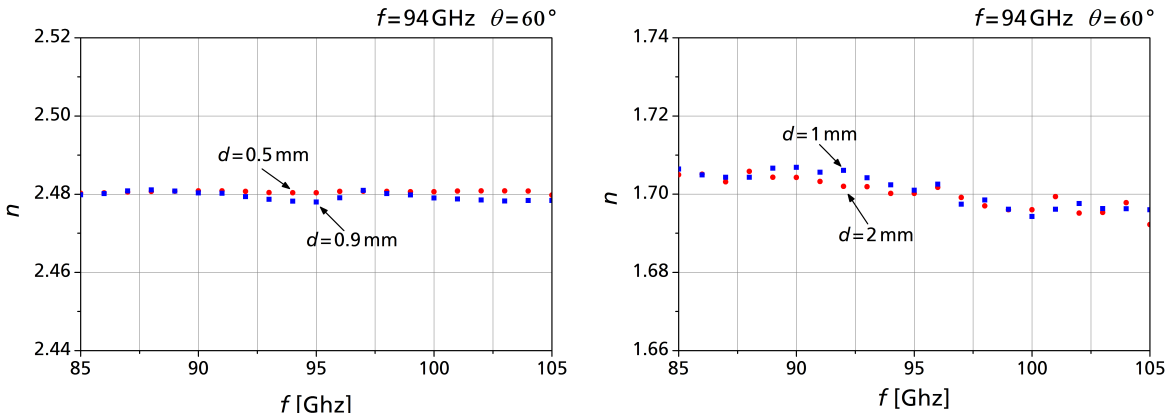

(a) FerroA6M-E sample (b) PVC sample

Figure 4.8: Influence of the sample thickness on spectroscopic mmW ellipsometry using a metal substrate.

It is noteworthy that the more challenging samples resulted in a less significant deviation. This might be due to the smaller difference in the sample thickness or, more likely, due to the apparent dispersion in the refractive index of PVC over the frequency band, which has also been previously observed [97]. However, compared to conventional microwave ellipsometry (cf. Figure 2.12), where

$$\overline{\sigma}_{\text{Std}} = 15\,\%, \tag{4.7}$$

the deviation is negligible in both cases and the measurement results are internally consistent.

In summary, spectroscopic mmW ellipsometry on metal substrates allows for high reproducibility of the measured refractive index from a statistical point of view. In addition, the results are unambiguous so that there is only a slight deviation between samples with different thickness.

4.2.4 Dispersion measurements

Spectroscopic mmW ellipsometry allows for detailed measurement of the refractive index of thin dielectrics over a wide frequency range. The method is therefore ideally suited for characterization of the strength of dispersion of a dielectric material, even if there is only a slight frequency dependence of the refractive index. For this purpose, the ellipsometer curves corresponding to the samples listed in Tables 4.1 and 4.2 were measured over the frequency range between 85 and 105 GHz in intervals of $\delta f = 1$ GHz. At every frequency point, the ellipsometer angles were evaluated in order to estimate the material parameters as described in section 3.3.2. The corresponding values of the refractive index are plotted over frequency in Figure 4.9. Since the thickness of the sample has no significant influence on the measurement results, only one sample made from FerroA6M-E, PVC and PMMA is shown for better clarity.

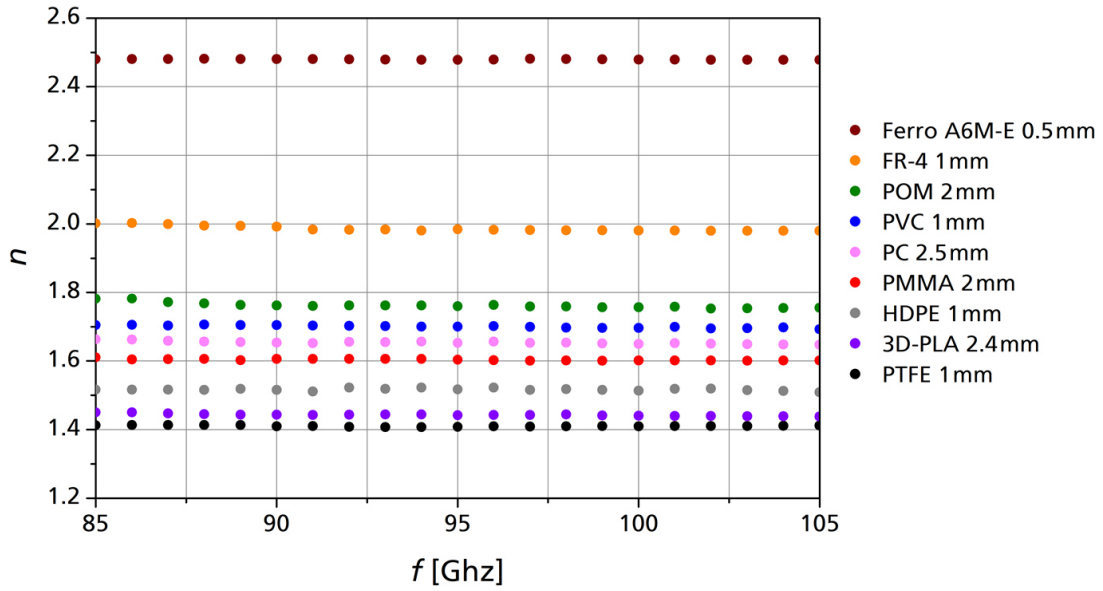

Figure 4.9: Measurement of the dispersion curves of various dielectric materials over the frequency range between 85 and 105 GHz. Spectroscopic mmW ellipsometry works well for both optimal and challenging samples.

As expected, the refractive indices corresponding to all the samples are unambiguously identifiable and the dispersion curves are comparably smooth. There are no notable outliers in any of the measurements. Furthermore, the novel method yields equally good results for the refractive index of both the challenging and the optimal samples. There is neither an obvious problem with very thin samples (0.5 mm) nor with particularly high ($n \approx 2.5$) or low ($n \approx 1.4$) refractive indices. Measurements of laminated and inhomogeneous materials are feasible. All results are in accordance with previously published values, where available (cf. Tables 4.1 and 4.2). Thus, compared to the standard method (cf. Figure 2.12), measurement accuracy is significantly enhanced by spectroscopic mmW ellipsometry using a metal substrate. Table 4.4 summarizes the average refractive index $\bar{n}$ and the corresponding standard deviation σ_n for all the samples under investigation. Therefore, the arithmetic mean of the measurements was calculated over the full frequency range. Since σ_n is one order of magnitude larger than the statistical error at single frequency measurements (cf. Table 4.3), there is a significant influence on the measurement which is related to the frequency. For an ideal, non-dispersive material, σ_n would directly represent the achievable measurement accuracy of the spectroscopic approach. However, the refractive index of most materials depends on the wavelength of the applied electromagnetic field. At microwave and millimeter wave frequency bands, material dispersion is mainly caused by dipolar relaxation (cf. section 2.1.2). Therefore, a Debye-type relaxation model is a good approximation for the evolution of the refractive index over mmW frequency bands:

$$n(f) = \sqrt{\epsilon_r^{\infty} + \frac{\epsilon_r^{0} - \epsilon_r^{\infty}}{1 + \gamma(f)^2}}, \tag{4.8}$$

Table 4.4: Average refractive index, standard deviation and relaxation time, measured for the frequency range between 85 GHz and 105 GHz.

Material	d [mm]	D [mm]	$\bar{n}$	σ_n	τ [ps]
Ceramic FerroA6M-E	0.9	175	2.479	0.001	8.1
Ceramic FerroA6M-E	0.5	175	2.481	0.001	7.3
Glass-reinforced epoxy laminate FR-4	1	300	1.986	0.008	56.5
Polyoxymethylene (POM)	2	200	1.762	0.008	58.3
Polyvinyl chloride (PVC)	2	200	1.700	0.004	37.4
Polyvinyl chloride (PVC)	1	200	1.701	0.004	35.8
Polycarbonate (PC)	2.5	250	1.654	0.004	44.2
Polymethyl methacrylate (PMMA)	2	200	1.604	0.003	25.2
Polymethyl methacrylate (PMMA)	1.5	200	1.605	0.003	24.6
High-density polyethylene (HDPE)	1	220	1.517	0.003	26.2
3D-printed polylactic acid (PLA)	2.4	200	1.443	0.003	9.4
Polytetrafluoroethylene (PTFE)	1	210	1.410	0.002	12.2

where ϵ_r^0 and ϵ_r^∞ are defined according to equations 2.5 and

$$\gamma(f) = 2\pi f \tau \frac{\epsilon_r^0 + 2}{\epsilon_r^\infty + 2}. \tag{4.9}$$

The parameters ϵ_r^0 and ϵ_r^∞ represent the hypothetical permittivity of the material for very low and very high frequencies, respectively. Since, the Debye relaxation model is not a valid approximation in these cases, ϵ_r^0 and ϵ_r^∞ are not actual physical properties of the material. Thus, the strength of dispersion is mainly related to the dipole relaxation time τ. Previous measurements indicate that τ is in the order of picoseconds for homogeneous polymers like PMMA or PVC [174–176]. Thus, the Debye relaxation model predicts that dielectric dispersion of common polymers or composites is comparably weak at mmW frequencies. If it can be reliably detected with spectroscopic mmW ellipsometry, this is a clear indication for high measurement accuracy.

Figure 4.10 shows an enlarged section of the dispersion measurements including the POM, PVC, PC and the PMMA sample. The Debye relaxation model (cf. equation 4.8) is fitted to the respective data in order to determine the dipole relaxation time τ. The model curves are represented by solid lines while the measured data is shown as filled circles. The determined relaxation times are summarized for all the samples in Table 4.4. Among this selection of materials, POM has the most dispersive refractive index. This is reflected by the steep slope of the Debye model and the comparably high value of the relaxation time τ. In contrast, PMMA is considerably less dispersive. This behavior has been previously observed in measurements using a free-space S-parameter method [97]. The refractive indices of the ceramic sample made from FerroA6M-E and of the low

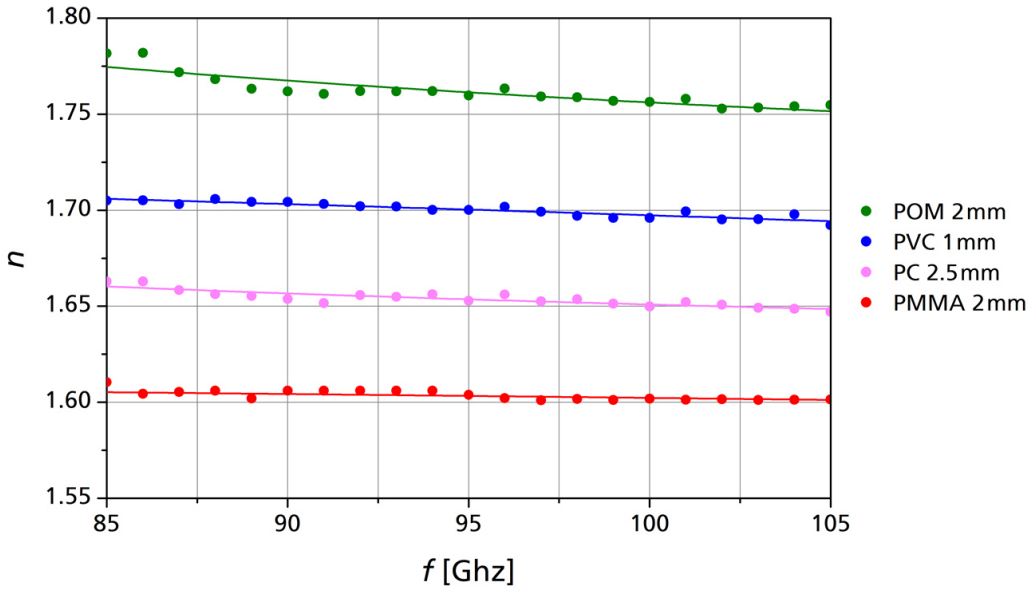

Figure 4.10: The strength of dispersion can be evaluated by fitting a Debye-type model to the measured data.

refracting materials PLA and PTFE are virtually constant over the frequency range between 85 GHz and 105 GHz and thus have the smallest relaxation times. In general, dispersion is too weak to be measured using spectroscopic mmW ellipsometry if τ is smaller than about 10 ps. For all the other samples, a slight decrease of the refractive index could be determined by means of the Debye relaxation model.

By comparing the standard deviation σ_n, corresponding to the average refractive index over the frequency range between 85 GHz and 105 GHz, to the respective dipole relaxation time τ, a clear correlation between these parameters can be found. A longer relaxation time implies a larger standard deviation. Thus, also σ_n is a good qualitative measure to estimate the strength of dispersion of a material, without further analysis. For virtually non-dispersive samples, such as FerroA6M-E or PTFE, the standard deviation is between $\sigma_n = 0.001$ and $\sigma_n = 0.002$. Accordingly, this defines the order of magnitude to which frequency stability of the refractive index is ensured. However, the parameter σ_n does, in general, not account for setup related errors. It is noteworthy that a very small relaxation time was measured for the 3D-printed PLA sample, but still σ_n is comparably large. Here, it is unlikely that the standard deviation is directly linked to dispersion. The reason for the comparably large value of σ_n is presumably caused by imprecisions in its thickness. The 3D printer that was used to fabricate this sample has a tolerance range of more than hundred micrometers. Since ellipsometry is very sensitive to the sample thickness, the refractive index measurement is more imprecise in this case.

4.2.5 Comparison of results

The main error sources for refractive index measurements are the dimension of the samples under investigation and line-of-sight loss due to antenna crosstalk. As shown in

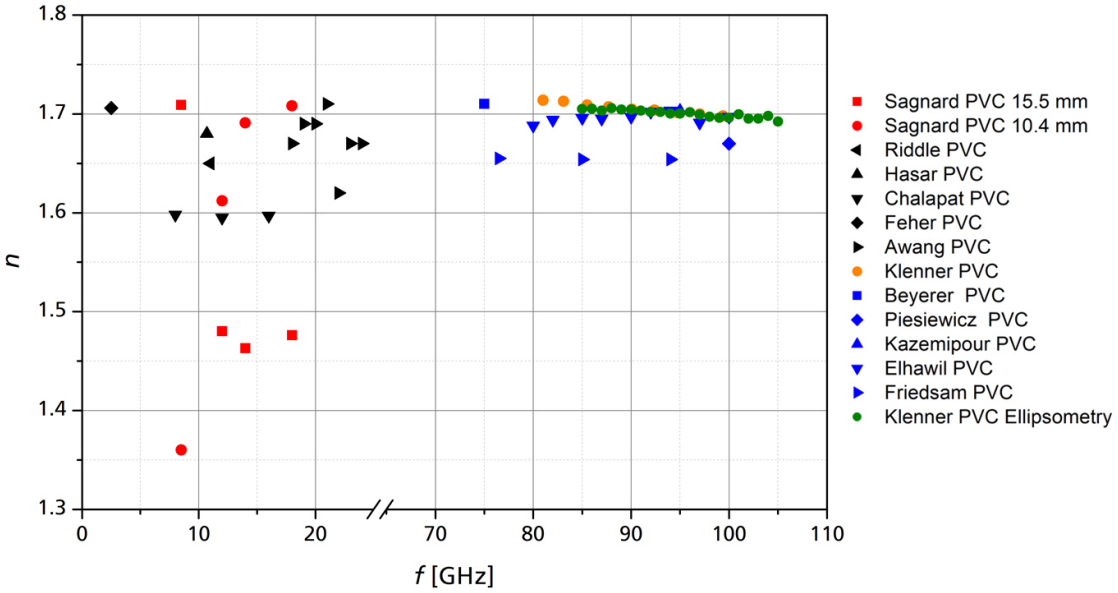

Figure 4.11: Comparison different microwave and millimeter wave measurements of the refractive index of PVC. on the left-hand side, the red data points show the results of conventional microwave ellipsometry and the black data points correspond to comparable S-parameter measurements. On the right-hand side, the green data points show the results of spectroscopic mmW ellipsometry. The blue and orange circles correspond to comparable S-parameter measurements. The orange data points have been measured by the author using a sample of exactly identical PVC.

Figure 4.5, an incidence angle of less than 60° is required to minimize line-of-sight interference effects. At this angle, the measured ellipsometer curve is falsified if the sample diameter is smaller than 175 mm (cf. Figure 4.4). Accordingly, if these two conditions are met, the statistical reproducibility and the frequency stability of the method are high so that the dispersion curves of the refractive index, obtained from mmW ellipsometry, are smooth and self-consistent with respect to sample thickness. This is already strong evidence that the improved method is not relevantly superimposed by systematic errors. The influence of possible misalignment of the Tx or Rx antennas or asymmetries in the beampath should depend on the sample thickness. In addition, the measured refractive indices are in accordance with previously published values, where available. However, comparison to other mmW refractive index measurements is difficult. The selection of comparable data is limited and the published values, even those corresponding to common, homogeneous polymers, typically differ by 5 % to 10 % between different experiments (cf. Table 4.1). Since the exact composition and processing of many modern dielectrics are confidential and vary from manufacturer to manufacturer, it is not feasible to determine whether this deviation is caused by slightly different material properties or imprecise measurements. Therefore it is particularly important to compare the results of spectroscopic mmW ellipsometry to independent measurements of samples made from exactly identical materials.

Figure 4.11 shows different measurements of the refractive index of PVC at frequencies around 10 GHz and 100 GHz. On the left-hand side, the results from con-

ventional microwave ellipsometry, which have already been shown in Figure 2.12, are summarized for better comparison. The red data points correspond to the ellipsometer measurements, while the black circles show results from other, comparable experiments [51, 52, 116–120]. On the right hand side, corresponding measurements in the frequency range around 100 GHz are summarized. The refractive index determined with spectroscopic mmW ellipsometry using a metal substrate is shown as green data points. For comparison, available data sets from other experiments, mostly based on classical S-parameter methods, are represented by blue symbols [90, 164, 177–179]. In addition, the orange data points show a mmW measurement, based on Fabry-Perot interferometry, where the material of the sample is exactly identical to the one used for spectroscopic mmW ellipsometry [97]. Since both of these independent PVC measurements are in very good accordance, possible systematic, setup related errors must be smaller than σ_n (cf. Table 4.4). Furthermore, the ellipsometer measurement is well within the confidence range of the other experiments, considering possible fabrication-related deviations in the dielectric properties of the different PVC samples.

4.2.6 Two-Point approximation

As shown in the previous section, the accuracy of spectroscopic mmW ellipsometry is significantly higher compared to the conventional approach. Unambiguous measurements are feasible with high frequency resolution and statistical reproducibility is high. The refractive index of a wide variety of samples can be reliably investigated as long as the sample size is at least 175 mm and the angle of incidence is not larger than 60°. Therefore, two of the main problems with conventional microwave ellipsometry are solved. However, the method still has the drawback of being comparably slow due to the mechanical rotation of the analyzer horn antenna. In section 3.4, it has been shown that a metallic substrate allows for an approximation method that reduces measurement time by a factor of about 100, if the absorbance of a sample is adequately low. The performance and limits of the methods have been investigated and discussed from a theoretical point of view. However, to ensure that the method does not falsify the result, it is obligatory to investigate the approximation method based on actual measurements.

PMMA is a comparably well known low-loss material. Several measurements of its loss tangent at mmW frequencies have been published previously. The values vary from $\tan\delta = 6 \times 10^{-4}$ to $\tan\delta = 30 \times 10^{-4}$ [152–154]. Thus, the material is a good reference for the two-point approximation. In contrast, the loss tangent of PVC is in the range between $\tan\delta = 50 \times 10^{-4}$ and $\tan\delta = 100 \times 10^{-4}$ [124, 180] at frequencies around 100 GHz. According to Figure 3.21, this corresponds to an amount of absorption that is just high enough to falsify the refractive index measurement, if the two-point approximation is used. Consequently, these materials are a good choice for experimental investigation of the approximation.

Figure 4.12 shows the refractive index of the 2 mm thick PMMA and PVC samples over the frequency range between 85 GHz and 105 GHz. For both measurements, the two-point approximation was used (blue data points) and is compared to the standard 360° analysis (red data points). While the approximation works well for the PMMA sample,

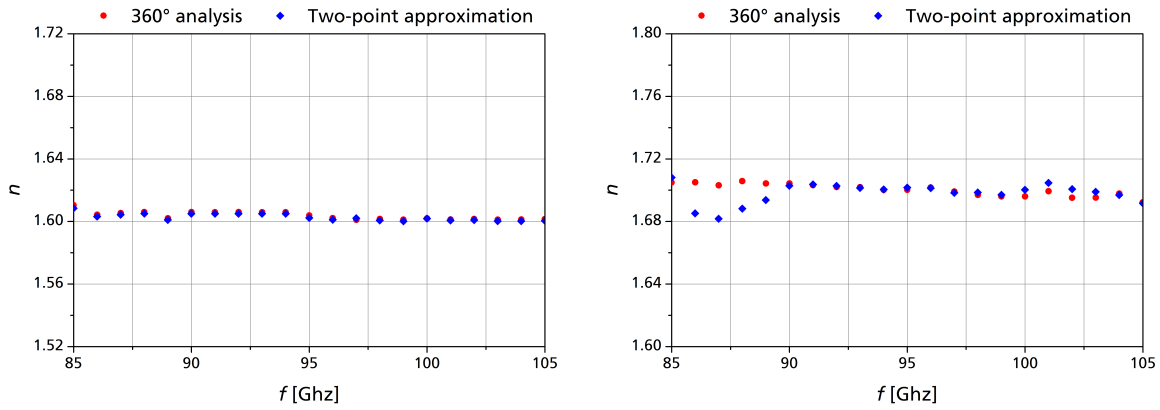

(a) PMMA sample (b) PVC sample

Figure 4.12: Refractive index measurement of 2 mm thick PMMA and PVC samples. The two-point approximation method works well for the low-loss PMMA sample but partly deviates from the 360° analysis for the PVC sample.

there is a noticeable deviation between the curves of the PVC samples at the frequency ranges around 87 GHz and 102 GHz. This is in good accordance with the simulations shown in Figure 3.21. Thus, the applicability of the approximation method can be estimated before the actual measurements. In addition, the two-point approximation can be used to qualitatively investigate the absorption of a sample. By comparison of the measured curves shown in Figure 4.12(b) to according simulations, an estimation of the lost tangent is feasible. In case of the PVC sample, Figure 3.21 indicates that the loss tangent will be in the range between $\tan\delta = 50 \times 10^{-4}$ and $\tan\delta = 100 \times 10^{-4}$, most likely closer to the higher value. Thus, this quick estimation is in accordance with previously published results.

4.3 Determination of the loss tangent

Precise characterization of the absorbance of a dielectric sample in the mmW regime is an even greater challenge than the measurement of the refractive index. Most plastic and building materials are fairly transparent for mmW radiation so that the measurands are only slightly influenced. Previously published values of the loss tangent at frequencies around 100 GHz vary by up to an order of magnitude between different free-space measurements of the same material [11, 12]. Conventional microwave ellipsometry seems to be particularly unfavorable. As shown in section 2.3.3, the loss tangent of a PVC sample is greatly overestimated compared to classical free-space methods. In addition, a relative measurement error of more than 38 % indicates, that conventional microwave ellipsometry is not suitable for reliable determination of the loss tangent. However, simulations show that spectroscopic mmW ellipsometry on a strongly reflecting substrate not only enhances the measurement accuracy with respect to the refractive index, but also is beneficial for loss tangent measurements (cf. Figure 3.19).

Table 4.5: Suitability of samples for loss tangent measurements using mmW ellipsometry.

Material	expected $\tan\delta \times 10^4$	suitable?
Polyoxymethylene (POM)	N/A	unknown
Polyvinyl chloride (PVC)	50-100 [123–125, 163, 164]	yes
Polycarbonate (PC)	1-25 [155–157]	no
Polymethyl methacrylate (PMMA)	5-75 [152–154]	yes
High-density polyethylene (HDPE)	1-3 [159–161]	no
Ceramic FerroA6M-E	50-150 [162]	yes
Glass-reinforced laminate FR-4	250-350 [147]	yes
3D-printed polylactic acid (PLA)	N/A	unknown
Polytetrafluoroethylene (PTFE)	3-6 [166–168]	no

In this section, it is shown that the loss tangent can indeed be determined with much higher precision compared to conventional microwave ellipsometry. However, the selection of suitable samples is restricted since very low-loss materials with $\tan\delta < 50 \times 10^{-4}$ can not be reliably characterized. Furthermore, small air gaps become a notable problem for thin samples such as the 0.5 mm thick FerroA6M-E ceramic platelet. Still, the method is powerful and yields good results for adequate samples.

4.3.1 Suitable samples

In addition to the requirements, which have been discussed in section 4.2.1, samples that can be used for reliable loss tangent measurements must fulfill further conditions. Simulations show that there is no measurable influence on the ellipsometer angle Ψ, if the absorption of mmW radiation within a material is very weak (cf. section 3.2.4). This allows for the two-point approximation, but has the drawback that it is not feasible to distinguish between low-loss materials with $\tan\delta < 50 \times 10^{-4}$ and hypothetical, ideal materials which are not absorbing at all. Accordingly, reliable loss tangent measurements are only possible for more strongly absorbing materials.

Table 4.5 summarizes available data on the loss tangent of the materials which have been selected for mmW ellipsometry in section 4.2.1. While there is no information available on the loss tangent of 3D-printed PLA and polyoxymethylene (POM) at frequencies around 100 GHz, the other materials can be classified in suitable and unsuitable samples. The glass-reinforced laminate FR-4 is the most strongly absorbing material and should be well suited for the loss tangent measurement. In contrast, the values available for PMMA and PVC are close to the minimal absorption that can theoretically be measured with the ellipsometer. There are experiments that report $\tan\delta > 50 \times 10^{-4}$ for both materials, but these samples are challenging. In the case of PC, HDPE and PTFE, absorption is too weak according to the simulations. Nevertheless, it is possible to evaluate

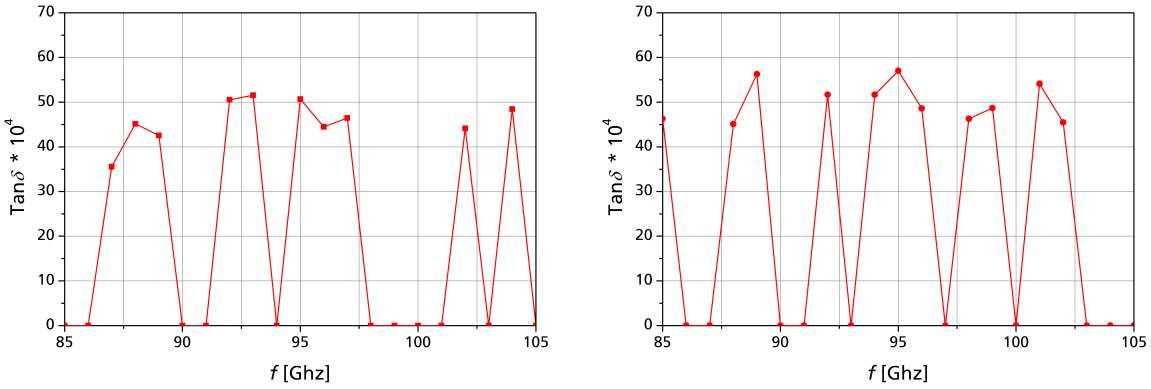

(a) HDPE sample (b) PTFE sample

Figure 4.13: Loss tangent of the weakly absorbing HDPE and PTFE samples. The optimization algorithm converges into zero if $\tan\delta$ is below a certain threshold. In this case, it is only feasible to state an upper limit of $\tan\delta \approx 50 \times 10^{-4}$.

the ellipsometer curves using the algorithm proposed in section 3.3.2. Thereby, both the refractive index and the loss tangent are obtained.

Figure 4.13 shows the result of this analysis for the HDPE and PTFE samples. For better clarity, the data points are connected by straight lines. The data is clustered in two groups. Some values are in the range around $\tan\delta \approx 50 \times 10^{-4}$ while the others are exactly at $\tan\delta = 0$. This behavior of the algorithm is typical for low loss samples. If $\tan\delta$ is smaller than about 40×10^{-4} to 50×10^{-4}, the influence of absorption is negligible in the optimization and the parameter converges into zero. At some frequencies, the algorithm did converge into a non-zero loss tangent, which is just strong enough to influence the optimization procedure. However, it should not be concluded that these data points represent the actual loss tangent of the sample. This is more likely an artifact of insufficient measurement accuracy. Generally, a significant amount of zeros in the loss tangent evaluation is a clear indicator that the sample is very weakly absorbing with an upper limit of $\tan\delta \approx 50 \times 10^{-4}$. This is already an important information since low-loss materials are desired for most modern mmW applications. In many cases, it is more important to ensure that attenuation of mmW radiation within the material is low or negligible than knowing the exact value of the loss tangent. Furthermore, the suitability of the unknown samples in Table 4.5 can be evaluated. Alongside the PC, HDPE and PTFE samples, also the analysis of the POM sample resulted in zeros in the loss tangent. Therefore, the material is considered as unsuitable for precise characterization of its absorbance using mmW ellipsometry. In contrast, the algorithm did properly converge in case of the 3D-printed PLA and the FerroA6M-E platelets as well as for the other samples from Tables 4.1 and 4.2.

4.3.2 Influence of sample thickness

As opposed to conventional microwave ellipsometry, the results of the refractive index measurement using spectroscopic mmW ellipsometry on a metal substrate do not de-

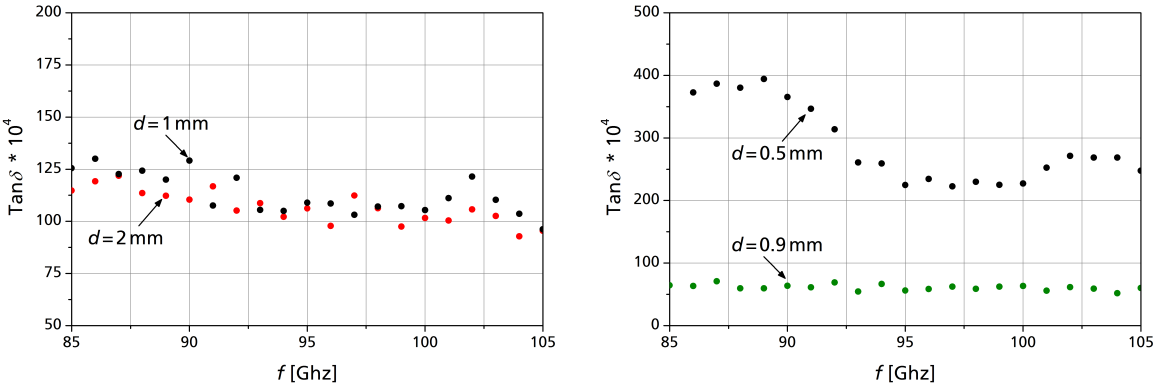

(a) PVC sample (b) FerroA6M-E sample

Figure 4.14: Influence of the sample thickness on the measured loss tangent. While the PVC measurements are in accordance, the loss tangent of the thin FerroA6M-E sample is overestimated, most likely due to a small air gap below the sample.

pend on the sample thickness. Even very thin samples with $d = 0.5\,\text{mm}$ can be reliably characterized as Figure 4.8 demonstrates. Since the loss tangent of a material mainly influences the ellipsometer angle Ψ, the expectable measurement accuracy is lower compared to the refractive index (cf. section 3.2.3). In addition, error sources like air gaps or antenna crosstalk seem to affect the ellipsometer angle Ψ more strongly than simulations predict (cf. Figure 4.3).

The attenuation of a microwave signal passing through a layer of dielectric material is exponentially decreasing with the layer thickness d, so that

$$P_{\text{out}} = P_{\text{in}} \exp\left(-\alpha_{\text{a}} d\right), \tag{4.10}$$

where P_{in} and P_{out} represent the power of the incoming and outgoing electromagnetic wave, and α_a is the attenuation coefficient of the material. For dielectrics with small loss where $\tan\delta \ll 1$, such as the samples shown in Table 4.5, α_{a} can be approximately related to the loss tangent [181, 182]:

$$\alpha_{\text{a}} \approx \frac{\pi f n}{c} \times \tan\delta. \tag{4.11}$$

Thus, the measurable attenuation between incoming and outgoing signals is very low if the sample thickness is in the micrometer regime. In case of the typical range of material parameters at mmW frequencies, the attenuation within a dielectric layer of 0.5 mm thickness is less than 1 % of the incoming signal. Even a very thin air gap of less than 30 µm can impact the result in this case. Therefore, the measurement of the loss tangent of thin samples is particularly challenging.

Figure 4.14 shows measurements of the loss tangent of four samples made from PVC and FerroA6M-E to investigate the influence of their thickness. The PVC samples are 1 mm and 2 mm thick, while the ceramic samples are thinner with a thickness of 0.9 mm and 0.5 mm. In comparison to the corresponding refractive index measurements (cf.

Figure 4.8), the relative divergence in the measured values is larger. Still, in case of the PVC sample, both curves are in good accordance with respect to the achieved accuracy. The relative difference between both measurements (cf. equation 4.4) is

$$\overline{\sigma}_{\mathrm{PVC}} = 7.4\,\% \tag{4.12}$$

and thus higher than the corresponding value obtained from the refractive index measurements (cf. equation 4.5). However, considering that $\overline{\sigma}_{\mathrm{PVC}}$ also suffers from the inaccuracy of the single measurements, and compared to the PVC measurement using conventional microwave ellipsometry (cf. section 2.3.3), where

$$\overline{\sigma}_{\mathrm{Std}} = 56.1\,\%, \tag{4.13}$$

this is a good result. In contrast, the loss tangent measurements of the FerroA6M-E samples are not consistent. The curve corresponding to the 0.5 mm thin sample resulted in strongly deviating values in the range around $\tan\delta = 300 \times 10^{-4}$. The 0.9 mm thick sample led to a more stable result at $\tan\delta \approx 60 \times 10^{-4}$. Accordingly, the relative difference between the measurements is very large:

$$\overline{\sigma}_{\mathrm{Ferro}} = 129\,\% \tag{4.14}$$

However, as the measurement of the thin sample is obviously falsified by a systematic effect, such as a significant air layer between sample and substrate (cf. section 4.1.1), $\overline{\sigma}_{\mathrm{Ferro}}$ is not a meaningful measure for the achievable accuracy in this case. The minimum thickness of samples, for which the loss tangent is not overestimated, also depends on the refractive index of the material in a nonlinear way. This can be shown by simulations similar to the ones in Figure 4.2. Thus, it is not feasible to quantitatively derive a limit which is generally valid for all the samples. Nevertheless, further experiments have revealed that a sample thickness of at least 1 mm is adequate to reduce the influence of air gaps for the selected samples in the current setup. If the sample stage of the ellipsometer is optimized to avoid air gaps, for instance by using a vacuum pump to place the samples, the minimal sample thickness for loss tangent measurements can be decreased.

4.3.3 Measurement results

One of the great benefits of ellipsometry is that, in general, two material parameters can be measured simultaneously [44, 45, 48]. There is no need for separate experiments to determine either the loss tangent or the refractive index. All the results on the loss tangent, which are presented in this section, were obtained from the same data and using the same algorithm that was used for evaluation of the refractive index in the previous section. However, the novel approach, using a strongly reflecting substrate, decouples the influence of the refractive index and the loss tangent on the measurement. In consequence, performance is significantly enhanced but the requirements on the samples are also decoupled. A material which is particularly well suited for measurement of the refractive index, such as a low loss dielectric, where the two-point approximation is

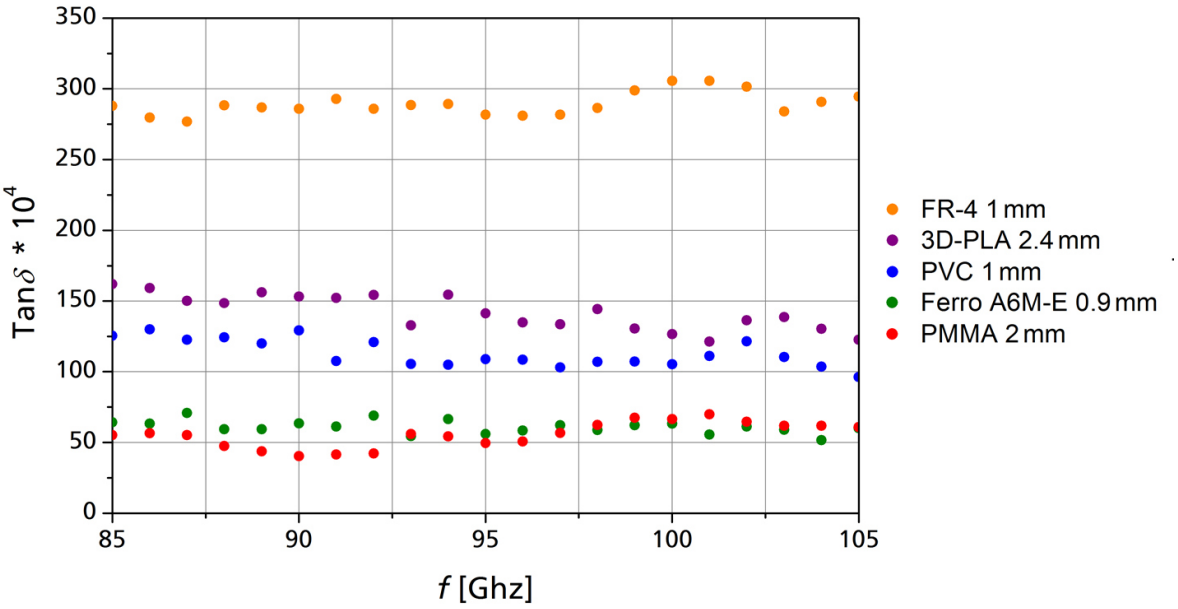

Figure 4.15: Loss tangent of several suitable samples atmmW frequencies. The lower limit for meaningful results is at $\tan\delta \approx 50 \times 10^{-4}$.

applicable, results in inconclusive data on the loss tangent as shown in Figure 4.13. On the other hand, for samples with high loss tangents, the two-point approximation is not valid so that measurement time must be increased, even if the refractive index is the main parameter of interest. If $\tan\delta > 500 \times 10^{-4}$, there is an increasing coupling between the ellipsometer angles Ψ and Δ, and the excellent measurement accuracy regarding the refractive index will most likely decrease (cf. Figure 3.16(b)). However, in practice, materials with such strong attenuation of mmW radiation only play a minor role, e.g. as dedicated mmW absorbers. Therefore, it is useful to discuss the requirements and results of the refractive index and the loss tangent measurements separately, even though the measured data and the processing algorithms are identical.

Figure 4.15 shows the loss tangent of the materials which have not been identified as unsuitable in Table 4.5, measured over the frequency range between 85 and 110 GHz. Only one sample thickness per material is shown for better clarity. Within the limits of accuracy of these measurements, slight dispersion effects can be suspected, but are not unequivocally apparent. The loss tangent of 3D-printed PLA, PVC and FerroA6M-E seems to be slightly decreasing, while the absorbance FR-4 and PMMA samples seems to be increasing with frequency. According to Figure 2.2, this indicates that the dipolar resonance frequency f_{max} is lower than 85 GHz for PLA, PVC and FerroA6M-E and higher than 105 GHz for FR-4 and PMMA. However, since the measurement accuracy is low compared to that of the dispersion curves of the refractive index, this behavior might also be caused by interfering effects instead of dipolar relaxation. A more quantitative analysis of the Debye parameters is therefore not meaningful.

The average values and the corresponding standard deviations are summarized in Table 4.6 for all the samples where the optimization algorithm did not converge into zeros. Apart from the 0.5 mm thin FerroA6M-E sample, where the loss tangent is clearly over-

Table 4.6: Average loss tangent and corresponding standard deviation, measured for the frequency range between 85 GHz and 105 GHz.

Material	d [mm]	D [mm]	$\overline{\tan\delta} \times 10^4$	$\sigma_{\tan\delta} \times 10^4$
Ceramic FerroA6M-E	0.5	175	288*	61*
Ceramic FerroA6M-E	0.9	175	61	5
Glass-reinforced epoxy laminate FR-4	1	300	289	8
Polyvinyl chloride (PVC)	2	200	107	8
Polyvinyl chloride (PVC)	1	200	113	10
Polymethyl methacrylate (PMMA)	2	200	55	9
Polymethyl methacrylate (PMMA)	1.5	200	52	7
3D-printed polylactic acid (PLA)	2.4	200	142	12

*Overestimation, most likely caused by an air gap between sample and substrate.

estimated (cf. Figure 4.14), the highest value was measured for the laminated FR-4 sample where $\tan\delta = (289 \pm 8) \times 10^{-4}$. This corresponds to a relative error of less than 3 %. In contrast, the lowest values that could be reliably determined using spectroscopic mmW ellipsometry are $\tan\delta = (52 \pm 7) \times 10^{-4}$ and $\tan\delta = (55 \pm 9) \times 10^{-4}$ for the PMMA sample. This corresponds to a maximum relative error of about 15 %. As expected from section 3.2.4, the measurement accuracy of the loss tangent increases with the absorbance of a material, but is considerably lower compared to that of the refractive index. This is a consequence of the decoupling of the ellipsometer angles Ψ and Δ and has been deliberately invoked to obtain the maximum accuracy on the refractive index measurement. However, the results for the loss tangent are in good accordance with previously published values (cf. Table 4.5) and the average error (excluding the 0.5 mm thin sample) is only about 9 %. This is also a very good result considering that samples with sub-wavelength thickness made from weakly absorbing materials have been chosen to demonstrate the full potential of the novel method.

4.4 Summary of experiments

The novel approach to mmW ellipsometry, that has been introduced in chapter 3, also induces new sources for systematic errors in the material parameter measurement. By specifically selecting samples with properties beyond the limits of the optimal working range of the ellipsometer (cf. Table 3.3), these error sources have been discussed based on actual measurements. At a maximum incidence angle of 60°, which is limited by antenna crosstalk, small samples with a diameter of 150 mm or less strongly influence the ellipsometer curve. Both, refractive index and loss tangent, are falsified in this case. Considering a safety margin for better placement of the samples, the measured minimal sample size is in good accordance with corresponding simulations. This is not the case for another significant error source, a small air layer that may occur between the sample

and the substrate. Its influence on the ellipsometer angle Ψ has turned out to be much stronger than predicted by simulations. Therefore the loss tangent measurement is more prone to error if thin samples with $d < 1\,\mathrm{mm}$ are investigated, where the influence of air gaps becomes considerable.

Using this information, a selection of samples has been presented to investigate the measurement accuracy with respect to the refractive index and the loss tangent for optimal and challenging conditions. It includes established homogeneous plastic and building materials, which have been comparably well characterized at mmW frequencies, such as PVC or PMMA as well as modern ceramic and composite materials or inhomogeneous, 3D-printed samples. The statistical reproducibility of the measurements is very high with a relative standard deviation of less than $0.05\,\%$, independently of the material. In addition, it has been shown that the results are unambiguous, consistent and the accuracy is high enough to reveal even weak dispersion effects of the refractive index. Furthermore, the measurements do not depend on the thickness of the sample and are in accordance with previously published results where available. Compared to previous approaches to microwave ellipsometry, this is a considerable improvement. As long as the loss tangent of a material is not significantly higher than 50×10^{-4}, the two-point approximation can be safely used to reduce the measurement time. The enhancement of the performance of mmW ellipsometry is based on the decoupling of the dependence of the ellipsometer angles Ψ and Δ on the refractive index and the loss tangent. In consequence, measurement of the loss tangent is a challenging task and the selection of suitable samples for spectroscopic mmW ellipsometry is more limited. Nevertheless, as long as $\tan\delta > 50 \times 10^{-4}$ and the sample thickness is at least $1\,\mathrm{mm}$, an uncertainty of averagely $9\,\%$ can be achieved. This also is a very good result compared to previous publications.

In summary, the experiments have essentially verified the predicted improvement of the performance of mmW ellipsometry using a strongly reflecting substrate, in both optimal and challenging cases. The novel method is therefore particularly interesting for detailed and accurate measurements of the refractive index of thin, dielectric samples over wide mmW frequency bands. Thus, it seems predefined for many industrial applications. Not only for characterization of modern vehicle parts, behind which millimeter wave sensors are placed for autonomous driving, but also for precise measurement of the geometry of plastic sheets or pipes or the analysis of laminated structures such ar wind power blades with respect to possible defects. In addition, spectroscopic mmW ellipsometry can be used to reliably determine whether or not the absorbance of a sample is stronger than $\tan\delta \approx 50 \times 10^{-4}$. In most cases, this information is already sufficient, e.g. to decide whether the attenuation within a material is low enough to be interesting for building a mmW sensor or dielectric focusing elements such as radar lenses. For more strongly absorbing materials, the exact value of the loss tangent can be determined with comparably high accuracy. This allows to classify materials that are used for building absorbers which are also important parts in many modern mmW sensors.

5 Conclusions

Precise characterization of novel dielectric materials at frequencies around 100 GHz and higher is an inevitable challenge in the development of the next generation of robust and versatile mmW sensors and sensor systems. Virtually any mmW signal that is used in advanced radar or communication systems interferes with dielectric materials in its surrounding. For instance, fully autonomous driving requires sophisticated signal analysis of radar sensors that are placed behind the vehicle chassis. Unknown or imprecise material parameters make this task unfeasible. Since mmW propagation is governed by the principles of refraction and diffraction, precise material measurements at this frequency range is a demanding task. A promising approach to mmW material characterization is to set up a free-space reflectometer and measure the scattering parameters over a preferably wide bandwidth using a vector network analyzer. Even though this method is now well established in mmW material characterization, it still has serious drawbacks, particularly with regard to industrial applications. Its accuracy depends to a large extend on the calibration of the measurement equipment, which can be complicated or even unfeasible, depending on the exact setup. Consequently, the method is not only less accurate than desired, but also cost-intensive and limited with respect to the range of samples that can be investigated. Thin or dispersive materials can, in general, not be satisfyingly characterized at mmW frequencies using conventional free-space methods.

Apart from classical S-parameter measurements, spectroscopic ellipsometry, a well established measurement technique at visible or infrared wavelengths, shows great promise to overcome the main challenges in mmW material analysis. Optical ellipsometry is not only very sensitive to small changes in the material parameters, but also allows for characterization of samples that are much thinner than the corresponding wavelength. In addition, in contrast to classical reflectometry, two material parameters can be determined simultaneously from a single measurement. A successful adaption of ellipsometry to the mmW regime could overcome some of the main limitations of state-of-the art material characterization at frequencies around 100 GHz. However, previous attempts have revealed that the experimental realization of microwave or mmW ellipsometry is more challenging than expected and that the method is inferior compared to other, more established methods. There are three core problems that must be solved in order to reliably adapt ellipsometry to the mmW regime: Insufficient measurement accuracy, ambiguous results and slow measurement speed. Only then can ellipsometry be a genuine improvement to mmW material analysis that opens up new applications, particularly in the automotive industry, where precise characterization of thin dielectric layers at mmW frequencies will be a major challenge in the near future.

In this thesis, a novel approach to mmW ellipsometry has been presented that addresses all of these challenges. Using a compact and versatile experimental setup, a comprehensive analysis of the critical measurands and how they influence the achievable

accuracy of mmW ellipsometry has been performed. It has been found that a strongly reflecting substrate is mandatory to not only improve the sensitivity of the measurement, but also to allow for unambiguous material parameter estimation and an approximation method that significantly reduces measurement time in many cases.

Spectroscopic mmW ellipsometry on a metal substrate

Since every ellipsometer curve is sinusoidal and can be normalized with respect to its average value for further analysis, the actual measurement is fully characterized by the maximum power $(P_{\mathrm{Rx}}/P_0)^{\max}$ and the corresponding angle of the Rx antenna $\phi_{\mathrm{A}}^{\max}$. Consequently, precise measurement of these two parameters is crucial for a reliable material parameter estimation. While $(P_{\mathrm{Rx}}/P_0)^{\max}$ can be measured accurately using modern power meters or spectrum analyzers, the uncertainty on the $\phi_{\mathrm{A}}^{\max}$ measurement is significant due to the polarization loss of the horn antennas. Using the standard approach to microwave ellipsometry, where the sample is surrounded by air, the real material parameters, such as the refractive index or the thickness, mainly influence $\phi_{\mathrm{A}}^{\max}$. Accordingly, measurement accuracy is insufficient. In addition, most dielectrics are relatively weakly absorbing in the mmW regime so that only a small amount of the transmitted signal is reflected to the receiver. Thus, also the imaginary part of the dielectric function can not be measured precisely. Since a deviation from the optimal angle of incidence would significantly reduce measurement accuracy, the only possibility to influence the outcome of the measurement independently from the sample, is by using an appropriate substrate. As shown in section 3.2, simulations based on different material models have revealed that a strongly reflecting metal, such as a copper or aluminum plate, inverts the influence of the material parameters on the measurements. If the loss tangent of a material is not higher than about 500×10^{-4}, the real material parameters only influence $(P_{\mathrm{Rx}}/P_0)^{\max}$, while a variation of the imaginary part of the dielectric function is exclusively reflected in $\phi_{\mathrm{A}}^{\max}$. Using this approach, the measurement accuracy regarding the refractive index has been significantly improved. However, at fixed frequencies the results are still ambiguous and the precision regarding the loss tangent is insufficient.

To attain the full potential of mmW ellipsometry, the method needs to be combined with the classical strengths of spectroscopic reflectometry by evaluating ellipsometric parameters along with interference effects over a wide bandwidth. As shown in section 3.3, the metallic substrate does not only decouple the influence of the material parameters on the ellipsometer measurement, but also enhances Fabry-Perot reflections within the dielectric. Thus, a more distinct power spectrum is obtained and even small differences in the refractive index down to $\delta n = 0.01$ can be unequivocally identified from the $(P_{\mathrm{Rx}}/P_0)^{\max}$ over f curve. In addition, measurement accuracy concerning the loss tangent greatly benefits from the spectroscopic approach. By evaluation of the frequency dependence of $\phi_{\mathrm{A}}^{\max}$, it has been shown that even the loss tangent of low-loss dielectrics can be accurately determined down to a lower limit of $\tan\delta \approx 50 \times 10^{-4}$. Simulated variations of only 0.001 are clearly distinguishable. In any case, the algorithm is well suited to determine whether or not the absorbance of a material is below the lower limit. Since low-loss materials are desired for most practical mmW applications, this is typically a more essential information than knowledge of the exact value of the loss tangent.

In the case of low-loss samples with $\tan\delta < 75 \times 10^{-4}$, using a metal substrate for mmW ellipsometry allows for an approximation method. Instead of a full rotation of the Rx antenna, it is sufficient to determine the power spectrum at only two analyzer angles. Thereby, mechanical movement is minimized and measurement time can be reduced by more than two orders of magnitude.

Measurement results

While mmW ellipsometry on a metal substrate is advantageous over the conventional approach from a theoretical point of view, it also involves new sources for errors. A small, unintentional air gap might occur between the dielectric and the substrate, when the sample is placed onto the ellipsometer. Repeated measurements have shown that air gaps are unproblematic if the refractive index is the main property of interest. However, the accuracy on the loss tangent suffers more strongly than expected from according simulations, particularly if the thickness of the sample is less than 1 mm. In this case, even a thin air gap of less than 30 µm influences the measurement. Furthermore, the strongly reflecting substrate falsifies the measurement if the dielectric platelets are too small or improperly placed. It has been demonstrated that a minimum sample diameter of $D = 150\,\text{mm}$ is sufficient to avoid significant reflections from the area around the sample, including a safety margin for appropriate placement.

Considering these fundamental limitations on the samples that can be used for mmW ellipsometry, a selection of materials has been chosen to demonstrate the performance of the novel method under optimal conditions as well as for more challenging cases. The dielectric properties of most homogeneous plastic and building materials, such as PMMA, PVC or HDPE, are within the optimal working range of the ellipsometer and have been comparably well characterized at mmW frequencies before. In contrast, there is little or no knowledge on the material parameters of modern laminates, ceramics or 3D-printed materials. Using spectroscopic mmW ellipsometry on a metal substrate, detailed and unambiguous dispersion curves have been measured for both optimal and challenging samples over a bandwidth of 25 GHz. A statistical analysis has demonstrated that the reproducibly of the ellipsometer measurement is very high. The average refractive index from 50 identical measurements is precise up to the forth decimal for both challenging and optimal samples. In addition, frequency stability of the spectroscopic measurements is high enough to reveal even weak dispersion in the refractive index by comparison to a Debye relaxation model as shown in section 4.2. Measurements of virtually non-dispersive materials, such as PTFE, have revealed that the standard deviation of the refractive index over the full frequency band is between $\sigma_n = 0.001$ and $\sigma_n = 0.002$. Since the determined values of the refractive index are in very good accordance with the results of other independent measurements (where available), setup related errors must be smaller than σ_n. In consequence, also the validity of the two-point approximation is in good accordance with the theoretical prediction and can be safely used for most low loss materials. Compared to the conventional approach to microwave ellipsometry this is a considerable improvement in measurement accuracy and measurement speed. In contrast to the refractive index, the analysis of the loss tangent is more limited. It has been shown that the algorithm is only capable of processing data from samples with

$\tan\delta > 50 \times 10^{-4}$. In addition, even small air layers of less than 30 µm between the dielectric and the substrate significantly falsify the measurement if the sample is thinner than about 1 mm. Nevertheless, the measured values are in accordance with previously published results and the average error over a frequency range of 25 GHz is only about 9 %. This is a very good result, considering that the method has been deliberately optimized for refractive index measurements.

Outlook

When ellipsometry was first considered at microwave frequencies, a straightforward approach to its experimental realization was chosen in order to investigate the general applicability of the method to the microwave regime. Therefore, the simplest case, homogeneous single-layer samples surrounded by air, was detailedly investigated throughout several measurements. In this thesis, an additional degree of freedom, a substrate on which the samples are placed, has been introduced to the method. By adjusting the theoretical framework of microwave ellipsometry, the desired properties of the substrate have been determined in a way to optimize the method for refractive index measurements. However, the formalism which has been developed in this thesis might also be used to find a substrate that allows for more precise absorption measurements. In general, an interesting task for future studies is to investigate the influence of more complex materials. The next logical step is to replace the single-layer sample on a substrate by a multilayer structure. At infrared or visible wavelengths, ellipsometry is already successfully used to characterize complex layered samples, such as hyperbolic metamaterials or organic structures [183–185]. Therefore, the two-layer configuration that has been presented in this thesis, must be extended to an n-layer system and corresponding multi-parameter models must be derived along with appropriate algorithms for processing.

In conclusion, spectroscopic ellipsometry is a promising method to further enhance the possibilities of microwave and mmW material characterization. Apart from the high measurement accuracy regarding the refractive index of dielectric samples with subwavelength thickness, the method also offers good prospects for investigation of material parameters of more complex structures. This makes the method particularly interesting for investigation of materials that are used for quasi-optical focusing of mmW communication signals or thin dielectric layers that interfere with a sensor signal, such as the parts of a vehicle chassis behind which mmW radars are placed. Since the development of novel plastic and building materials is also a vivid field of research [186–189], accurate mmW material characterization also is a key task for numerous future applications that are yet incalculable. Spectroscopic mmW ellipsometry on metal substrates can thereby play an important role to complement and verify the corresponding catalog of material parameters at frequencies around 100 GHz and higher.

Bibliography

[1] Millman. *Microelectronics*. en. McGraw-Hill Education Pvt Limited, 2001.

[2] J. C. Whitaker. *Microelectronics 2nd Edition*. en. CRC Press, Nov. 2005.

[3] A. Mcafee and E. Brynjolfsson. *The Second Machine Age*. de. Plassen Verlag, Oct. 2014.

[4] K. Schwab. *The Fourth Industrial Revolution*. en. World Economic Forum, Jan. 2016.

[5] B. Müller, O. Herzog, and K.-I. Eiermann. *Advanced Manufacturing Industry 4.0 and Urban Development: Discussion Paper*. en. 2014.

[6] A. Gilchrist. *Industry 4.0: The Industrial Internet of Things*. en. Apress, June 2016.

[7] S. Yurish. *Sensors and Signals*. en. IFSA Publishing, Oct. 2015.

[8] J. A. Nanzer. *Microwave and Millimeter-wave Remote Sensing for Security Applications*. en. Artech House, 2012.

[9] Z. Tong. *Silicon Millimeter-Wave Imaging Systems for Security and Biomedical Applications*. en. North Carolina State University, 2015.

[10] H. Jo et al. *Biomedical Engineering: Frontier Research and Converging Technologies*. en. Springer, July 2015.

[11] A. J. Bur. "Dielectric properties of polymers at microwave frequencies: a review". In: *Polymer* 26.7 (1985), pp. 963–977.

[12] J. W. Lamb. "Miscellaneous data on materials for millimetre and submillimetre optics". en. In: *International Journal of Infrared and Millimeter Waves* 17.12 (Dec. 1996), pp. 1997–2034.

[13] V. R. K. Murthy, S. Sundaram, and B. Viswanathan. *Microwave Materials*. en. Springer Science & Business Media, Mar. 2013.

[14] A. K. Kulshreshtha and C. Vasile. *Handbook of Polymer Blends and Composites*. en. iSmithers Rapra Publishing, 2002.

[15] B. Cantor, P. Grant, and C. Johnston. *Automotive Engineering: Lightweight, Functional, and Novel Materials*. en. CRC Press, Feb. 2008.

[16] S. Thomas et al. *Handbook of Biopolymer-Based Materials: From Blends and Composites to Gels and Complex Networks*. en. John Wiley & Sons, Apr. 2013.

[17] A. Bandyopadhyay and S. Bose. *Additive Manufacturing*. en. CRC Press, Sept. 2015.

[18] M. Schiementz. *Postprocessing Architecture for an Automotive Radar Network*. en. Cuvillier Verlag, 2005.

[19] V. Issakov. *Microwave Circuits for 24 GHz Automotive Radar in Silicon-based Technologies*. en. Springer Science & Business Media, Aug. 2010.

[20] D. Kissinger. *Millimeter-Wave Receiver Concepts for 77 GHz Automotive Radar in Silicon-Germanium Technology*. en. Springer Science & Business Media, Mar. 2012.

[21] V. Jain and P. Heydari. *Automotive Radar Sensors in Silicon Technologies*. en. Springer Science & Business Media, Sept. 2012.

[22] *Sensors and Data Management for Autonomous Vehicles report 2015*. Tech. rep. Yole Développement group, Oct. 2015.

[23] J Wenger. "Automotive mm-wave radar: Status and trends in system design and technology". In: *Automotive Radar and Navigation Techniques (Ref. No. 1998/230), IEE Colloquium on*. IET. 1998, pp. 1–1.

[24] J. Wenger. "Automotive radar-status and perspectives". In: *Compound Semiconductor Integrated Circuit Symposium, 2005. CSIC'05. IEEE*. IEEE. 2005, 4–pp.

[25] H. H. Meinel. "Evolving automotive radar?From the very beginnings into the future". In: *Antennas and Propagation (EuCAP), 2014 8th European Conference on*. IEEE. 2014, pp. 3107–3114.

[26] R. K. Jurgen. *Adaptive cruise control*. Tech. rep. SAE Technical Paper, 2006.

[27] A. Vahidi and A. Eskandarian. "Research advances in intelligent collision avoidance and adaptive cruise control". In: *IEEE transactions on intelligent transportation systems* 4.3 (2003), pp. 143–153.

[28] S. Heuel and H. Rohling. "Pedestrian classification in automotive radar systems". In: *Radar Symposium (IRS), 2012 13th International*. IEEE. 2012, pp. 39–44.

[29] E. Schubert et al. "Target modeling and deduction of automotive radar resolution requirements for pedestrian classification". In: *International Journal of Microwave and Wireless Technologies* 7.3-4 (2015), pp. 433–441.

[30] L. F. Chen et al. *Microwave Electronics: Measurement and Materials Characterization*. English. 1 edition. Chichester: Wiley, Apr. 2004.

[31] R. D. Hollinger et al. "Microwave characterization of dielectric materials from 8 to 110 GHz using a free-space setup". en. In: *Microwave and Optical Technology Letters* 26.2 (July 2000), pp. 100–105.

[32] J. Krupka. "Frequency domain complex permittivity measurements at microwave frequencies". en. In: *Measurement Science and Technology* 17.6 (2006).

[33] A. Kumar, S. Sharma, and G. Singh. "Measurement of Dielectric Constant and Loss Factor of the Dielectric Material at Microwave Frequencies". English. In: *Progress In Electromagnetics Research* 69 (2007), pp. 47–54.

[34] J. W. Schultz. *Focused Beam Methods: Measuring Microwave Materials in Free Space*. en. John Schultz, Oct. 2012.

[35] U. Bakshi and V. U. Bakshi. *Electronic Measurements*. en. Technical Publications, Jan. 2007.

[36] E. DeRijk. "Mm-wave and Terahertz (THz) Materials Measurements and Characterization". In: *European Microwave Week (EuMW)*. Paris, 2015.

[37] F. Gerhardes and D. Nüßler. "E-Band Material Characterization - Using a Unique and Novel VNA Architecture". In: *European Microwave Week (EuMW)*. London, 2016.

[38] M. Hiebel. *Fundamentals of Vector Network Analysis*. en. Rohde & Schwarz, 2007.

[39] N. Shoaib. *Vector Network Analyzer (VNA) Measurements and Uncertainty Assessment*. en. Springer, Oct. 2016.

[40] F. Purroy and L. Pradell. "New theoretical analysis of the LRRM calibration technique for vector network analyzers". In: *IEEE Transactions on Instrumentation and Measurement* 50 (Oct. 2001), pp. 1307–1314.

[41] D. F. Williams, J. C. M. Wang, and U. Arz. "An optimal vector-network-analyzer calibration algorithm". In: *IEEE Transactions on Microwave Theory and Techniques* 51.12 (Dec. 2003), pp. 2391–2401.

[42] U. Stumper and T. Schrader. "Influence of Different Configurations of Non-ideal Calibration Standards on Vector Network Analyzer Performance". In: *IEEE Transactions on Instrumentation and Measurement* 61.7 (July 2012).

[43] A. A. Savin et al. "Estimation of complex residual errors of calibrated two-port vector network analyzer". In: *Microwave Measurement Conference (ARFTG), 2014 83rd ARFTG*. June 2014, pp. 1–4.

[44] R. M. A. Azzam and N. M. Bashara. *Ellipsometry and polarized light*. en. North-Holland, Apr. 1987.

[45] H. Tompkins and W. McGahan. *Spectroscopic ellipsometry and reflectometry: a user's guide*. English. New York: Wiley, 1999.

[46] H. Fujiwara. *Spectroscopic Ellipsometry: Principles and Applications*. en. John Wiley & Sons, Sept. 2007.

[47] P. Drude. "Ueber die Gesetze der Reflexion und Brechung des Lichtes an der Grenze absorbirender Krystalle". en. In: *Annalen der Physik* 268.12 (Jan. 1887), pp. 584–625.

[48] H. Tompkins, E. Irene, and E. A. Haber. *Handbook of Ellipsometry*. Englisch. Norwich, NY : Heidelberg, Germany: William Andrew Inc, Jan. 2005.

[49] P. Stetiu and B. Hannover. "Ellipsometrie en microondes". In: *Journees Caracterization Microondes et Materiaux*. Mar. 2000, pp. 281–284.

[50] F. Sagnard, D. Seetharamdoo, and V. Le Glaunec. “Reflection and transmission ellipsometry data analysis for measuring the complex permittivity of a single layer material at microwave frequencies”. en. In: *Microwave and Optical Technology Letters* 33.6 (June 2002), pp. 443–448.

[51] F. Sagnard, F. Bentabet, and C. Vignat. “In situ measurements of the complex permittivity of materials using reflection ellipsometry in the microwave band: theory (part I)”. In: *IEEE T. Instrumentation and Measurement* 54.3 (2005), pp. 1266–1273.

[52] F. Sagnard, F. Bentabet, and C. Vignat. “In situ measurements of the complex permittivity of materials using reflection ellipsometry in the microwave band: experiments (Part II)”. In: *IEEE T. Instrumentation and Measurement* 54.3 (2005), pp. 1274–1282.

[53] Y. Xianwang, J. Minning, and L. Mingxiang. “Numerical Simulation of Ellipsometry Measurement in Millimeter-Wave Band”. In: *2008 China-Japan Joint Microwave Conference*. Sept. 2008, pp. 723–726.

[54] K. Tsuzukiyama et al. “Ellipsometry for Measurement of Complex Dielectric Permittivity in Millimeter-Wave Region”. In: IEEE, Oct. 2003, pp. 487–490.

[55] L. R. Lawson and H. A. Yousif. “Standing Wave Effects in Microwave Ellipsometry”. English. In: *Progress In Electromagnetics Research Letters* 14 (2010), pp. 51–58.

[56] P. I. Deffenbaugh, R. C. Rumpf, and K. H. Church. “Broadband Microwave Frequency Characterization of 3-D Printed Materials”. In: *IEEE Transactions on Components, Packaging and Manufacturing Technology* 3.12 (Dec. 2013), pp. 2147–2155.

[57] J.-M. L. Floch et al. “Dielectric material characterization techniques and designs of high-Q resonators for applications from micro to millimeter-waves frequencies applicable at room and cryogenic temperatures”. In: *Review of Scientific Instruments* 85.3 (Mar. 2014), p. 031301.

[58] R. G. Pierce et al. “SU-8 2000 Millimeter Wave Material Characterization”. In: *IEEE Microwave and Wireless Components Letters* 24.6 (June 2014), pp. 427–429.

[59] X. Wang and A. Stelzer. “Millimeter-Wave Material Characterization Using Laminated Waveguides”. In: *IEEE Transactions on Microwave Theory and Techniques* 62.8 (Aug. 2014), pp. 1762–1771.

[60] H. P. Fu, C. Yang, and J. G. Ma. “Challenges of measuring the complex permittivity and permeability of thin materials in millimeter wave regimes”. In: July 2016, pp. 1–2.

[61] S. Kim et al. “A Free-Space Measurement Method for the Low-Loss Dielectric Characterization Without Prior Need for Sample Thickness Data”. In: *IEEE Transactions on Antennas and Propagation* 64.9 (Sept. 2016), pp. 3869–3879.

[62] W. Bolton. *Electrical and Magnetic Properties of Materials*. English. Longman, Dec. 1991.

[63] B. H. Bransden and C. J. Joachain. *Physics of Atoms and Molecules*. English. 2 edition. Harlow, England ; New York: Pearson, June 2003.

[64] E. Fermi. "Zur Quantelung des idealen einatomigen Gases". In: *Zeitschrift für Physik* 36.11-12 (1926), pp. 902–912.

[65] P. A. Dirac. "On the theory of quantum mechanics". In: *Proceedings of the Royal Society of London A: Mathematical, Physical and Engineering Sciences*. Vol. 112. 762. The Royal Society. 1926, pp. 661–677.

[66] H. V. Keer. *Principles of the Solid State*. en. New Age International, Jan. 1993.

[67] B. V. Suresh. *Solid State Devices and Technology*. en. Pearson Education India, Sept. 2010.

[68] P. YU and M. Cardona. *Fundamentals of Semiconductors: Physics and Materials Properties*. en. Springer Science & Business Media, Apr. 2010.

[69] P. Hofmann. *Solid State Physics: An Introduction*. en. John Wiley & Sons, Nov. 2011.

[70] P. Robert. *Electrical and Magnetic Properties of Materials*. English. Norwood, MA: Artech House Publishers, June 1988.

[71] P. S. Neelakanta. *Handbook of Electromagnetic Materials: Monolithic and Composite Versions and Their Applications*. en. CRC Press, June 1995.

[72] K. S. Cole and R. H. Cole. "Dispersion and absorption in dielectrics I. Alternating current characteristics". In: *The Journal of chemical physics* 9.4 (1941), pp. 341–351.

[73] K. S. Cole and R. H. Cole. "Dispersion and absorption in dielectrics II. Direct current characteristics". In: *The Journal of Chemical Physics* 10.2 (1942), pp. 98–105.

[74] J. C. Slater and N. H. Frank. *Electromagnetism*. en. Courier Corporation, Mar. 2012.

[75] F. Kremer and A. Schönhals, eds. *Broadband Dielectric Spectroscopy*. en. Berlin, Heidelberg: Springer Berlin Heidelberg, 2003.

[76] E. L. Ginzton. *Microwave measurements*. en. McGraw-Hill, 1957.

[77] M. N. Afsar et al. "The measurement of the properties of materials". In: *Proceedings of the IEEE* 74.1 (Jan. 1986), pp. 183–199.

[78] D. L. Hollway and G. J. A. Cassidy. "An instrument for dielectric measurements in the frequency range 100-300 Mc/s". In: *Proceedings of the IEE - Part III: Radio and Communication Engineering* 99.62 (Nov. 1952), pp. 364–372.

[79] J. Baker-Jarvis. *Transmission/reflection and short-circuit line permittivity measurements*. eng. National Institute of Standards and Technology (U.S.)

[80] W. C. Chew, K. J. Olp, and G. P. Otto. "Design and calibration of a large broadband dielectric measurement cell". In: *IEEE Transactions on Geoscience and Remote Sensing* 29.1 (Jan. 1991), pp. 42–47.

[81] J. Baker-Jarvis et al. *Transmission/reflection and short-circuit line methods for measuring permittivity and permeability*. eng. National Institute of Standards and Technology (U.S.), 1992.

[82] Z. Abbas, R. D. Pollard, and R. W. Kelsall. "Determination of the dielectric constant of materials from effective refractive index measurements". In: *IEEE Transactions on Instrumentation and Measurement* 47.1 (Feb. 1998), pp. 148–152.

[83] N. Marcuvitz. *Waveguide Handbook*. en. IET, 1951.

[84] Z. Abbas, R. D. Pollard, and R. W. Kelsall. "A rectangular dielectric waveguide technique for determination of permittivity of materials at W-band". In: *IEEE Transactions on Microwave Theory and Techniques* 46.12 (Dec. 1998), pp. 2011–2015.

[85] R. Luebbers. "Effects of waveguide wall grooves used to hold samples for measurement of permittivity and permeability". In: *IEEE Transactions on Microwave Theory and Techniques* 41.11 (Nov. 1993), pp. 1959–1964.

[86] J. Musil and F. Zacek. "Microwave Measurements of Complex Permittivity by Free Space Methods and Their Applications.(Translation)". In: *Academia, 1986,* (1986), p. 275.

[87] E. Nyfors. "Industrial Microwave Sensors: A Review". en. In: *Subsurface Sensing Technologies and Applications* 1.1 (2000), pp. 23–43.

[88] R. G. Nitsche, J. Preissner, and E. M. Biebl. "A free space technique for measuring the complex permittivity and permeability in the millimeter wave range". In: *Microwave Symposium Digest, 1994., IEEE MTT-S International*. May 1994, 1465–1468 vol.3.

[89] A. C. Lynch et al. "Free-wave measurement of permeability and permittivity of ferrites at millimetre-wave frequencies". In: *IEE Proceedings - Science, Measurement and Technology* 142.2 (Mar. 1995), pp. 169–175.

[90] G. L. Friedsam and E. M. Biebl. "A broadband free-space dielectric properties measurement system at millimeter wavelengths". In: *1996 Conference on Precision Electromagnetic Measurements Digest*. June 1996, pp. 210–211.

[91] D. Bourreau, A. Peden, and S. L. Maguer. "A Quasi-Optical Free-Space Measurement Setup Without Time-Domain Gating for Material Characterization in the W-Band". In: *IEEE Transactions on Instrumentation and Measurement* 55.6 (Dec. 2006), pp. 2022–2028.

[92] A. Kazemipour et al. "Design and Calibration of a Compact Quasi-Optical System for Material Characterization in Millimeter/Submillimeter Wave Domain". In: *IEEE Transactions on Instrumentation and Measurement* 64.6 (June 2015), pp. 1438–1445.

[93] P. F. Goldsmith. *Quasioptical Systems: Gaussian Beam Quasioptical Propogation and Applications*. English. 1 edition. Piscataway, NJ: Wiley-IEEE Press, Jan. 1998.

[94] D. Ghodgaonkar, V. Varadan, and V. Varadan. "Free-space measurement of complex permittivity and complex permeability of magnetic materials at microwave frequencies". In: *IEEE Transactions on Instrumentation and Measurement* 39.2 (Apr. 1990), pp. 387–394.

[95] *Measurement Techniques for Complex Permeability and Permittivity of Highly Conductive Materials at Microwave Frequencies*. en. Defense Technical Information Center, 1966.

[96] R. J. Collier and A. D. Skinner. *Microwave Measurements*. en. IET, 2007.

[97] M. Klenner et al. "Investigation of dielectric properties of multilayer structures consisting of homogeneous plastics and liquid solutions at 75-110 GHz". en. In: *Journal of Sensors and Sensor Systems* 4.1 (Mar. 2015), pp. 125–131.

[98] A. W. Rudge. *The Handbook of Antenna Design*. en. IET, Jan. 1982.

[99] I. Rolfes and B. Schiek. "Calibration Methods for Free Space Dielectric Microwave Measurements with a 4-Channel-Network-Analyzer". In: Sept. 2002, pp. 1–4.

[100] I. Rolfes and B. Schiek. "Calibration methods for microwave free space measurements". In: *Adv. Radio Sci.* 2 (May 2005), pp. 19–25.

[101] A. Basu. *An Introduction to Microwave Measurements*. en. CRC Press, Dec. 2014.

[102] D. R. Lima et al. "Accuracy of GRL calibration considering time domain gating for the calculation of permittivity parameter in free space technique". In: *Microwave and Optoelectronics Conference (IMOC), 2015 SBMO/IEEE MTT-S International*. Nov. 2015.

[103] N. Zhang et al. "A broadband free-space dielectric measurement system". In: *2015 IEEE MTT-S International Microwave Workshop Series on Advanced Materials and Processes for RF and THz Applications (IMWS-AMP)*. July 2015, pp. 1–3.

[104] A. M. Hassan, J. Obrzut, and E. J. Garboczi. "A Q-Band Free-Space Characterization of Carbon Nanotube Composites". In: *IEEE Transactions on Microwave Theory and Techniques* 64.11 (Nov. 2016), pp. 3807–3819.

[105] T. W. Kang et al. "Free-space measurement of the complex permittivity of liquid materials at millimeter-wave region". In: *2016 Conference on Precision Electromagnetic Measurements (CPEM 2016)*. July 2016, pp. 1–2.

[106] T. Dakin and C. Works. "Microwave dielectric measurements". In: *Journal of Applied Physics* 18.9 (1947), pp. 789–796.

[107] W. B. Weir. "Automatic measurement of complex dielectric constant and permeability at microwave frequencies". In: *Proceedings of the IEEE* 62.1 (1974), pp. 33–36.

[108] D. G. Aguirre. *Measurement of permittivity and permeability of microwave materials*. US Patent 4,507,602. Mar. 1985.

[109] R. Azzam and N. Bashara. *Ellipsometry and polarized light*. English. Amsterdam: Elsevier, 1999.

[110] F. Sagnard. "Determination of complex permittivity and thickness of a single-layer material using reflection ellipsometry at several angles of incidence". In: *Microwave and Optical Technology Letters* 35.2 (2002), pp. 154–157.

[111] K. Riedling. *Ellipsometry for Industrial Applications*. en. Springer Science & Business Media, Dec. 2012.

[112] E. Hecht. *Optik*. de. Oldenbourg Verlag, 2005.

[113] F. Sagnard et al. "Microwave measurements of the complex permittivity of construction materials using Fresnel reflection coefficients and reflection ellipsometry". In: *IEEE Antennas and Propagation Society International Symposium, 2001*. Vol. 1. 2001, 626–629 vol.1.

[114] L. I. Nass. *Encyclopedia of PVC, Second Edition: Compounding Processes, Product Design, and Specifications - Volume 3 of 4 (Print)*. en. CRC Press, Aug. 1992.

[115] C. E. Wilkes et al. *PVC Handbook*. en. Hanser, 2005.

[116] B. Riddle, J. Baker-Jarvis, and J. Krupka. "Complex permittivity measurements of common plastics over variable temperatures". In: *IEEE Transactions on Microwave Theory and Techniques* 51.3 (Mar. 2003), pp. 727–733.

[117] U. C. Hasar. "Permittivity Measurement of Thin Dielectric Materials from Reflection-Only Measurements Using One-Port Vector Network Analyzers". English. In: *Progress In Electromagnetics Research* 95 (2009), pp. 365–380.

[118] K. Chalapat et al. "Wideband Reference-Plane Invariant Method for Measuring Electromagnetic Parameters of Materials". In: *IEEE Transactions on Microwave Theory and Techniques* 57.9 (Sept. 2009), pp. 2257–2267.

[119] L. E. Feher. *Energy Efficient Microwave Systems: Materials Processing Technologies for Avionic, Mobility and Environmental Applications*. en. Springer Science & Business Media, Apr. 2009.

[120] Z. Awang et al. "A Free-Space Method for Complex Permittivity Measurement of Bulk and Thin Film Dielectrics at MIcrowave Frequencies". en. In: *Progress In Electromagnetics Research B* 51 (2013), pp. 307–328.

[121] R. H. Burgess. *Manufacture and Processing of PVC*. en. CRC Press, Nov. 1981.

[122] J. Leadbitter, J. A. Day, and J. L. Ryan. *PVC: Compounds, Processing and Applications*. en. iSmithers Rapra Publishing, Jan. 1994.

[123] D. K. Ghodgaonkar, V. V. Varadan, and V. K. Varadan. "A free-space method for measurement of dielectric constants and loss tangents at microwave frequencies". In: *IEEE Transactions on Instrumentation and Measurement* 38.3 (June 1989), pp. 789–793.

[124] G. L. Friedsam and E. M. Biebl. "Precision free-space measurements of complex permittivity of polymers in the W-band". In: *Microwave Symposium Digest, 1997., IEEE MTT-S International*. Vol. 3. June 1997, 1351–1354 vol.3.

[125] N. Tamyis, A. Ramli, and D. K. Ghodgaonkar. "Free space measurement of complex permittivity and complex permeability of magnetic materials using open circuit and short circuit method at microwave frequencies". In: *Student Conference on Research and Development, 2002. SCOReD 2002*. 2002, pp. 394–398.

[126] A. Tessmann et al. "Metamorphic HEMT MMICs and Modules for Use in a High-Bandwidth 210 GHz Radar". In: *IEEE Journal of Solid-State Circuits* 43.10 (Oct. 2008), pp. 2194 –2205.

[127] A. Bangert et al. "W-band MMIC VCO with a large tuning range using a pseudomorphic HFET". In: *Microwave Symposium Digest, 1996., IEEE MTT-S International*. Vol. 2. June 1996, 525–528 vol.2.

[128] S. Kang, J. C. Chien, and A. M. Niknejad. "A W-Band Low-Noise PLL With a Fundamental VCO in SiGe for Millimeter-Wave Applications". In: *IEEE Transactions on Microwave Theory and Techniques* 62.10 (Oct. 2014), pp. 2390–2404.

[129] R. Weber et al. "A 92 GHz GaN HEMT voltage-controlled oscillator MMIC". In: *2014 IEEE MTT-S International Microwave Symposium (IMS2014)*. June 2014, pp. 1–4.

[130] F. Thome, S. Maroldt, and O. Ambacher. "Prospects and Limitations of Stacked-FET Approaches for Enhanced Output Power in Voltage-Controlled Oscillators". In: *IEEE Transactions on Microwave Theory and Techniques* 64.3 (Mar. 2016), pp. 836–846.

[131] N. Pohl et al. "SiGe Bipolar VCO With Ultra-Wide Tuning Range at 80 GHz Center Frequency". In: *IEEE Journal of Solid-State Circuits* 44.10 (Oct. 2009), pp. 2655–2662.

[132] N. Pohl, T. Jaeschke, and K. Aufinger. "An Ultra-Wideband 80 GHz FMCW Radar System Using a SiGe Bipolar Transceiver Chip Stabilized by a Fractional-N PLL Synthesizer". In: *IEEE Transactions on Microwave Theory and Techniques* 60.3 (Mar. 2012), pp. 757–765.

[133] C. Balanis. *Antenna theory: analysis and design*. English. Hoboken, NJ: Wiley Interscience, 2005.

[134] H. J. Visser. *Antenna Theory and Applications*. en. John Wiley & Sons, Jan. 2012.

[135] Singal. *Wireless Communications*. en. Tata McGraw-Hill Education, 2010.

[136] W. L. Stutzman and G. A. Thiele. *Antenna Theory and Design*. en. John Wiley & Sons, May 2012.

[137] J. Moré. "The Levenberg-Marquardt algorithm: Implementation and theory". In: *Numerical Analysis*. Ed. by G. A. Watson. Lecture Notes in Mathematics 630. Springer Berlin Heidelberg, Jan. 1978, pp. 105–116.

[138] M. Ocker. *Untersuchungen zur Millimeterwellen-Bilderfassung mit aktiver Bestrahlung*. 2012.

[139] E. E. Kriezis, D. P. Chrissoulidis, and A. G. Papagiannakis. *Electromagnetics and Optics*. en. World Scientific, 1992.

[140] R. Zoughi. *Microwave Non-Destructive Testing and Evaluation Principles*. en. Springer Science & Business Media, Dec. 2012.

[141] I. Webman, J. Jortner, and M. H. Cohen. "Theory of optical and microwave properties of microscopically inhomogeneous materials". In: *Physical Review B* 15.12 (June 1977), pp. 5712–5723.

[142] D. K. Schroder. *Semiconductor Material and Device Characterization*. en. John Wiley & Sons, Feb. 2006.

[143] D. Misra et al. "Noninvasive electrical characterization of materials at microwave frequencies using an open-ended coaxial line: test of an improved calibration technique". In: *IEEE Transactions on Microwave Theory and Techniques* 38.1 (Jan. 1990), pp. 8–14.

[144] Y. Rao and C. P. Wong. "Material characterization of a high-dielectric-constant polymer-ceramic composite for embedded capacitor for RF applications". en. In: *Journal of Applied Polymer Science* 92.4 (May 2004), pp. 2228–2231.

[145] M. N. Afsar and K. J. Button. "Millimeter-wave dielectric measurement of materials". In: *Proceedings of the IEEE* 73.1 (Jan. 1985), pp. 131–153.

[146] L. A. Belov, S. M. Smolskiy, and V. N. Kochemasov. *Handbook of RF, Microwave, and Millimeter-wave Components*. en. Artech House, 2012.

[147] R. Sturdivant. *Microwave and Millimeter-Wave Electronic Packaging*. en. Artech House, Dec. 2013.

[148] M. Klenner et al. "Characterization of quasi-optical focusing systems at W-band frequencies". In: *Microwave Conference (EuMC), 2015 European*, pp. 311–314.

[149] A. Cataldo, E. D. Benedetto, and G. Cannazza. *Advances in Reflectometric Sensing for Industrial Applications*. en. Morgan & Claypool Publishers, Jan. 2016.

[150] K. K. Sharma. *Optics: Principles and Applications*. en. Academic Press, Sept. 2006.

[151] D. Kühlke. *Optik Grundlagen und Anwendungen*. German. Frankfurt am Main: Harri Deutsch, 2011.

[152] W. L. Brooks et al. "Absorption of millimeter waves in dielectric solids". In: *JOSA* 43.12 (1953), pp. 1191–1194.

[153] M. Halpern et al. "Far infrared transmission of dielectrics at cryogenic and room temperatures: glass, Fluorogold, Eccosorb, Stycast, and various plastics". In: *Applied Optics* 25.4 (1986), pp. 565–570.

[154] M. N. Afsar. "Precision millimeter-wave measurements of complex refractive index, complex dielectric permittivity, and loss tangent of common polymers". In: *IEEE Transactions on Instrumentation and Measurement* 1001.2 (1987), pp. 530–536.

[155] M. Lee et al. "Millimeter-wave dielectric properties of electro-optic polymer materials". In: *Applied physics letters* 81.8 (2002), pp. 1474–1476.

[156] A. Kilian, J. Weinzierl, and L.-P. Schmidt. "Permittivity measurement techniques at 24 GHz for automotive polymer composites including thin films and paint foils". In: *Microwave Conference (GeMIC), 2008 German*. VDE. 2008, pp. 1–4.

[157] T. Shimizu and Y. Kobayashi. "Millimeter wave measurements of some low-loss dielectric plates by a novel cut-off circular waveguide method". In: *Microwave Conference, 2002. 32nd European*. IEEE. 2002, pp. 1–4.

[158] F. Rutz. *Terahertz-Zeitbereichsspektroskopie: zerstörungsfreie Charakterisierung von Polymeren und Verbundwerkstoffen*. de. Fraunhofer-IRB-Verlag, 2007.

[159] J. Birch, J. Dromey, and J Lesurf. "The optical constants of some common low-loss polymers between 4 and 40 cm- 1". In: *Infrared Physics* 21.4 (1981), pp. 225–228.

[160] J. Birch and K. F. Ping. "An interferometer for the determination of the temperature variation of the complex refraction spectra of reasonably transparent solids at near-millimetre wavelengths". In: *Infrared Physics* 24.2 (1984), pp. 309–314.

[161] J. Birch. "Systematic errors in dispersive fourier transform spectroscopy in a non-vacuum environment". In: *Infrared physics* 34.1 (1993), pp. 89–93.

[162] A. A. Hanzaz. "LTCC system for high frequency applications". In: *Proceedings of the International MultiConference of Engineers and Computer Scientists*. Vol. 2. IMECS Hong Kong. 2012.

[163] A. Elhawil et al. "A Quasi-Optical Free-Space Method for Dielectric Constant Characterization of Polymer Materials in mm-wave Band". In: *Proceedings of 12th Annual Symposium of the IEEE/LEOS Benelux*. Dec. 2007, pp. 187–190.

[164] A. Kazemipour et al. "Wideband frequency-domain material characterization up to 500 GHz". In: *2014 39th International Conference on Infrared, Millimeter, and Terahertz waves (IRMMW-THz)*. Sept. 2014, pp. 1–2.

[165] A. R. Djordjevic et al. "Wideband frequency-domain characterization of FR-4 and time-domain causality". In: *IEEE Transactions on Electromagnetic Compatibility* 43.4 (2001), pp. 662–667.

[166] K. Breeden and A. Sheppard. "A note on the millimeter and submillimeter wave dielectric constant and loss tangent value of some common materials". In: *Radio Science* 3.2 (1968), pp. 205–205.

[167] R. Haas and P Zimmermann. "22-GHz Measurements of Dielectric Constants and Loss Tangents of Castable Dielectrics at Room and Cryogenic Temperatures (Short Papers)". In: *IEEE Transactions on Microwave Theory and Techniques* 24.11 (1976), pp. 881–883.

[168] F. I. Shimabukuro et al. "A quasi-optical method for measuring the complex permittivity of materials". In: *IEEE transactions on microwave theory and techniques* 32.7 (1984), pp. 659–665.

[169] E. Marsh. *Composites in Infrastructure - Building New Markets*. en. Elsevier, Dec. 2000.

[170] L. Hollaway, M. K. Chryssanthopoulos, and S. S. J. Moy. *Advanced Polymer Composites for Structural Applications in Construction: ACIC 2004 : Proceedings of the Second International Conference, Held at the University of Surrey, Guildford, UK on 20-22 April 2004*. en. Woodhead Publishing, 2004.

[171] J. Murphy. *The Reinforced Plastics Handbook*. en. Elsevier, Oct. 2013.

[172] H. Lipson and M. Kurman. *Fabricated: The New World of 3D Printing*. en. John Wiley & Sons, Jan. 2013.

[173] *Additive Manufacturing Technologies: 3D Printing, Rapid Prototyping, and Direct Digital Manufacturing*.

[174] A. K. Jonscher. "Dielectric relaxation in solids". In: *Journal of Physics D: Applied Physics* 32.14 (1999), R57.

[175] G. Williams. "Dielectric Relaxation". en. In: *Encyclopedia of Polymer Science and Technology*. John Wiley & Sons, Inc., 2002.

[176] A Tanwar et al. "Microwave dielectric relaxation study of poly (methyl methacrylate) and polysulphone in dilute solutions". In: *Indian Journal of Pure and Applied Physics* 44.7 (2006), p. 548.

[177] R. Piesiewicz et al. "Properties of Building and Plastic Materials in the THz Range". en. In: *International Journal of Infrared and Millimeter Waves* 28.5 (Mar. 2007), pp. 363–371.

[178] A. Elhawil et al. "A Quasi-Optical Free-Space Method for Dielectric Constant Characterization of Polymer Materials in mm-wave Band". In: *Proceedings of 12th Annual Symposium of the IEEE/LEOS Benelux December 17-18 (2007) Brussels Belgium*. IEEE/LEOS Benelux, Dec. 2007, pp. 187–190.

[179] J. Beyerer and F. P. León. *OCM 2013 - Optical Characterization of Materials - conference proceedings*. en. KIT Scientific Publishing, 2013.

[180] D. K. Ghodgaonkar, V. V. Varadan, and V. K. Varadan. "A free-space method for measurement of dielectric constants and loss tangents at microwave frequencies". In: *IEEE Transactions on Instrumentation and measurement* 38.3 (1989), pp. 789–793.

[181] R. K. Shevgaonkar. *Electromagnetic Waves*. en. Tata McGraw-Hill Education, Oct. 2005.

[182] C. Yeh and F. Shimabukuro. *The Essence of Dielectric Waveguides*. en. Springer Science & Business Media, June 2008.

[183] D. Yokoyama and C. Adachi. "In situ real-time spectroscopic ellipsometry measurement for the investigation of molecular orientation in organic amorphous multilayer structures". In: *Journal of Applied Physics* 107.12 (2010).

[184] J. Bousquet et al. "Spectroscopic ellipsometry of homoepitaxial diamond multilayers and delta-doped structures". In: *Applied Physics Letters* 104.2 (2014).

[185] T Tumkur et al. "Permittivity evaluation of multilayered hyperbolic metamaterials: Ellipsometry vs. reflectometry". In: *Journal of Applied Physics* 117.10 (2015).

[186] A Sayyadi-Shahraki et al. "A new temperature stable microwave dielectric ceramic with low-sintering temperature in Li 2 TiO 3–Li 2 Zn 3 Ti 4 O 12 system". In: *Journal of Alloys and Compounds* 597 (2014), pp. 161–166.

[187] M. Sebastian, R Ubic, and H Jantunen. "Low-loss dielectric ceramic materials and their properties". In: *International Materials Reviews* 60.7 (2015), pp. 392–412.

[188] J. Choi and H.-T. Jung. "A new triple-layered composite for high-performance broadband microwave absorption". In: *Composite Structures* 122 (2015), pp. 166–171.

[189] M. Samper et al. "New environmentally friendly composite laminates with epoxidized linseed oil (ELO) and slate fiber fabrics". In: *Composites Part B: Engineering* 71 (2015), pp. 203–209.

List of Publications

Journals

M. Klenner et al. “Spectroscopic Measurement of Material Properties Using an Improved Millimeter-Wave Ellipsometer Based on Metallic Substrates”. In: *IEEE Transactions on Instrumentation and Measurement* PP.99 (2016), pp. 1–9.

M. Klenner et al. “Investigation of dielectric properties of multilayer structures consisting of homogeneous plastics and liquid solutions at 75–110 GHz”. English. In: *Journal of Sensors and Sensor Systems* 4.1 (Mar. 2015), pp. 125–131.

Conference Proceedings

M. Klenner et al. “Material characterization using a compact W-band ellipsometer”. In: *2016 46th European Microwave Conference (EuMC)*. Oct. 2016.

M. Klenner et al. “A portable W-band radar system for enhancement of infrared vision in fire fighting operations”. In: *Millimetre Wave and Terahertz Sensors and Technology IX*. Vol. 9993. 2016.

M. Klenner et al. “Characterization of quasi-optical focusing systems at W-band frequencies”. In: *Microwave Conference (EuMC), 2015 European*. Sept. 2015, pp. 311–314.

M. Klenner et al. “Analysis of Dielectric Properties of Layered Plastics at W-Band Frequencies”. In: *ITG/GMA Symposium; Proceedings of Sensors and Measuring Systems 2014; 17*. June 2014, pp. 1–4.

M. Klenner et al. “Compact quasi-optical focusing system for a 94 GHz FMCW radar”. In: *Radar Symposium (IRS), 2014 15th International*. June 2014, pp. 1–3.

M. Klenner et al. “Multilayer material analysis using an active millimeter wave imaging system”. In: *Radar Symposium (IRS), 2013 14th International*. Vol. 1. 2013, pp. 207–213.

Co-Authored

A. Hülsmann et al. “Radar system components to detect small and fast objects”. In: *Terahertz Physics, Devices, and Systems - Advanced Applications in Industry and Defense*. Baltimore/Md, May 2015, p. 94830C.

Acknowledgment

I wish to express my sincere appreciation to everyone who contributed to this thesis. First of all, I would like to thank Prof. Dr. Oliver Ambacher, my supervisor and former head of the Fraunhofer Institute for Applied Solid State Physics (IAF), for giving me the unique opportunity to do a doctorate that combines the investigation of fundamental physical principles with the exciting world of high frequency electronics. Apart from many fruitful discussions, I want to point out how much his annual doctoral seminars have helped me to develop my scientific skills.
I am more than grateful to my technical advisor Dr. Axel Hülsmann as well as to the whole ME-SY group of the Microelectronics department at the Fraunhofer IAF and particularly to my colleague Christian Zech. Without the excellent working conditions, their unreserved support and confidence in my capabilities, it would not have been possible to achieve the ambitious goal of developing a novel approach to millimeter wave ellipsometry within the past three years.
Furthermore, I would like to thank

- the head of our business unit Dr. Michael Schlechtweg and the head of our department Dr. Jutta Kühn for valuable discussions on high frequency electronics, reliable and detailed proofreading of my publications and this thesis, as well as for their constant willingness for support.
- Dr. Rüdiger Quay and Dr. Friedbert van Raay for their assistance in defining my goals and not losing track of them, especially in the early stages of this thesis.
- Benjamin Baumann for designing the PCBs used for signal generation and voltage supply of the ellipsometer.
- Martin Zink for the CAD-drawings of the mechanical construction of the ellipsometer and his assistance with assembly and adjustment of the experimental setup.
- Olivia Lehmann for additional CAD-drawings of new components used for optimization of the ellipsometer.
- the team of the mechanical workshop at the Fraunhofer IAF for consultation as well as precise and reliable fabrication of all the mechanical parts of the ellipsometer.

In deepest sorrow, I have to express my everlasting gratitude to the most important person for this thesis: Sarah-Katharina Meisenheimer, my beautiful wife and one of the most talented physicists I have known. Sarah passed away unexpectedly but peacefully while we were both working on the very last pages of our doctoral theses, after sharing not only our private lives but also most parts of our scientific careers. Some of the central ideas in this thesis resulted from our extraordinary discussions when we were jogging, preparing dinner or playing golf at the coastlines of western Scotland during our honeymoon. You have been invaluable for my academic growth. I miss you so much!